THE SOUND OF MOVING BODIES

by

Kenneth Steven Brentner

Corpus Christi College

December 1990

Submitted for the degree of Doctor of Philosophy to the University of Cambridge. This research was carried out in the Department of Engineering of the University of Cambridge and at NASA Langley Research Center.

Acknowledgements.

This work was carried out during the period of October 1987 through December 1990, under the supervision of Professor J. E. Ffowcs Williams. His encouragement and guidance were most helpful both while I was in residence at Cambridge and during my time at NASA Langley Research Center.

I also wish to express my most sincere thanks to Dr. F. Farassat for his helpful discussions, exhortation, and strong encouragement. Dr. Farassat has been an important role model for me throughout my career. I am also grateful for the several other colleagues at NASA Langley for their assistance, support, and encouragement while I was working on this research.

During the three years of my research, I have been financially supported by NASA Langley Research Center, to whom I am grateful for granting me the freedom to pursue this research.

Finally, I owe more than I know to my family for their enduring love and patience.

Declaration.

This work was carried out solely by the author, and no part has been submitted for a degree at any other university.

Permission to copy.

I give my consent for this dissertation, if approved for a higher degree, to be made available for copying and inter-library loan providing due acknowledgement is made by the person consulting the thesis for any information obtained or results quoted.

Contents

The mind of man plans his ways,
But the Lord directs his step.

Proverbs 16:9

Introduction

Background

The theory of aerodynamic sound was developed by Lighthill *[1]* through the introduction of the acoustic analogy. This analogy views the limited fluctuating fluid region as an external stress field acting on the uniform acoustic medium at rest. Thus by rearrangement of the usual statements of mass and momentum conservation into an inhomogeneous wave equation, Lighthill found a general procedure for estimating the intensity of the sound produced in terms of the fluid flow. The acoustic analogy proceeds with the assumption that the localized flow field is unaffected by the acoustic field, completing the separation between aerodynamics and acoustics. While others have described the acoustic radiation as driven by distributions of sources, the acoustic analogy gave a consistent and rational way to determine the strength of these sources. Even though the analogy separates the acoustics from the full fluid dynamics problem, physical insight is needed in determining the necessary information from the aerodynamic flow.

The extension of Lighthill's theory to include surfaces in the flow was first made by Curle *[2]* in 1955, and generalized to sound produced by surfaces in arbitrary motion by Ffowcs Williams and Hawkings *[3]* in 1969. The Ffowcs Williams and Hawkings (FW–H) equation has found great success, especially as a tool for estimating the sound generated by propellers and helicopter rotors. This success may be partially attributed to Ffowcs Williams and Hawkings giving several forms for the source terms. Using the theory of generalized functions in the derivation, Ffowcs Williams and Hawkings choose a source description of monopole, dipole and quadrupole terms, which have come to be known as thickness, loading, and quadrupole terms respectively. Although this particular description

is not unique, it yields meaningful results when each the sources are considered individually. For example in Farassat's *[4]* early work, which used the FW–H equation as its foundation, only the thickness noise was calculated for helicopter rotors because of the difficulty in determining the aerodynamic field. Later the contribution of the loading source was added as experimental and computational results became available.

The volume source, or quadrupole, has been a subject of lively discussion and speculation in rotor noise prediction often because of the difficulty in assessing its importance when the flow is complicated. It has been argued by Farassat*[4]* that the quadrupole may be neglected when the turbulent flow region is small, as in the case of very thin propellers or low speed rotors. However, probably the most fundamental reason that the volume term has not been included in many analyses is because it requires a detailed knowledge of the flow field around the body in advance. Until recently this information was nearly impossible to attain. Indeed, many numerical prediction codes based on the FW–H equation have neglected the quadrupole source term precisely because of the inability to determine the correct source strength together with the analytical and numerical difficulties in dealing with a volume distribution of sources.

As propellers and helicopter rotor speeds approach sonic speed, it is no longer prudent to neglect the quadrupole source, since any argument based on the normal ordering of monopole, dipole and quadrupole becomes meaningless. Hanson and Fink *[5]* were the first to demonstrate through numerical calculations the importance of the quadrupole source for high speed propellers, while Schmitz and Yu *[6]* have found similar results for helicopter rotors. Ffowcs Williams *[7]* has shown that in some cases the quadrupole term may be the *most* significant source term.

Today prediction methods based on the FW–H equation are quite advanced. One good example is that of Schultz and Splettstoesser *[8]* where model scale helicopter rotor noise is compared to an approximate prediction of all three source terms of the FW–H equation. The aerodynamic blade pressure was measured on the blade and used as input in the acoustic theory. Predictions were good for all the cases presented, which included high speed impulsive and blade vortex interaction noise. Unfortunately, when a prediction is needed we do not generally have the luxury of having measured blade surface pressures. Even so accurate results are still necessary. Determining the time dependent surface pressure, not to mention the pressure and velocities of the fluid particles near the body, is difficult. These calculations are especially troublesome when the volume source is most needed; i.e. when the flow is transonic and sophisticated aerodynamic analyses are needed. Although current high speed computers and present day computational fluid dynamics (CFD) methods may allow one to predict the aerodynamic field, much of the advantage of formulating the acoustic problem separately from the aerodynamics problem is lost. Indeed the development and operation of the CFD codes is a major task in its own right.

Farassat *[9]* has proposed to reduce the quadrupole from a volume source to an effective surface source by considering the time dependent shock surfaces as the primary contributor in the full volume source. Recognizing that the shock is a discontinuity in the fluid and guided by the mathematics, Farassat has shown that a shock surface noise contribution should improve the complete rotor noise calculation when shocks exist. While surface integration is preferable to volume integration in the acoustic calculations, this path demands more information from the aerodynamicist. In theory the entire flow field is not needed, but in practice the calculation of the full time dependent, three dimensional flow field will only be the first step in determining the shock location, geometry, and strength.

Two alternate approaches to the FW–H for predicting the sound of moving bodies have been pursued in the past few years. The first alternative is to consider the FW–H equation as an integral equation and solve for the entire flow field. Long *[10]*, Farassat and Myers *[11]*, Brandão*[12,13]* , and Lee *[14]* have all attempted to solve singular integral equations based on the FW–H equation with varying degrees of success. Hanson *[15]* and Das *[16]* have developed integral methods based on aeroacoustic ideas. Morino and his colleagues*[17,18]* have used a similar mathematical approach for propeller and helicopter aerodynamics. The acoustic integral equation has the advantage that the method used for aerodynamic and acoustic calculations is unified, yet it is apparently difficult to implement a nonlinear method along these lines. While this approach does not seem to take any advantage of recent progress made in CFD, it is hoped that much of the experience learned in developing noise prediction codes can be transferred directly to the development of aerodynamic codes based on the FW–H equation. It is also hoped that new codes developed along this line would not be significantly more complex than present day noise prediction codes. Ffowcs Williams *[19]* describes how this idea has been the motivation for acoustic diffraction problems, however, in general, diffraction theory has only been applied to simple geometries.

The second alternative to the FW–H equation recognizes that a major effort is required to develop and use CFD codes just to determine the input for the FW–H equation. Since the acoustic fluctuations are part of the complete fluid dynamics problem, there is no fundamental reason not to solve the combined acoustics and aerodynamics field using an unsteady CFD code. This approach has the advantage that the nonlinear features in the flow, like shocks, are accounted for automatically along with local sound speed variation and convection effects. These effects are included in the FW–H quadrupole source, albeit

in a somewhat unnatural way. The difficulty with this approach is that non-physical boundary conditions and numerical dissipation are required for stable numerical methods, even though they may cause potentially insurmountable problems in the simultaneous calculation of aerodynamics and acoustics. Also the acoustic quantities are several orders of magnitude smaller than the aerodynamic quantities, a condition which implies that very accurate solutions are required. To achieve a high level of accuracy, the flow field must be resolved sufficiently by the computational grid. Finally, only near field solutions will be possible in the foreseeable future since execution times and memory requirements inherently limit job sizes.

Korkan, Von Lavante, and Bober *[20]* have overcome the near field limitation by combining a non-linear Euler calculation for a high speed propeller with a Kirchhoff formulation to determine the sound outside the computational grid. Thus linear acoustics is used in the region where appropriate and the near field calculation is completely nonlinear; all in the spirit of the acoustic analogy. Ffowcs Williams and Hawkings suggested that their formulation could be used as a Kirchhoff formula, but it took the advancement of both the digital computer and computational fluid dynamics for this to become feasible.

The results of Korkan et. al.*[20]* were not as good as one might hope, but their work did bring to the surface many of the issues, such as grid resolution, artificial viscosity, etc., which must be addressed. Purcell, Strawn, and Yu *[21]* as well as Lyrintzis and George *[22]* have applied the Kirchhoff approach to idealized helicopter rotor problems but there is some question about the extension of their work to complete three dimensional rotating blades. For this reason, Farassat and Myers *[23]* have given a new derivation of Morgans' *[24]* original Kirchhoff formulation using the modern mathematics of generalized functions

and differential geometry, extending the result to include a control volume in arbitrary motion.

The numerical coupling of a nonlinear inner solution with a linear outer solution for combined near and far field acoustics prediction appears to be an efficient use of the numerical tools at hand. This methodology depends crucially upon an inner solution which is accurate in both space and time within the entire control volume. The pressure, density, and fluid velocities along with their time and spatial derivatives at the control surface will be required as input into the Kirchhoff formulation. Clearly if there are significant damping or dispersion errors in a CFD solution, the outer acoustic solution cannot be accurate. Hence the coupled solution depends significantly on the inner solution.

Outline of the Dissertation

Two groups of problems are considered in this dissertation in order that some of the relevant issues in predicting the acoustic field of bodies moving at high speed may be examined. Since the quadrupole source has been shown to be important for accurate noise prediction but is both analytically and numerically difficult to evaluate, an analysis of this source term is made in Part A for the incompressible limit. While it is clear from Hanson and Fink*[5]* that the quadrupole will be most effective when the flow field is transonic, it is difficult to calculate exact solutions for transonic flow. For the idealized case of inviscid, incompressible flow, however, the exact solution for a circular cylinder is well known and it is shown that the contribution to the pressure field by each of the thickness, loading and quadrupole terms can be calculated separately and exactly. In this case, it is shown that the lift on the cylinder due to circulation is divided equally between the loading source and the quadrupole source.

These results are generalized for the case of a Joukowski airfoil. Here it is found that that the volume source can be eliminated for incompressible flow by manipulating the quadrupole and changing variables. This new incompressible version of the FW–H equation is compared with thin airfoil theory showing the role of the quadrupole in an aerodynamic theory is to enable lift generation. The case of a vortex passing a circular cylinder is also considered, where it is found that the quadrupole is required to account for the concentrated vorticity in the field. Keep in mind that in Part A the emphasis is upon the role of the FW–H source terms rather than the solution of the inviscid, incompressible flow past a cylinder.

For the second part of this work, it is postulated that CFD will play an important role in the future of acoustics; either to provide input into the quadrupole source term or to calculate directly the near field acoustics. In Part B, a finite volume, multistage time stepping, Euler code is used to investigate the use of present day CFD algorithms for the direct calculation of acoustics. The two dimensional, compressible, inviscid flow about an accelerating or decelerating circular cylinder is used as a model problem. The time evolution of the energy transfer from the cylinder to the fluid, as the cylinder is moved from rest to some nontrivial velocity, is clearly seen. Energy is the main quantity of interest in the calculations since various components of energy have physical meaning. By examining the temporal and spatial characteristics of the numerical solution, a distinction can be made between the propagating acoustic energy, the convecting energy associated with the entropy change in the fluid, and the energy contained in the local aerodynamic field. Systematic variation of the cylinder acceleration shows that the radiated acoustic energy depends strongly upon the rate of acceleration or deceleration.

Longhorn *[25]* has found that for an impulsively started sphere there is an equipartition between the kinetic energy in the local flow field and the propagating acoustic energy, in the low Mach number limit. In our calculations for the impulsively started cylinder, we find that an equipartition between of the energy in local aerodynamic field and the energy transported to the far field through propagation and convection exists. This is an extension of the low Mach number results. When the Mach number exceeds the critical Mach number and shocks persist in the steady state flow field, there is no longer an equipartition of energy since the cylinder continues to do work on the fluid, offsetting the drag associated with the shock. The additional energy input into the fluid convects downstream from the cylinder along with the newly generated vorticity.

Unlike the low Mach number situation, the energy of the aerodynamic field has a potential energy component, due to the significant second order compression of the fluid, in addition to kinetic energy. In our calculations, energy which leaves the control volume is divided between acoustic energy and energy associated with the change of entropy in the fluid. The computational grid has a large effect on the ratio of acoustic energy to entropy associated energy, while the role of the artificial viscosity seems to be of second order. We have found that the entropy terms were nearly negligible in all cases where the cylinder was started slowly. The calculations in Part B both give insight in to the interesting nonlinear interactions which occur when the cylinder is rapidly started as well as the numerical aspects of predicting the acoustics as part of the unsteady aerodynamic field.

Part A: Exact Calculation of Quadrupole Field

Introduction

In an effort to gain a new understanding about the FW–H quadrupole in both acoustic and aerodynamic applications, we have chosen some simple problems for which the incompressible flow field can be determined analytically using the two dimensional velocity potential. For a circular cylinder, each of the source terms are calculated separately and compared with the exact potential solution. The forces on the cylinder due to pressure are compared as well. This problem helps to explain the results and difficulties of Brandão's application*[12,13]* of the FW–H equation to aerodynamics.

The circular cylinder solution suggests a new description of the quadrupole term which is useful in identifying the volume and surface terms immediately from the exact solution. As an example, the problem of a circular cylinder moving near a vortex filament is examined to demonstrate the role of vorticity in the aerodynamic field. Following this, the contribution of the volume and surface sources are determined for a Joukowski airfoil. Each of these cases illustrate the various contributions of each of the source terms for incompressible flows. Finally the aerodynamic role of the quadrupole source is discussed along with a summary of Part A. Another analytical consideration of the role of quadrupole sources for exact *compressible* flow problems is given by Ffowcs Williams*[7]*.

The Incompressible FW–H equation

The differential form of the Ffowcs Williams – Hawkings equation may be written as

$$\left[\frac{\partial^2}{\partial t^2} - c_o^2 \frac{\partial^2}{\partial x_i \partial x_i}\right](\rho' H(f)) = \frac{\partial}{\partial t}(\rho_o v_n \delta(f)) - \frac{\partial}{\partial x_i}(p_{ij} n_j \delta(f)) + \frac{\partial^2}{\partial x_i \partial x_j}(T_{ij} H(f)) \quad (1)$$

where c is the sound speed, ρ is the density, ρ' is the density perturbation, and the subscript o refers to the value of the variables in the undisturbed medium. Lighthill's stress tensor, T_{ij}, is defined

$$T_{ij} = \rho u_i u_j + p_{ij} - c_o^2 \rho' \delta_{ij} \quad (2)$$

where u_i is the fluid velocity, p_{ij} is the compressive stress tensor, and δ_{ij} is the Kröeneker delta. In equation (1) the derivatives are to be interpreted as generalized derivatives, while $H(f)$ and $\delta(f)$ are the Heaviside and Dirac delta functions respectively. The surface of the body is described by the equation $f = 0$ with f being defined such that $\nabla f = \hat{\mathrm{n}}$, the outward unit normal vector. Note that the monopole and dipole terms, commonly referred to as thickness and loading sources, act only on the surface $f = 0$ while the quadrupole source acts throughout the volume $f > 0$. The velocity term v_n in the thickness source is the component of the body velocity normal to the body surface.

For an incompressible, inviscid fluid, $\rho' = 0$ and $p_{ij} = p\delta_{ij}$. The FW–H equation may then be written

$$\nabla^2(p' H(f)) = -\frac{\partial}{\partial t}(\rho v_n \delta(f)) + \frac{\partial}{\partial x_i}(p' n_i \delta(f)) - \frac{\partial^2}{\partial x_i \partial x_j}(\rho u_i u_j H(f)). \quad (3)$$

The subscript o on the variable ρ has been dropped since the density is constant and the perturbation pressure p' is used rather than p to emphasize the fluctuation in pressure and simplify accounting later. This is allowable since $\nabla^2 p' = \nabla^2 p$. Equation (3) can also be obtained by first using the isentropic relation $p' = c^2 \rho'$ and then allowing the speed of

sound c to approach infinity to account for incompressibility. To obtain a solution to this equation, we need to determine the strength of each source term.

Velocity Potential Solution for a Circular Cylinder

The velocity potential for a circular cylinder of radius a, in a frame of reference in which the cylinder is moving, is unsteady and known to be

$$\phi(\mathbf{x},t) = -\frac{a^2}{r}\mathbf{v}(t)\cdot\hat{\mathbf{r}} - \frac{K\theta}{2\pi}. \tag{4}$$

Here r,θ are the polar coordinates of $\mathbf{x}$ with respect to the cylinder center $\hat{\mathbf{x}}_o$, $\mathbf{v}(t)$ is the cylinder velocity, K is the bound circulation on the cylinder, and $\hat{\mathbf{r}}$ is a unit vector in the direction from the cylinder center to $\mathbf{x}$. See figure 1. The pressure perturbation, given by the Bernoulli equation, is

$$p' = p - p_o = -\frac{1}{2}\rho u^2 - \rho\frac{\partial\phi}{\partial t} \tag{5}$$

where

$$u^2 = |\nabla\phi|^2 = \frac{a^4}{r^4}v^2 + \frac{Ka^2}{\pi r^3}v_t + \frac{K^2}{4\pi^2 r^2} \tag{6}$$

$$\frac{\partial\phi}{\partial t} = -\frac{a^2}{r^2}\{v_n^2 - v_t^2\} - \frac{a^2}{r}\frac{d\mathbf{v}}{dt}\cdot\hat{\mathbf{r}} + \frac{Kv_t}{2\pi r}\ . \tag{7}$$

Here $v_n = \mathbf{v}\cdot\hat{\mathbf{n}}$ and $v_t = \mathbf{v}\cdot\hat{\mathbf{t}}$ are the components of velocity normal and tangential to the surface, respectively. Note that for the circular cylinder $\hat{\mathbf{r}}$ and $\hat{\mathbf{n}}$ are equivalent while $\hat{\mathbf{n}}$ and $\hat{\mathbf{t}}$ are both unit vectors. Also notice that $p' \to 0$ as $r \to \infty$ as required by the physics of the problem. These terms are written out so that they may be compared with the solution gained from the FW–H equation.

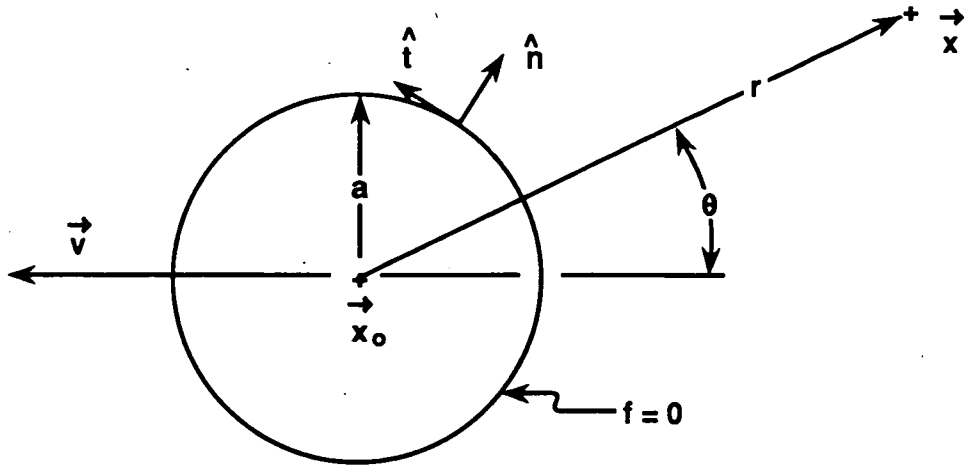

Figure 1. This figure shows the geometry of the circular cylinder and the definitions of the variables used in the calculations.

Acoustic Solution for a Circular Cylinder

The solution of the incompressible FW–H equation (3), which we will call the acoustic solution, can be obtained using the two dimensional free space Green's function of the Laplace equation, $G(\mathbf{x};\mathbf{y}) = \ln|\mathbf{x}-\mathbf{y}|/2\pi$, since the pressure and velocity fields are known and the geometry is simple. The Green's function solution for the model equation

$$\nabla^2\phi(\mathbf{x},t) = Q(\mathbf{x},t) \tag{8}$$

is given by

$$2\pi\phi(\mathbf{x},t) = \int_{-\infty}^{\infty}\int_{-\infty}^{\infty} Q(\mathbf{y},t)\ln|\mathbf{x}-\mathbf{y}|d\mathbf{y}. \tag{9}$$

The free space Green's function is appropriate since the source $Q(\mathbf{x},t)$ is a generalized function which extends the ordinary function to the entire two dimensional space. The presence of the generalized functions $\delta(f)$ and $H(f)$ remind us that the source terms in the FW–H equation have been extended as part of its derivation. Farassat discusses the powerful technique of extending ordinary functions in references*[4,26]* .

In Appendix A1, the integration for each of the source terms in the FW–H equation is carried out analytically. When this is done, the pressure perturbations obtained are

$$p'_t = \frac{\rho}{2}\left\{\frac{a^2}{r^2}(v_n^2 - v_t^2) + \frac{a^2}{r}\frac{d\mathbf{v}}{dt}\cdot\hat{\mathbf{r}}\right\} \tag{10}$$

$$p'_l = \frac{\rho}{2}\left\{\frac{a^2}{r^2}(v_n^2 - v_t^2) + \frac{a^2}{r}\frac{d\mathbf{v}}{dt}\cdot\hat{\mathbf{r}} - \frac{Kv_t}{\pi r}\right\} \tag{11}$$

and

$$p'_q = -\frac{\rho}{2}\left\{\frac{a^4}{r^4}v^2 + \frac{Ka^2}{\pi r^3}v_t + \frac{K^2}{4\pi^2 r^2}\right\}. \tag{12}$$

Here the subscripts t, l, and q on p' refer to the thickness, loading and quadrupole contributions, respectively. The subscripts n and t on v refer to the normal and tangential components of the cylinder velocity. It is immediately clear when comparing these equations with the potential solution, equations (5-7), that the thickness and loading sources correspond exactly to $-\rho\partial\phi/\partial t$ and the quadrupole contribution corresponds to $-\rho u^2/2$. This finding warrants further exploration to determine if this correspondence will be true in general or if it depends upon the unique geometry of the circular cylinder. Remember that these results apply when ϕ is defined for the case of a moving body in a stationary fluid.

Notice that the complete far field solution is given by the thickness and loading terms, but if there is circulation, $K \neq 0$, and no acceleration of the cylinder, $d\mathbf{v}/dt = 0$, the quadrupole contribution can be as important as the thickness term. The quadrupole serves to provide a near field pressure adjustment to the thickness and loading pressures. In effect the linearized pressure perturbation, $p' = -\rho\partial\phi/\partial t$, is determined by the thickness and loading sources alone, while the quadrupole accounts for the local kinetic energy in the fluid. Figure 2 shows the relative contributions of each of the source terms for a cylinder with circulation. This incompressible solution, which contains no acoustics, highlights that

it is possible to use the FW–H equation to predict the aerodynamic pressure field as well as acoustic pressure perturbations.

Force on the Cylinder

The force on the cylinder can now be calculated by integrating the pressure over the cylinder surface. The force per unit length is found to be

$$\mathbf{F} = \mathbf{F}_t + \mathbf{F}_l + \mathbf{F}_q \tag{13}$$

where

$$\mathbf{F}_t = -\frac{1}{2} m \frac{d\mathbf{v}}{dt} \tag{14}$$

$$\mathbf{F}_l = -\frac{1}{2} m \frac{d\mathbf{v}}{dt} + \frac{1}{2} \rho K (\mathbf{v} \times \hat{\mathbf{k}}) \tag{15}$$

$$\mathbf{F}_q = \frac{1}{2} \rho K (\mathbf{v} \times \hat{\mathbf{k}}) \, . \tag{16}$$

Here $m = \rho \pi a^2$ which is the added mass of the cylinder and $\hat{\mathbf{k}} = \hat{\mathbf{n}} \times \hat{\mathbf{t}}$. The force composed of $\mathbf{F}_t$ and the first term of $\mathbf{F}_l$ is an inertial force needed to accelerate the added mass while the force composed of $\mathbf{F}_q$ and the second part of $\mathbf{F}_l$ is a lift force due to circulation. The inertial force is independent of the quadrupole, due to the symmetry of the cylinder, but one half of the lift force is given by the quadrupole term. This implies that if the FW–H equation is to be used for aerodynamic calculations, the quadrupole may be important for lifting problems.

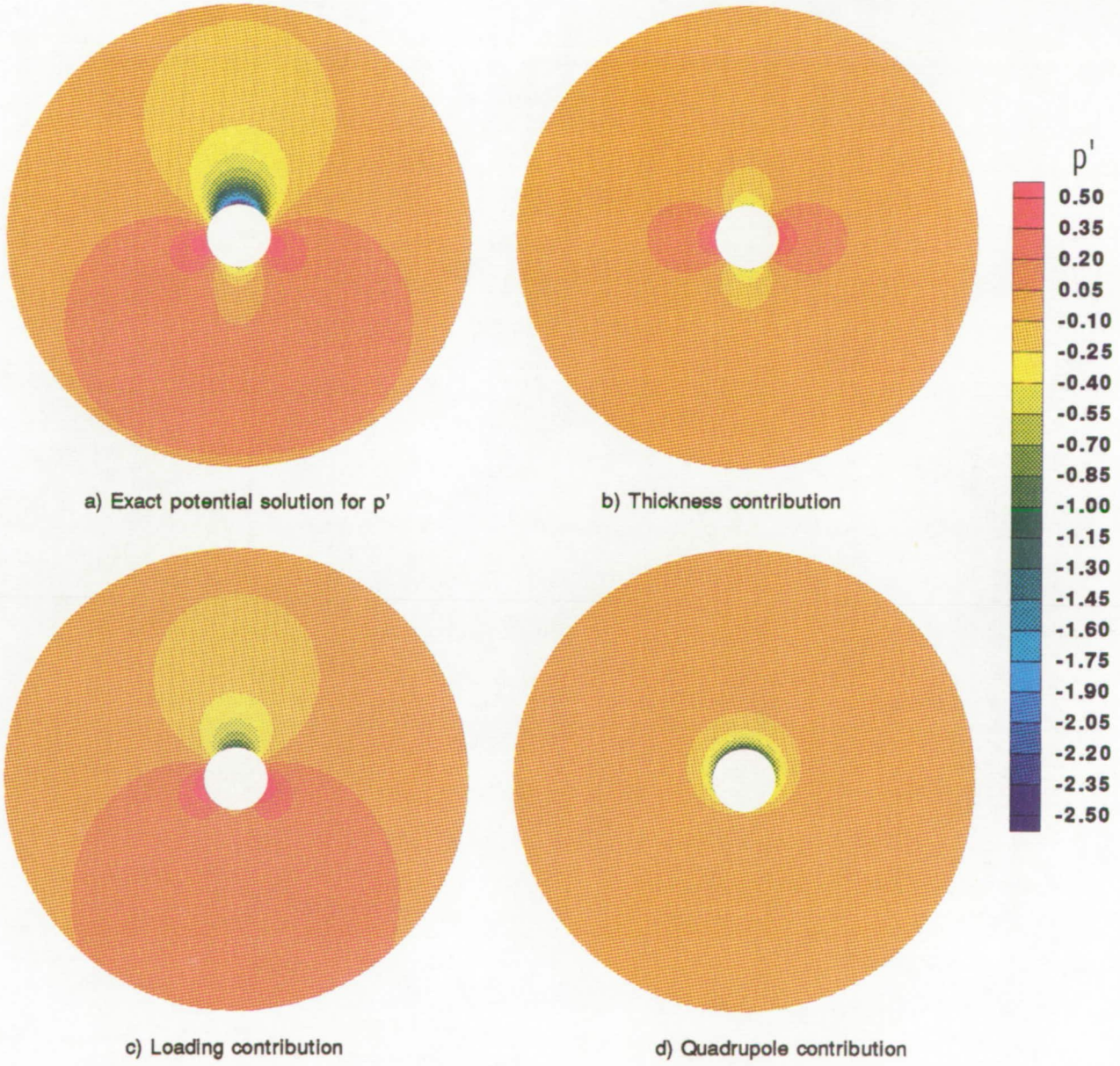

Figure 1. The pressure perturbation around a circular cylinder, radius $a = 1.0$, moving at a velocity $v = 1.0$, and with circulation $K = \pi$.

A New Quadrupole Description

Before a more definitive statement is made, let us first return to examine the way in which the quadrupole term was simply related to $\rho u^2/2$. In Appendix A2 it is shown that with no loss of generality the quadrupole term in the incompressible FW–H equation can be rewritten

$$\frac{\partial^2}{\partial x_i \partial x_j}\{\rho u_i u_j H(f)\} = \nabla^2\{\frac{1}{2}\rho u^2 H(f)\} + \rho\nabla\cdot\{\boldsymbol{\zeta}\times\mathbf{u}H(f)\} + \rho\nabla\cdot\{(v_n\mathbf{u} - \frac{1}{2}u^2\hat{\mathbf{n}})\delta(f)\} \tag{17}$$

where $\boldsymbol{\zeta} = \nabla\times\mathbf{u}$ is the local vorticity of the fluid and ρ is constant. The surface term arises from the gradient of the generalized function $H(f)$. The second term on the right hand side is zero for an irrotational flow ($\nabla\times\mathbf{u} = 0$). This form of the quadrupole clearly shows that if we only consider the linear solution, i.e. drop the $\rho u^2/2$ terms, that we still have a volume source and a surface source remaining. Hence the linearized solution is not equivalent to neglecting the quadrupole. This is not clear upon examining the original form of the quadrupole. The purpose of deriving this quadrupole expression is to separate explicitly the $\rho u^2/2$ part from the other parts, but (17) does have the advantage of showing the role of vorticity in the aerodynamic field.

It is also useful to rewrite the thickness term

$$\frac{\partial}{\partial t}\{\rho v_n \delta(f)\} = -\nabla\cdot\{\rho v_n \mathbf{v}\delta(f)\} + \rho\frac{d\mathbf{v}}{dt}\cdot\hat{\mathbf{n}}\delta(f) \tag{18}$$

which is a form similar to the previous equation. The derivation of this relation is found in Appendix A2 as well. The incompressible form of the FW–H equation may now be written

$$\nabla^2\{p'H(f)\} = -\nabla^2\{\frac{1}{2}\rho u^2 H(f)\} - \rho\nabla\cdot\{(\boldsymbol{\zeta}\times\mathbf{u})H(f)\} - \nabla\cdot\{\rho v_n(\mathbf{u}-\mathbf{v})\delta(f)\} + \nabla\cdot\{(p' + \frac{1}{2}\rho u^2)\hat{\mathbf{n}}\delta(f)\} - \rho\frac{d\mathbf{v}}{dt}\cdot\hat{\mathbf{n}}\delta(f)\ . \tag{19}$$

This new equation displays elements similar to Powell's theory of vortex sound *[27]* where the quadrupole source region is identified with the vorticity of compact eddies in the flow. The second source term in equation (19) is restricted to the region in the flow where the vorticity is nonzero, while the third source term is written in such a way that it may be interpreted as a vortex sheet of strength $u_t - v_t$ over the surface, since $\mathbf{u} - \mathbf{v} = (u_t - v_t)\hat{\mathbf{t}}$ on the surface. For the important case of irrotational flow the volume source of this new equation is exactly $-\rho u^2/2$, as was the case for the circular cylinder. In the following problems it will be possible to calculate the exact potential solution and then directly identify the volume and surface components in the modified FW–H equation, equation (19).

It is well to point out that if the body rotates this will affect both the first and last surface terms since the velocity $\mathbf{v}$ will have an additional rotational component. This explains the apparent discrepancy for the case of a circular cylinder rotating about its axis while also translating. If the cylinder rotates, the first surface source term appears to have a strength which depends upon the rotation rate of the cylinder, but the change in the last surface term exactly accounts for this apparent ambiguity. This must be the case for an inviscid fluid.

Upon examination of the modified FW–H equation, we see that a change of variables from p' to $B = p' + \rho u^2/2 = -\rho \partial\phi/\partial t$ is appropriate. This choice of variables, which is related to the variable Howe *[28]* used for his nonlinear analogy, transforms the FW–H equation into

$$\begin{aligned}\nabla^2(BH(f)) =& \nabla \cdot \left\{ \left(B\hat{\mathbf{n}} - \rho v_n(u_t - v_t)\hat{\mathbf{t}}\right)\delta(f)\right\} - \rho\frac{d\mathbf{v}}{dt}\cdot\hat{\mathbf{n}}\delta(f) \\ & - \rho\nabla\cdot\left((\boldsymbol{\zeta}\times\mathbf{u})H(f)\right). \end{aligned} \tag{20}$$

Here the variable B is actually the linearized pressure perturbation. The linear contribution of the original quadrupole is now represented by the vorticity term and the $\rho v_n u_t$ surface term. Notice that for an irrotational flow, the volume source term disappears, a reasonable result since the Laplace equation can be solved uniquely from the boundary data.

An alternate derivation given in Appendix A2 makes it easy to see that we can also write

$$\nabla^2\big(BH(f)\big) = \nabla\cdot(B\hat{\mathbf{n}}\delta(f)) - \rho\frac{\partial \mathbf{u}}{\partial t}\cdot\hat{\mathbf{n}}\delta(f) - \rho\nabla\cdot\big((\boldsymbol{\zeta}\times\mathbf{u})H(f)\big). \tag{21}$$

If we now recognize that $\nabla\phi = \mathbf{u}$ and $B = -\rho\partial\phi/\partial t$, we find that (21) can be written in the form

$$\nabla^2\big(BH(f)\big) = \nabla\cdot\big(B\hat{\mathbf{n}}\delta(f)\big) + \nabla B\cdot\hat{\mathbf{n}}\delta(f) - \rho\nabla\cdot\big((\boldsymbol{\zeta}\times\mathbf{u})H(f)\big). \tag{22}$$

This version shows that when there is no vorticity in the fluid, the solution can be expressed in terms of B on the surface alone, but it does not give much physical insight into the solution. This equation can be manipulated to give similar forms which are in terms of the fluid vorticity and B on the surface.

Solution for Circular Cylinder with a Vortex

Now we will consider a circular cylinder moving past a vortex to demonstrate the utility of arranging the source terms as a combination of surface terms, kinetic energy term, and vorticity term in equation (19). This example is chosen to demonstrate the role of the volume source terms when a region of vorticity exists in the aerodynamic field. For this problem, the complex velocity potential can be found using the Milne-Thomson circle theorem *[29]* to be the sum of the velocity potential of the cylinder alone, the free vortex alone, and an image vortex system. If z_1 is the position of the free vortex expressed

as a complex variable, $z_1 = x_1 + iy_1$, the image vortex system consists of a vortex of equal strength to the free vortex at the cylinder center, and a vortex of equal strength and opposite sense at the image point $z_2 = a^2/\overline{z}_1$. Here the overbar indicates the complex conjugate of the complex number. The complex velocity potential for the problem is written

$$w(z) = \frac{-Va^2}{z} + \frac{i(K+\Gamma)\ln(z)}{2\pi} + \frac{i\Gamma\ln(z-z_1)}{2\pi} - \frac{i\Gamma\ln(z-z_2)}{2\pi} \tag{23}$$

after dropping a constant. In this expression the cylinder has a velocity of magnitude v directed at an angle α to the x axis, expressed as the complex velocity $V = v(\cos\alpha + i\sin\alpha)$. The pressure perturbation p' is, from Bernoulli's equation, equal to $-\rho\partial\phi/\partial t - \rho u^2/2$, i.e.

$$p' = -\frac{1}{2}\rho\left|\frac{\partial w}{\partial z}\right|^2 - \rho\mathrm{Re}\left(\frac{\partial w}{\partial t}\right) \tag{24}$$

where

$$\frac{\partial w}{\partial z} = \frac{Va^2}{z^2} + \frac{i(K+\Gamma)}{2\pi z} + \frac{i\Gamma}{2\pi(z-z_1)} - \frac{i\Gamma}{2\pi(z-z_2)} \tag{25}$$

and

$$\frac{\partial w}{\partial t} = -V\frac{\partial w}{\partial z} - \frac{i\Gamma}{2\pi}\left(\frac{V_1}{(z-z_1)} - \frac{V_2}{(z-z_2)}\right). \tag{26}$$

Here $\partial w/\partial z$ is the complex conjugate of the fluid velocity written in complex form, i.e. $\partial w/\partial z = u_1 - iu_2$, and V_1, V_2 are the complex velocities of the free and image vortices. Although it is convenient for our purpose to write the velocities of the vortices as separate quantities, they are not independent. The velocity of the free vortex is that which a fluid particle at the position of the vortex center would have due to the combined velocity field of the cylinder and image vortex system, while the velocity of the image vortices is related to both the position and velocity of the free vortex relative to the cylinder.

This particular problem highlights a situation where the vorticity term in the volume source must not be neglected. Since the vorticity is concentrated at the point $\mathbf{x}_1$, the vorticity vector $\boldsymbol{\zeta}$ can be written $-\Gamma\delta(\mathbf{x}-\mathbf{x}_1)\hat{\mathbf{k}}$ where Γ is the strength of the vortex and $\hat{\mathbf{k}} = \hat{\mathbf{n}} \times \hat{\mathbf{t}}$ is a unit vector in the z direction. The pressure contribution of the free vortex may then be written

$$p'_v = \frac{1}{2\pi}\nabla \cdot \int_{f>0} \rho\Gamma\hat{\mathbf{k}} \times \mathbf{u}\delta(\mathbf{y}-\mathbf{x}_1)\ln|\mathbf{x}-\mathbf{y}|d\mathbf{y} = \rho\Gamma\hat{\mathbf{k}} \times \mathbf{u}\Big|_{\mathbf{x}_1} \cdot \frac{(\mathbf{x}-\mathbf{x}_1)}{2\pi|\mathbf{x}-\mathbf{x}_1|^2} \tag{27}$$

which may be rewritten in terms of complex variables as

$$p'_v = \rho\mathrm{Re}\Big\{\frac{i\Gamma V_1}{2\pi(z-z_1)}\Big\}. \tag{28}$$

This can be recognized immediately as part of $\partial\phi/\partial t$ in equations (24) and (26). For this problem, the linear pressure perturbation, $-\rho\partial\phi/\partial t$, is the sum of the surface terms and the free vortex alone. The surface source contribution differs from the cylinder alone solution by exactly the contribution of the image system of the free vortex. Powell *[30]* and Ffowcs Williams *[31]* have shown this is true for turbulent boundary layers on a plane boundary as well. Notice that the contribution from the vortex alone in the flow field is part of $\partial\phi/\partial t$ rather than $\rho u^2/2$. Thus the role of the volume source is primarily the inclusion of the free vortex pressure perturbation and secondarily to provide a nonlinear coupling of the various source components through the kinetic energy of the fluid. This suggests approximating the solution by the linear pressure perturbation, which neglects the nonlinear $\rho u^2/2$ part of p'. Figure 3 shows this approximation compared to the exact solution. The figure shows that this approximation varies little from the complete solution except in the vicinity of the free vortex and near the cylinder surface.

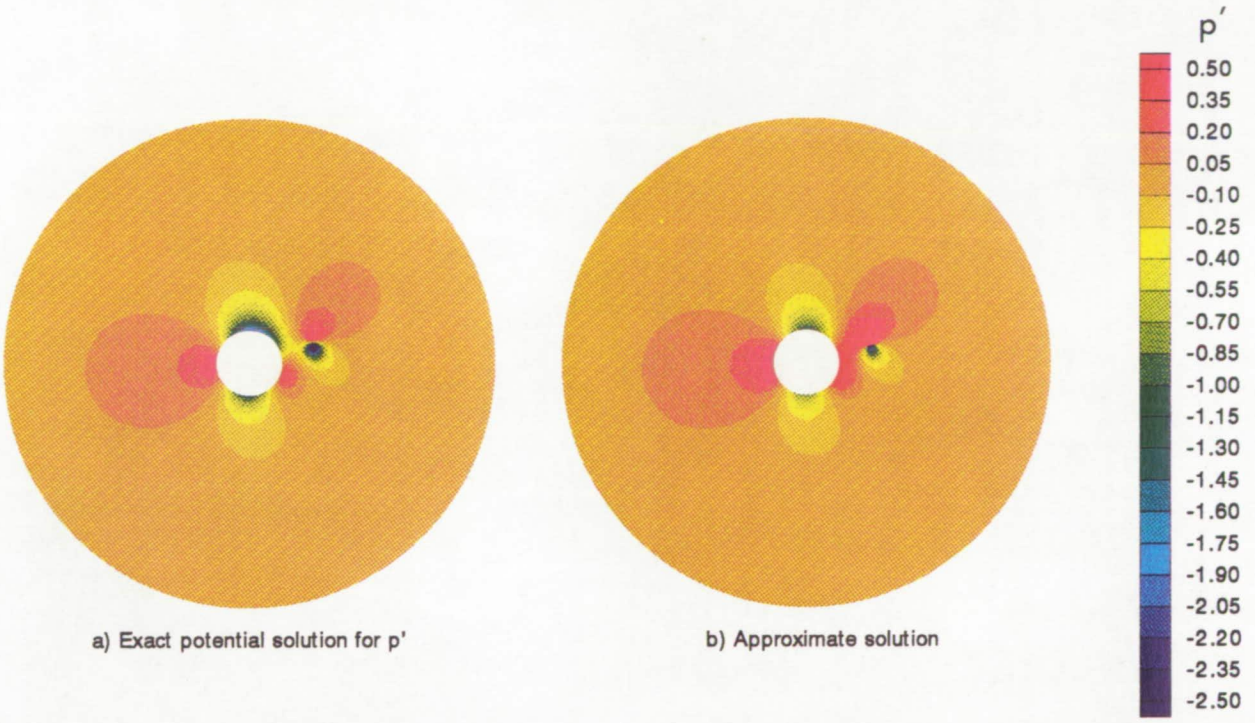

Figure 3. Comparison of p' and $-\rho\partial\phi/\partial t$ for a circular cylinder moving in proximity to a free vortex. ($V = 1.0$, $K = 2.0$, $\Gamma = -2.0$, Vortex position $(r_1, \theta_1) = (2.,\ 15\ \text{deg.})$)

Solution for the Joukowski Airfoil

Now as a further example consider the case of a Joukowski airfoil in an incompressible flow. The exact solution is readily obtained using the Joukowski transformation, $\zeta = z + 1/z$, to transform the complex velocity potential $w(z)$ for the circular cylinder. The pressure perturbation p' can be written

$$p' = -\frac{1}{2}\rho\left|\frac{dw}{d\zeta}\right|^2 - \rho\mathrm{Re}(V\frac{dw}{d\zeta}) \tag{29}$$

where the airfoil has a steady complex velocity V and $dw/d\zeta$ is the conjugate of the complex fluid velocity. The value for $dw/d\zeta$ is obtained by transforming the solution for the circular cylinder with a free stream moving past into the ζ plane and then subtracting

the freestream velocity. The freestream is removed since the velocity potential must be given in a frame of reference where the body is moving in a still fluid. Once this is done we find

$$\frac{dw}{d\zeta} = (\overline{V} - \frac{Va^2}{(z-z_o)^2} + \frac{iK}{2\pi(z-z_o)}) \Big/ \frac{\partial \zeta}{\partial z} - \overline{V} \tag{30}$$

where $\overline{V}$ is the conjugate of V and z_o is the center of the circular cylinder. Clearly an analytical term by term integration of the original FW–H equation using the potential solution is difficult for even this simple airfoil geometry. There is no vorticity in the flow field, therefore we can use the new quadrupole description to identify the volume and surface contribution to p' immediately from Bernoulli's equation. Unfortunately such a separation is not possible with the original form of the FW–H equation.

In Figure 4 the surface source contribution is compared with the velocity potential solution for a cambered airfoil at angle of attack. In this figure, it is evident that the volume source, $-\rho u^2/2$, has a negligible effect away from the airfoil. In figure 5, the pressure coefficient on the surface of the airfoil is compared with the surface and volume components, $-\rho \partial\phi/\partial t$ and $-\rho u^2/2$. The volume source contribution is most important near the forward stagnation point, and we can see by comparing the difference in pressure on the upper and lower surface of the airfoil for each component that the volume source term plays a significant role in the lift generation.

Aerodynamic Implications of the Quadrupole

From what we have already seen from the three previous examples, it is clear that the volume source term may be safely considered to have negligible influence on the pressure perturbation far away from the body. Recall however that the FW–H quadrupole accounts for half of the lift on a circular cylinder with circulation and the volume source term in the

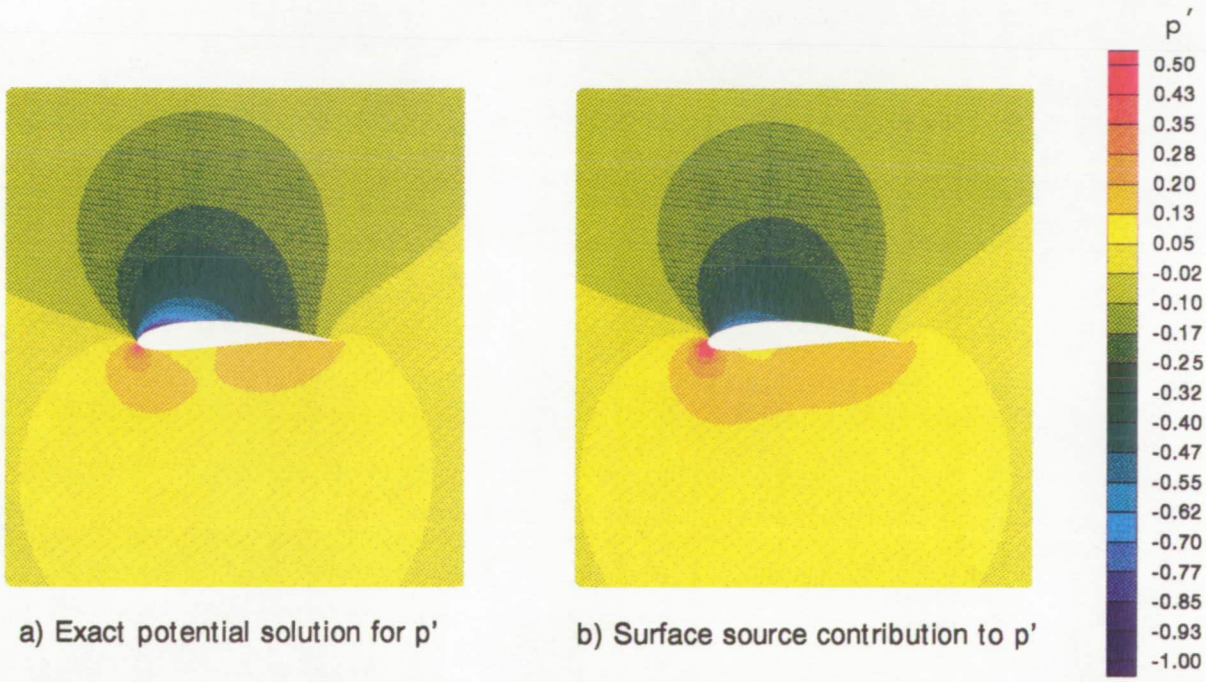

Figure 4. The pressure perturbation components for a flow ($v = 1.0$) about a Joukowski airfoil ($a = 1.13$, $z_o = -.11 + .10i$) at $\alpha = 5$deg.

Joukowski airfoil problem produced a smaller, yet significant part of the total lift. These apparently contradictory observations indicate that the quadrupole is important in any aerodynamic theory based on the the aeroacoustic approach. Without going far from our central purpose it is possible to shed some light on the role of the quadrupole source in aerodynamics.

As we begin to consider aerodynamics, it is important to realize that the primary purpose of aerodynamics is to determine the loading on the body, rather than to determine the perturbations far away from the body. For incompressible flow especially, it is obvious that it would be more straightforward to solve the Laplace equation for either the velocity potential or the acceleration potential using Green's theorem to obtain the aerodynamic solution. The attraction of an aeroacoustic based aerodynamics theory is that it would be

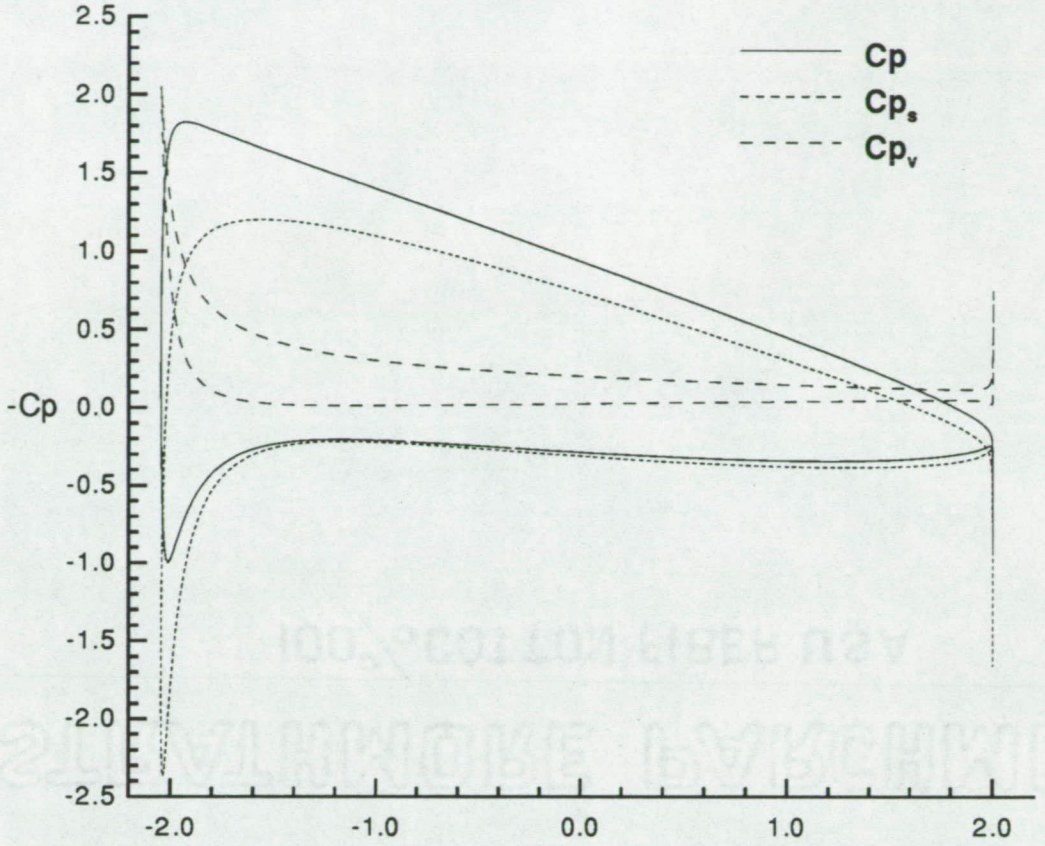

Figure 5. A comparison of pressure coefficient contribution from the surface source, Cp_s, and the volume source, Cp_v with the total pressure coefficient, $Cp = 2p'/(\rho U_\infty^2)$, for a Joukowski airfoil ($a = 1.13$, $z_o = -.11 + .10i$) at $\alpha = 5$deg.

unified with the acoustics, and hence one theory and one computer code could be used to solve the entire aero/acoustic problem. It is also possible that in developing such a theory new understanding may be gained by using an acoustic point of view. Further, the theory may be more general in nature, more robust, or its implementation numerically superior in some way.

Long[10] and Farassat and Myers[11] were the first to use the FW–H equation for aerodynamic problems. Long started with a linearized derivation of the FW–H equation in which he eliminated the quadrupole from the start, as is common practice in the prediction of the acoustic field of rotating blades. He was able to develop a singular integral equation which was useful for the thickness problem, but Long was forced to resort to an ad hoc numerical conditioning to achieve a lifting solution. Curious about this result, Farassat and Myers[11] have shown that the angle of attack problem becomes an eigenvalue problem in Long's case and cannot be solved, even though the unsteady aerodynamics problem is well posed. This finding seems to be supported by our earlier incompressible result where we have found that quadrupole did not contribute to the force on the cylinder due to unsteady motion. Brandão[12,13] has also developed an aerodynamics theory based on the FW–H equation but has reduced most of his work to the case of an incompressible fluid for simplicity. Since there has been some confusion about the results of aerodynamic theory based on the FW–H equation, we provide some insight into these problems in this section.

The steady incompressible form of Brandão's[12] aerodynamic integral equation may be written

$$p'(\mathbf{x},t) - \frac{1}{4\pi}\int_{f=0} \frac{p'\hat{\mathbf{n}}\cdot\hat{\mathbf{r}}}{r^2}dS = \frac{1}{4\pi}\int_{f=0} \frac{\rho v_n \mathbf{v}\cdot\hat{\mathbf{r}}}{r^2}dS \tag{31}$$

where $\hat{\mathbf{r}} = (\mathbf{x}-\mathbf{y})/|\mathbf{x}-\mathbf{y}|$, $r = |\mathbf{x}-\mathbf{y}|$, and dS is an element of the three dimensional surface $f = 0$. This is a singular Fredholm integral equation of the second kind for the unknown variable p'. Equation (31) is also the incompressible limit of Long's equation. We can develop a similar integral equation based on equation (20) by using the three dimensional Green's function for the Laplace equation for unbounded space. Having done

this, the steady form becomes

$$B(\mathbf{x},t) - \frac{1}{4\pi}\int\limits_{f=0} \frac{B\hat{\mathbf{n}}\cdot\hat{\mathbf{r}}}{r^2}dS = -\frac{1}{4\pi}\int\limits_{f=0} \frac{\rho v_n(\mathbf{u}-\mathbf{v})\cdot\hat{\mathbf{r}}}{r^2}dS - \frac{1}{4\pi}\int\limits_{f>0} \frac{\rho(\boldsymbol{\zeta}\times\mathbf{u})\cdot\hat{\mathbf{r}}}{r^2}dV. \quad (32)$$

This equation is valid for steady motion in an incompressible fluid and is closely related to the acceleration potential method. It differs from the normal acceleration potential theory in that it also accounts for the wake of a lifting body through the volume integral on the right hand side. In Appendix A3 it is demonstrated that classical thin airfoil theory can be obtained from the two dimensional form of equation (32) for both thickness and lifting cases. With this knowledge, we can compare (32) with Brandão's equation to determine where the quadrupole is important.

Examining (31) and (32), we can see that if we use the linearized pressure, i.e. if we let $B \rightarrow p'$, the two equations are similar except for the absence in Brandão's equation of the $\mathbf{u}\cdot\hat{\mathbf{r}}$ term in the first integral on the right hand side and the lack of any volume integral. As we noticed earlier, this combination of $\mathbf{u}-\mathbf{v}$ can be thought of as a vortex sheet around the body which, in the three dimensional case, trails off the body forming a wake. The strength of this sheet is responsible for the lift generation, a feature absent when the quadrupole is neglected.

Brandão*[13]* recognized that the induced velocity acting through the quadrupole must be important for the lifting problem and used this as justification for an alternate interpretation of $\mathbf{v}$ on the surface. Brandão replaced $\mathbf{v}\cdot\hat{\mathbf{r}}$ with $(v_n\hat{\mathbf{n}} + q\hat{\mathbf{t}})\cdot\hat{\mathbf{r}}$, where q was determined iteratively during the numerical solution process. Having done this, Brandão's results improved somewhat for blunt bodies with no lift, but the results were still unsatisfactory for lifting bodies. Equation (32) should have no such difficulty since it is shown, in Appendix A3, to give Munk's Vortex-sheet theory *[32]* result for lifting thin airfoils. For

the two dimensional case, the volume integral is not needed if the wake is idealized by the Kutta condition.

While equation (32) has been useful in the present discussion, in practical application it has the disadvantage that the fluid velocity **u** on the surface is regarded as being given. In general **u** will not be known and cannot be measured on the surface since real fluids obey the no-slip condition on the surface of a body. This can be overcome if equation (22) is used as the starting point since it is written in terms of the variable B alone on the surface. Since this equation is equivalent to the acoustic equation used in Appendix A3, it should also reduce to slender body theory and Munk's vortex sheet theory under the assumptions of thin airfoil theory, even though it is more general than either of these theories. A further drawback, however, is that this form is only valid for an incompressible flow and it is not clear whether a compressible analog can be derived with the desired utility. In addition, an acoustic approach is probably complicated for the transonic case when the acoustic and aerodynamic fields are no longer distinct. In transonic flows, finite strength shocks may generate vorticity and the local speed of sound will vary. Accounting for these important effects will require the use of the full volume source term. Thus it is probably more natural for transonic flows to consider the numerical solution to the Euler or Navier–Stokes equations directly.

Conclusions

The aim of part A has been to gain more understanding of the importance of the quadrupole source in the FW–H equation. By using the incompressible flow solution, the *exact* contribution from each of the source terms in the FW–H equation was seen for both thick and thin bodies. For the special geometry of the circular cylinder, the sum of

the thickness and loading contributions to p' is proportional to $\partial\phi/\partial t$, when the velocity potential ϕ is written in a frame of reference fixed to the undisturbed medium. The quadrupole contribution is $-\rho u^2/2$ in this frame.

In general, the quadrupole source of the FW–H equation can be divided into a group of surface terms and volume terms. The particular form of the surface source terms given in the new description is similar to that of the thickness and loading source terms in the original FW–H equation. The new volume source terms are related to the vorticity and kinetic energy of the fluid. This rearrangement of the FW–H quadrupole clearly shows that the quadrupole source has a contribution to even the linear pressure perturbation through the surface source terms and the vorticity term. In the special case of the circular cylinder, only the nonlinear, kinetic energy term of the quadrupole is nonzero, however.

From the incompressible problems considered we can conclude that the quadrupole source term in the FW–H equation has two primary functions. As the only volume source term, the quadrupole is obviously necessary to account for any vorticity in the fluid. This was evident for the vortex-cylinder interaction considered. The quadrupole also provides a nonlinear coupling through the kinetic energy term. This is a localized effect, which nonetheless is important when the FW–H equation is applied to the aerodynamics problem since it accounts for a signficant portion of the steady lift.

It is significant that both slender body theory and vortex sheet theory can be derived from the new incompressible form of the FW–H equation because this shows that the full incompressible form of the FW–H equation may be considered as the fundamental governing equation. Further development would be required to solve the singular integral equation in Appendix 3, even though Long, Farassat and Myers, and Brandão have already laid the groundwork. Developing an analogous compressible source description would be

much more complicated. A consideration of the compressible flow field is necessary to gain further understanding, so in Part B a numerical study of the compressible flow about a circular cylinder is carried out.

Part B: Numerical Calculation of Sound Generated in a Compressible Fluid.

Introduction

While the exact analysis of an incompressible flow field is useful, many of the important fluid dynamics phenomena can only be studied in a fully compressible flow. Transonic flows in particular are difficult to calculate analytically with any generality, yet with the computational techniques and computer power available today we can learn a great deal about complex, nonlinear flow fields by using computational fluid dynamics (CFD). In part B we have numerically solved the Euler equations, together with the continuity and energy equations, for the two dimensional problem of a circular cylinder accelerating from rest and the related problem of a decelerating the cylinder. The Euler equations were chosen because we specifically want to consider the case of an ideal, inviscid fluid so that the artificially viscous nature of the discrete numerical algorithm may be observed independently. The Euler equations are also useful because they allow us to consider transonic flow fields containing shock waves.

A brief discussion of the numerical procedure is followed by an investigation of an accelerating cylinder. The transient process of starting the cylinder impulsively to Mach 0.4 is presented in detail, then other starting scenarios are considered. In this analysis, we find that the energy of the fluid is a useful quantity to track since we are ultimately interested in the acoustic energy flux generated by accelerating the body. As we consider energy, Myers' exact energy corollary *[33]* suggests physically meaningful partitioning of energy. When the energy is separated into kinetic, potential, and entropy terms along with the flux of these terms out of a control volume, we are able to observe the transfer

of energy from one form to another as a function of time. When a cylinder is started impulsively, we find an equipartition between the local kinetic and potential energy and the flux of acoustic and entropy energy out of the near field. This equipartition of energy is evident until the velocity of the cylinder reaches the critical Mach number, at which time the flow field contains shocks in the steady flow field. When this happens, the cylinder must continually input energy into the system to offset the shock induced drag.

The case of a cylinder decelerating to rest is also considered. We find that if the cylinder is stopped impulsively, nearly half of the kinetic energy is rapidly transformed into potential energy as the energy in the local field propagates away as sound. Unfortunately a significant portion of the acoustic energy propagating away from the cylinder is converted to entropy energy, if the rate of deceleration is high. This is probably a numerical limitation which can be identified for the high acceleration cases as well.

Normally entropy energy, i.e. the energy associated with increases in the fluid entropy, is due either to an increase in entropy across shocks or to fluid viscosity. Since we have an inviscid fluid, only entropy generated by shock waves has physical meaning. In the final section of part B, we consider the potential sources of the entropy energy in our calculations. We find that when the final velocity of the cylinder is near the critical Mach number, a shock forms during a rapid start up process and entropy is generated. We also demonstrate that the implicit damping – due to the discrete nature of the algorithm, and the explicit damping – added for numerical stability, are both numerical mechanisms for the transfer of energy into the entropy energy term. We have found that the implicit damping related to the grid resolution is of primary importance and that the entropy energy term gives a quantitative indication of the validity of the numerical solution for the sound.

Numerical Method

The Euler equations were chosen as the appropriate set of governing equations since they represent the physical characteristics of both sound and shock waves. The Euler equations also allow rotational flows to be considered if vorticity is generated by a shock or input into the system as an initial condition. In addition, the artificial viscosity of the discrete numerical solution is suspected of adversely affecting the calculated acoustic solution, therefore it is best to treat the inviscid problem first. With the assumption of an inviscid fluid, we need to remember that the solution for the circular cylinder will not be physically realizable since viscous separation is fundamental in the real problem. The advantage, however, is that any viscous phenomenon observed in the calculations must be related to the discrete nature of the numerical solution.

A finite volume method with multistage time stepping of the Jameson type*[34,35]* was programmed to solve the two dimensional Euler equations. This method is a cell centered scheme which is second order accurate in space and time in this implementation. The central difference methods of this type produce good solutions in smooth regions of the flow, but are prone to oscillations in the neighborhood of shock waves. These oscillations require the explicit addition of dissipative terms. In the present code, Jameson's adaptive blending of second and fourth order dissipation is used. The fourth order term provides a low level of background dissipation while the second order term provides a higher level of dissipation near shocks. The adaptive nature of the dissipation comes through the use of a switch, based on the pressure gradient, which turns on the second order dissipation when the gradient becomes large. The action of this adaptive dissipation on propagating acoustic waves is not well understood.

A five stage, Runge-Kutta like, time stepping scheme is used with the dissipative terms evaluated only in the first two stages to reduce the number of computations. This combination is second order accurate in time. Non-reflecting boundary conditions, based on the extrapolation of the linearized characteristic variables, are used at the outer computational boundaries. Symmetry is assumed between the upper and lower half planes. Therefore computations are carried out only in the upper half plane and symmetry boundary conditions are applied on the x axis. The surface boundary conditions consist of a statement of no flow through the body surface together with a linear extrapolation of the pressure onto the surface.

One slightly unusual feature of the Euler code developed for this work is that the computational grid is moving rather than fixed. Thus, unlike most two dimensional aerodynamic codes, the body is moving through a stationary fluid and the dependent variables are specified in a reference frame fixed to the undisturbed medium. The Euler equations appropriately modified for a moving control volume are written in vectorial form as

$$\frac{\partial \mathbf{U}}{\partial t} + \nabla_{\mathbf{X}} \cdot \vec{\mathbf{F}} = 0 \tag{1}$$

where

$$\mathbf{U} = \begin{Bmatrix} \rho \\ \rho u \\ \rho v \\ \rho E \end{Bmatrix} \qquad \text{and} \qquad \vec{\mathbf{F}} = \mathbf{U}(\vec{q} - \vec{v}) + p \begin{Bmatrix} 0 \\ \hat{i} \\ \hat{j} \\ \vec{q} \end{Bmatrix}$$

which is the conservative form of the Euler equations. Here $\mathbf{U}$ is the vector of dependent variables – density, momentum, and total energy; $\vec{q}$ is the fluid velocity (u, v); $\vec{v}$ is the velocity of the grid – normally the body velocity; and $\hat{i}$, $\hat{j}$ are the unit vectors in the coordinate directions. In these equations, the subscript $\mathbf{X}$ indicates that the spatial independent variables are moving with the control volume. The $\mathbf{U}\vec{v}$ term in the flux matrix $\vec{\mathbf{F}}$

arises from the time derivative of the moving coordinates. Since these additional terms will always be apparent in the flux matrix when the control volume is moving, the subscript X will not be included in subsequent equations. A moving grid was chosen to simplify the treatment for an accelerating body and to cast the problem in a frame of reference familiar to acousticians. The development of the equations for a moving control volume is addressed in more detail in Appendix B.

The calculations presented have been nondimensionalized; length by the cylinder radius, density and sound speed by the their values in the undisturbed fluid. With this particular nondimensionalization the pressure in the undisturbed medium is $1/\gamma$, where γ is the ratio of specific heats, and the speed of the body is equivalent to the Mach number of the body. An advantage of this system is that sound waves travel at a velocity close to unity plus the local convection speed. Thus it is fairly easy to determine where wave fronts should be expected, especially for an impulsive motion of the body.

The finite volume, multistage time stepping method of Jameson was chosen for this work based on several considerations. One attraction is that this method has been used in the CFD community for several years and is efficient and robust. Secondly, the various parts of the method are distinct from each other and therefore may be changed independently. For example, there are many alternate time stepping procedures available if one changes the number of stages and the weighting coefficients of each stage. Indeed the stability and efficiency of the algorithm can be changed considerably while still keeping second order, or higher, time accuracy. Likewise, Jameson*[36,37]* has shown that the algorithm can be transformed into an upwind or total variation diminishing (TVD) formulation by changing the form of the explicitly added dissipation. In addition, the flux balance can be changed from the cell centered, central difference scheme to a nodal scheme and there

is no particular difficulty in using this method on unstructured grids. This flexibility has not been utilized in this work, but it was a driving factor in choosing this method and will benefit future research using this code. A more detailed description of the precise numerical implementation is given in Appendix B.

The Accelerating Cylinder

The process of accelerating a body can be a potent noise source if the rate of acceleration is sufficiently large. It is natural then to consider the transient behavior of the compressible flow field in this situation. Several model problems have been studied analytically for various limiting conditions. Ffowcs Williams and Lovely *[38]* considered the case of a sphere that is suddenly brought into a low Mach number translation in an inviscid, compressible fluid. G. I. Taylor *[39]* also considered a sphere which, after an impulsive start, decelerated due to the drag induced by the transient pressure field. In each case, there is an equipartition of energy between the kinetic energy in the local flow around the body and the radiated acoustic energy. Longhorn*[25]* also found that the work required to start a sphere impulsively was twice the amount needed if the sphere was started slowly. The additional work required to rapidly accelerate the sphere supplies the acoustic energy which radiates as an intense sound. Each of these analyses are based on low Mach number motion, a limiting assumption we wish to remove.

Hill *[40]* carried out a similar analysis determining the linear wave field induced by the sudden starting of an infinite wavy plane. He also found an equitation of energy between the steady evanescent field following the surface and the outwardly traveling sound for the case of subsonic surface phase speed. Hill's problem displayed rather interesting transient behavior for the cases of subsonic, supersonic, and exactly sonic phase speeds. Nevertheless

none of the analytical approaches are able to adequately include the important nonlinear effects found in transonic flow.

Description of the Starting Process.

With these examples in mind, we shall first consider the transient flow field around a circular cylinder which has impulsively started in Mach 0.4 leftward translation. By examining this case in some detail we will be able to interpret the results for other Mach numbers and accelerations. The computational grid used for these calculations is a polar grid which models half of the flow field. The azimuthal direction is divided into 95 cells while the radial dimension of the grid cells increases linearly up to ten cylinder radii from the center of the cylinder, after which the radial increment remains constant. Figure 1 shows the inner part of the computational domain. Notice in figure 1 that the grid resolution is very fine, especially near the cylinder surface.

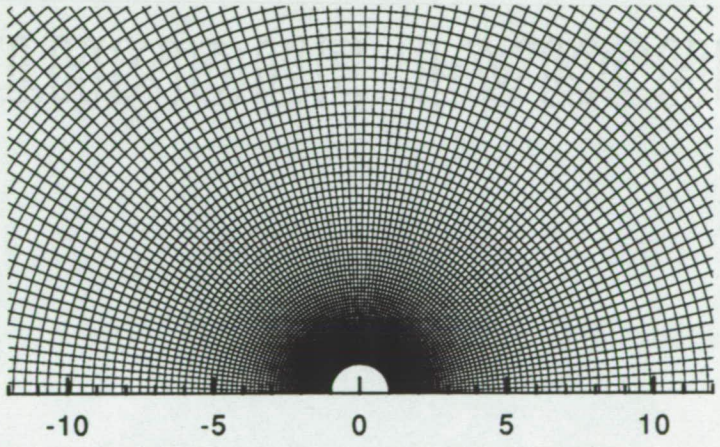

Figure 1. This is the inner part of the computational grid used for the numerical calculations. The grid is divided into constant azimuthal increments of $\Delta\theta = .0331$ radians and linearly increasing Δr from the surface to 10 radii from the cylinder center, after which Δr remains constant. The initial value of $\Delta r = .0397$ near the cylinder surface. The x axis is shown in the figure to provide a spatial scale of reference.

When the cylinder impulsively starts moving leftward, an expansion wave propagates behind the cylinder while a compression moves ahead of it. This is seen in the time history sequence of density perturbation contours plotted in figure 2. In figure 2 the density perturbation ρ' is scaled by $r^{1/2}$, r being the distance from the cylinder center, to offset the effect of cylindrical spreading. The expansion moves away from the cylinder more quickly, due to the motion of the cylinder. The steady flow field around the cylinder is nearly established by t=20.0. A careful look at figure 2 will also reveal that the rightward moving expansion is followed by a weaker recompression and the leftward moving compression by a weak expansion. The calculations show evidence that the signal has a sharp wavefront and the characteristic tail of cylindrical waves. Note that in all the contour plots the maximum value on the legend does not indicate the absolute maximum in the plot, but the regions colored with the maximum color should be understood to be greater than or equal to the maximum on the legend. Likewise the minimum color should be interpreted as less than or equal to the legend minimum, although some effort has been made to ensure that the maximum and minimum values in the contour region are not greatly different from the legend range. The values plotted in the contour plots are at the center of the grid cells, hence in some of the figures a small wedge shaped void is noticeable along the x axis. This is an artifact of the plotting. Contour plots of the pressure perturbation p' are nearly indistinguishable from the density perturbation and hence are not plotted.

The surface pressure coefficient is plotted in figure 3. In the figure, $-C_p$ is plotted against x so that the negative pressure peak is plotted upward, as is commonly done in aerodynamics. Immediately after the impulsive start the pressure on the surface corresponds to $p' = \rho_o c_o v_n$, which is expected for an impulsive motion. The transition from the asymmetric to the symmetric pressure distribution as the flow reaches steady state

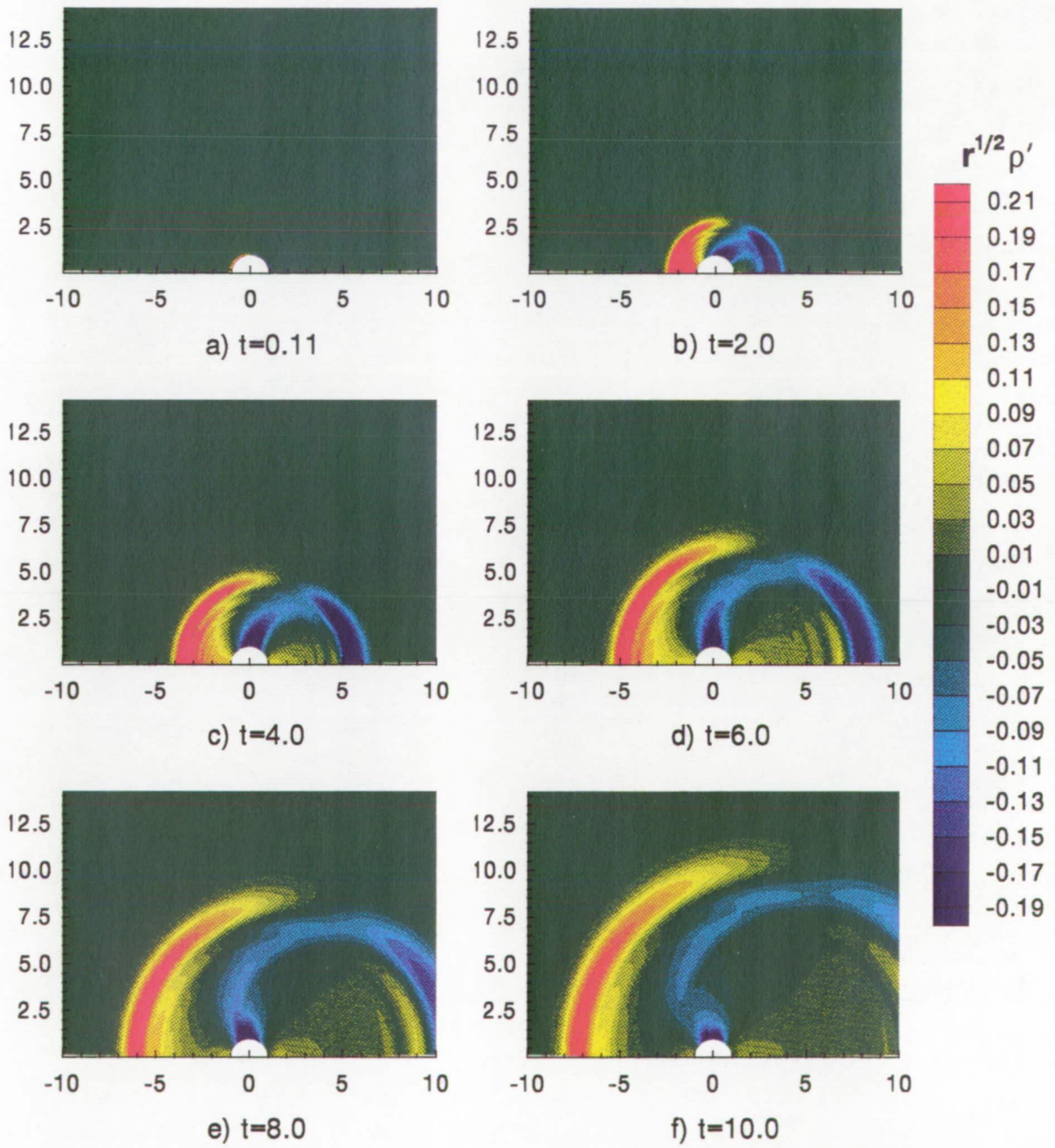

Figure 2. This figures shows a time sequence of density perturbation ρ' contours for the cylinder impulsively started to Mach 0.4. The density perturbation has been scaled by $r^{1/2}$ to account for cylindrical spreading. Here r is the distance from the cylinder center.

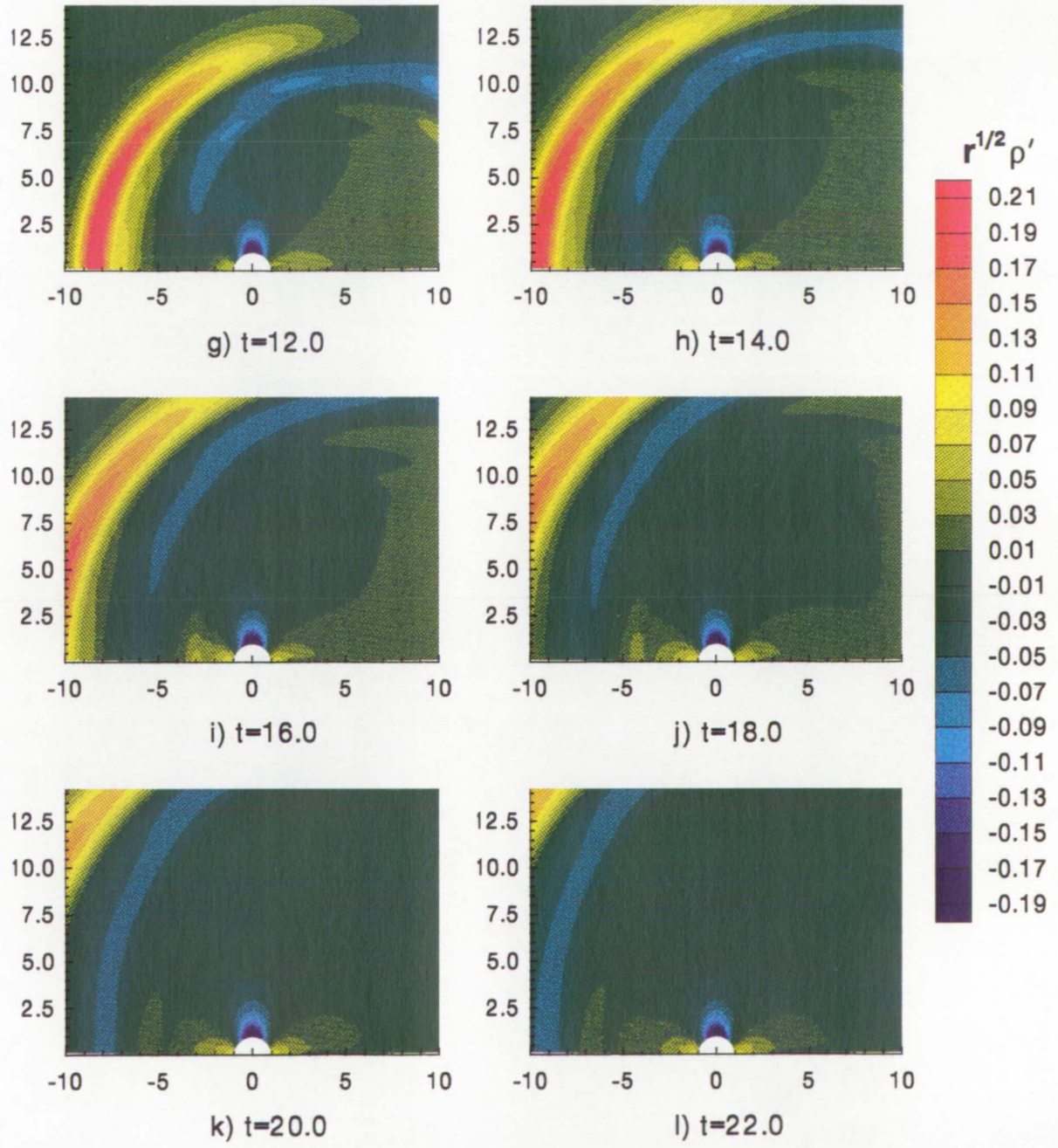

Figure 2.(continued) This figures shows a time sequence of density perturbation ρ' contours for the cylinder impulsively started to Mach 0.4. The density perturbation has been scaled by $r^{1/2}$ to account for cylindrical spreading. Here r is the distance from the cylinder center.

is seen in figures 3a-l. In the density perturbation contours it was not readily apparent that a shock forms at the cylinder surface, although this might be expected since we are impulsively staring the cylinder and M=0.4 is very close to the critical Mach number for the cylinder. From $t = 2.0$ to $t = 10.0$, in figures 3b-f, the shock formation and subsequent forward motion is easily seen. As the shock reaches the top of the cylinder it weakens as it continues to move forward until it finally disappears. The surface pressure distribution then tends toward the steady potential flow solution. Since the steady state solution is unique, it does not depend upon the time history, but the transient flow field and the work required to maintain the cylinder velocity during the transient phase vary greatly with the manner in which the steady state flow is achieved. This will be discussed in more detail later.

Another interesting point to consider is that when a shock wave is present in the flow field, in general it will not be isentropic and hence by Crocco's theorem (see for example Liepmann and Roshko *[41]*) vorticity may be generated. The existence of either vorticity or entropy in the field is of interest since the generation of these cannot be accounted for in an inviscid fluid without nonlinearities. Plotting the vorticity contours in figure 4 confirms the supposition that vorticity is generated. In the figures we see that from the time the shock forms at $t = 4.0$ until the shock disappears at nearly $t = 8.0$, a vortex forms and grows in strength. After the shock disappears, the vortex follows the cylinder surface and subsequently convects with the fluid away from the cylinder. As the cylinder travels away from the vortex, the vortex diffuses as a result of its interaction with a symmetrical vortex of opposite sense on the other side of the symmetry plane. The vorticity magnitude plotted in figure 4 was calculated numerically from the dependent variables using the program PLOT3D *[42]*.

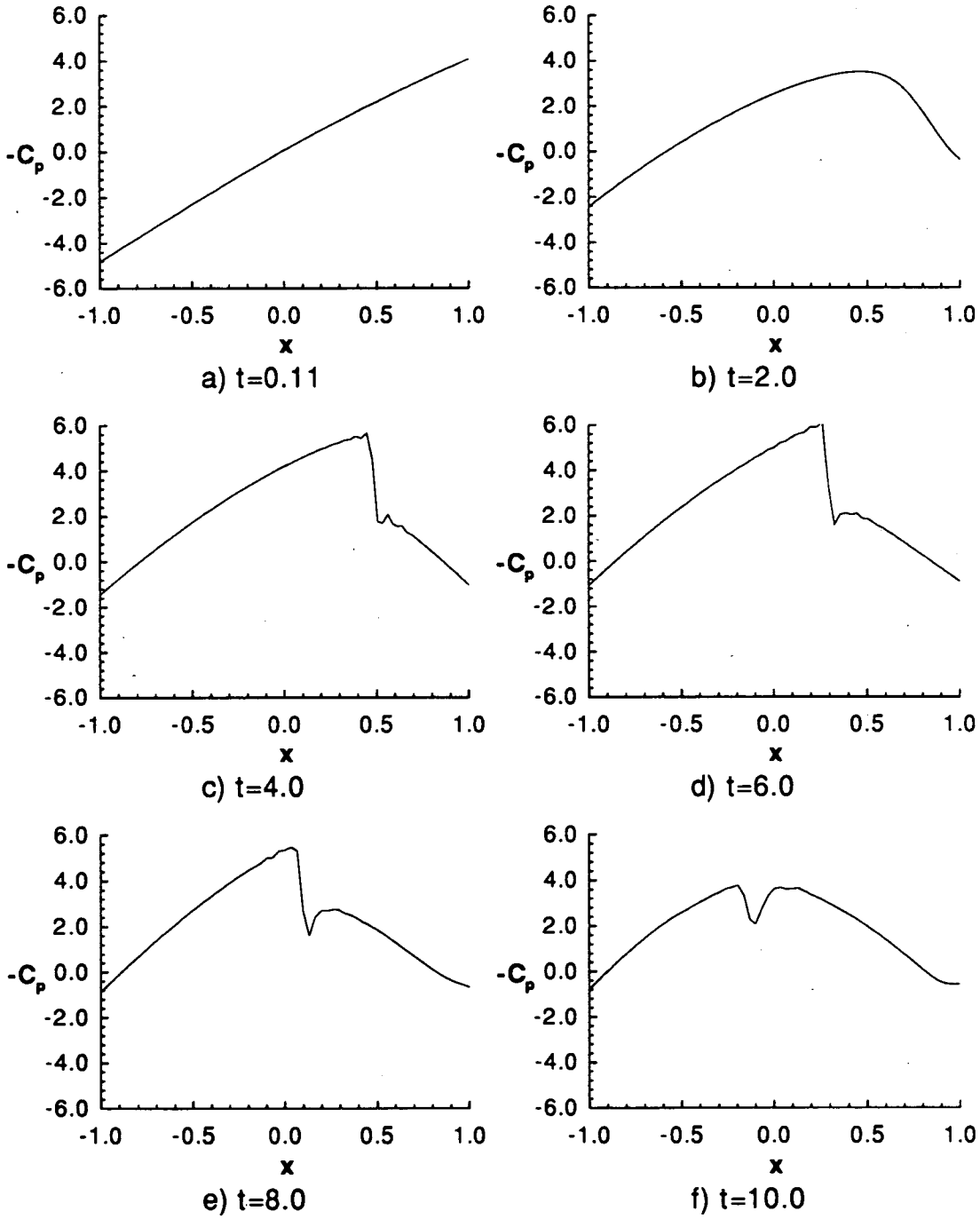

Figure 3. This figure is a time sequence of the pressure coefficient on the cylinder surface for a cylinder impulsively started to Mach 0.4. The pressure coefficient is defined as $C_p = 2(p - p_o)/(\rho_o v^2)$.

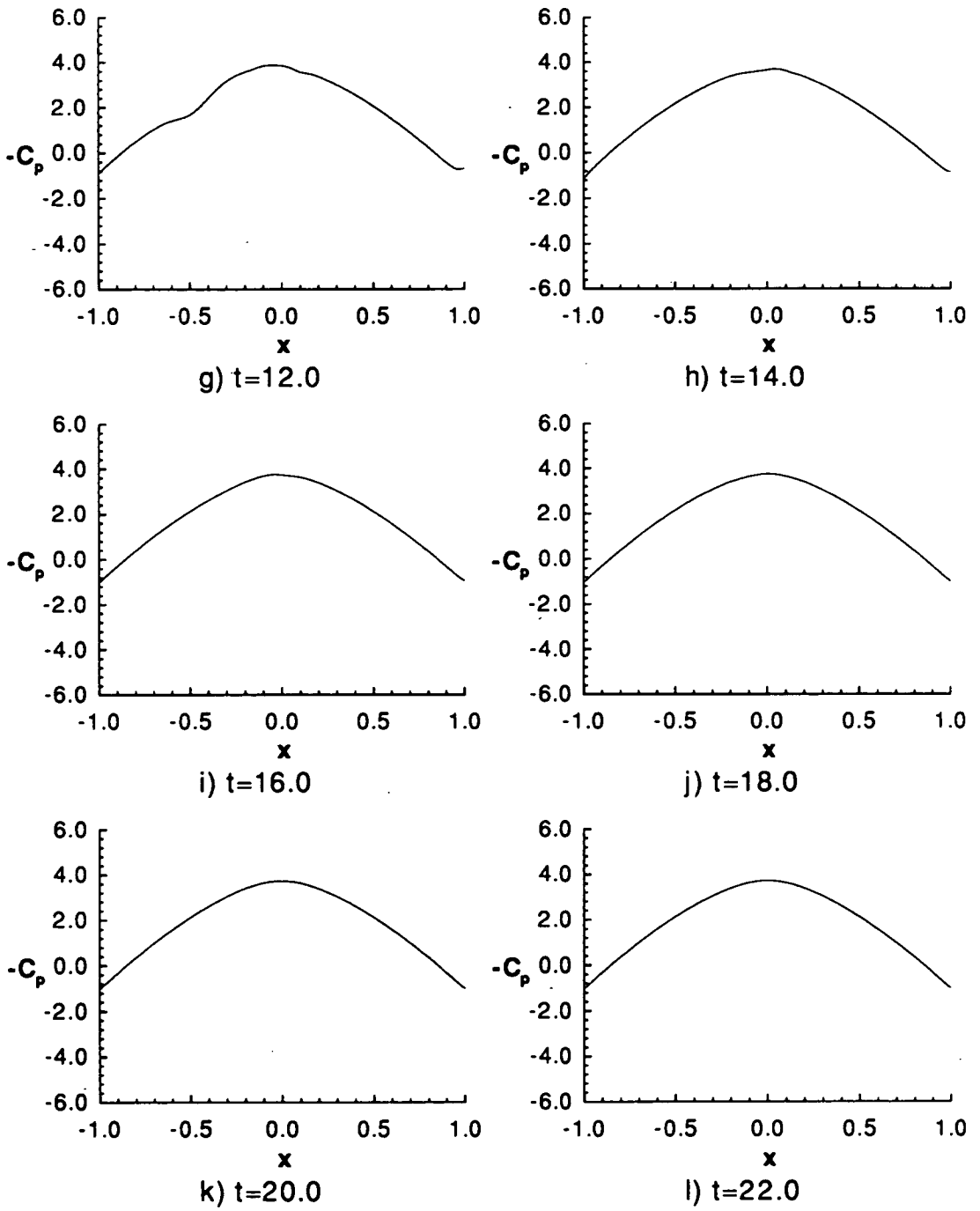

Figure 3.(Continued) This figure is a time sequence of the pressure coefficient on the cylinder surface for a cylinder impulsively started to Mach 0.4. The pressure coefficient is defined as $C_p = 2(p - p_o)/(\rho_o v^2)$.

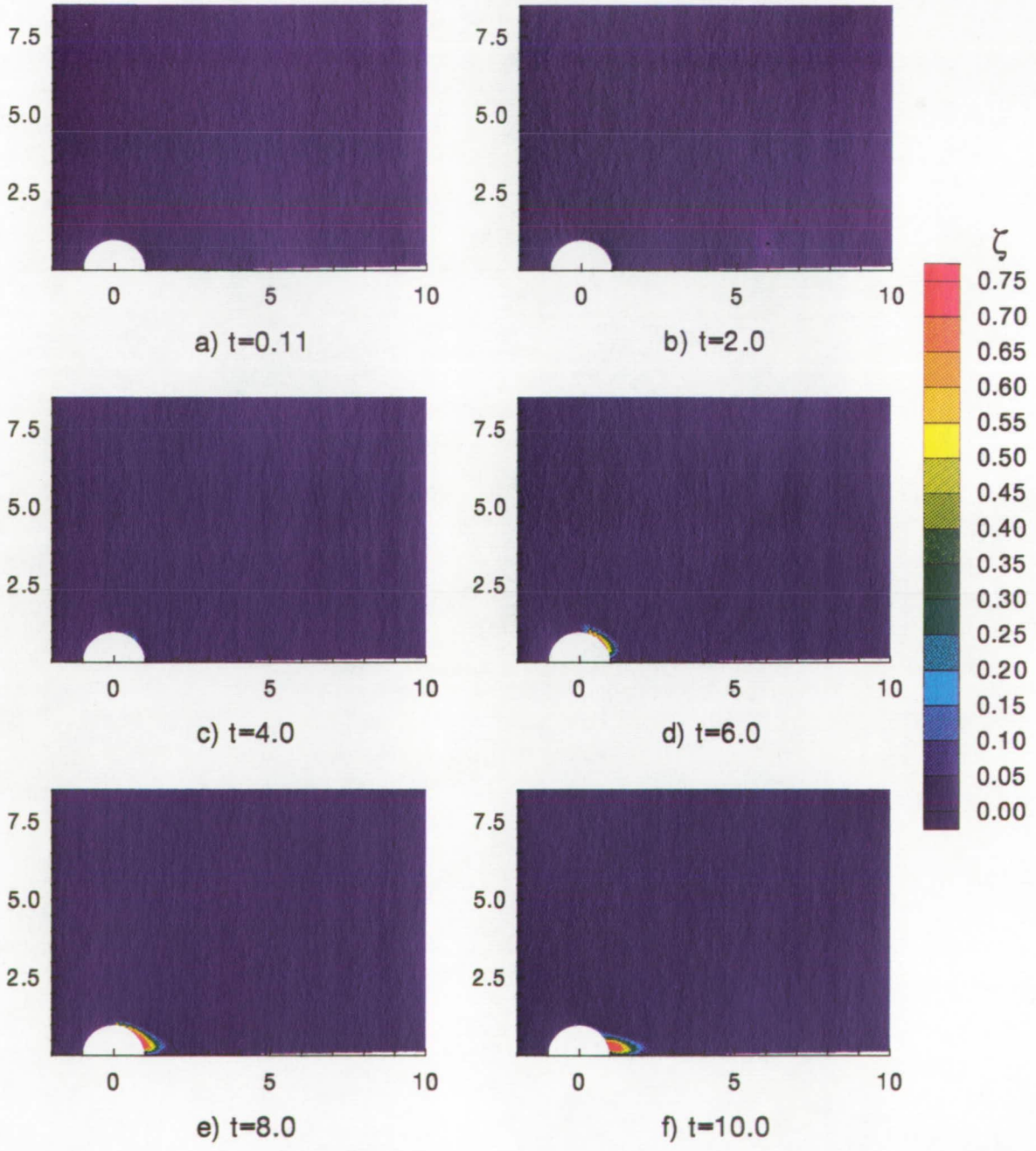

Figure 4. This figure shows the vorticity magnitude contours, for a cylinder impulsively started to Mach 0.4, at various times.

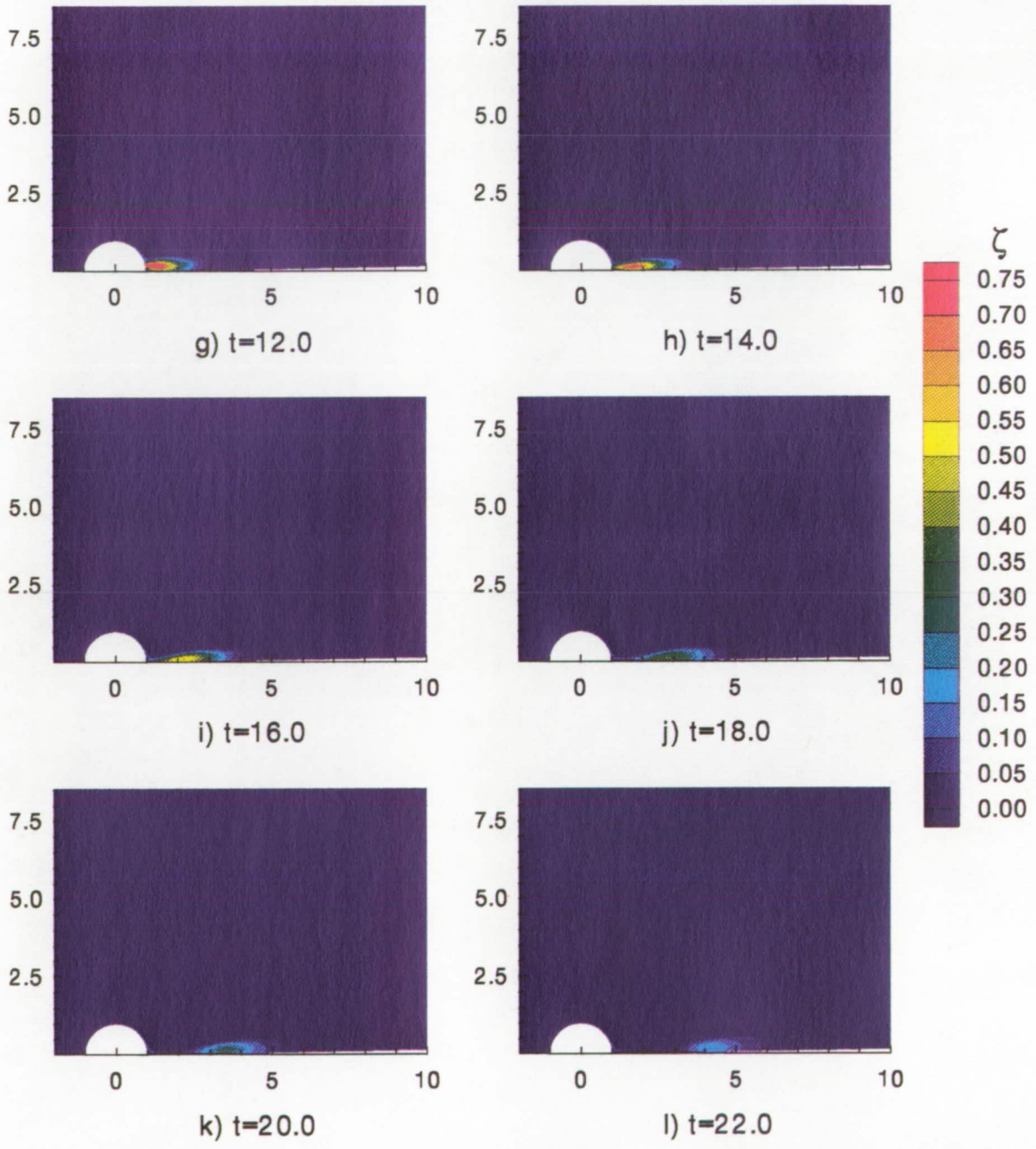

Figure 4.(Continued) This figure shows the vorticity magnitude contours, for a cylinder impulsively started to Mach 0.4, at various times.

Energy Partition.

Now that we qualitatively understand the physics of the startup process, it is useful to discuss the problem more quantitatively in order to compare various cases. Longhorn*[25]* has done this by examining the work required to accelerate a sphere to low Mach number translation using a variety of acceleration rates. If we look at the work required to accelerate the cylinder, we can develop an energy balance which describes the distribution of the various components of energy as a function of time. Energy flux out of some control volume will give us a measure of acoustic energy flux and energy flux due to convection processes. For the impulsively started cylinder, we will be able to distinguish between these types of energy by their propagation speeds, since clearly the acoustic energy will propagate at the fluid velocity and sound speed combined rather than the convection velocity, i.e. the velocity of fluid particles relative to the cylinder.

Myers has recently developed an exact energy corollary*[33]* which is well suited for our consideration of energy transport in flow fields which may include shock waves and vorticity. Myers' result is a generalization of the concept of acoustic energy, which he recognized from a perturbation expansion of the general energy equation of fluid mechanics. Since this corollary is exact, it is uniquely appropriate for the nonlinear problems we are considering. For our case of perturbation about an undisturbed inviscid fluid, we can write Myers' corollary as

$$\frac{\partial \varepsilon}{\partial t} + \nabla \cdot \vec{\mathcal{F}} = 0. \tag{2}$$

where

$$\varepsilon = \rho\left(h - h_o + \frac{u^2}{2} - T_o(s - s_o)\right) - (p - p_o) \tag{3}$$

and

$$\vec{\mathcal{F}} = \rho\left(h - h_o + \frac{u^2}{2} - T_o(s - s_o)\right)\vec{q}. \tag{4}$$

In these equations, h is the specific enthalpy, $e + p/\rho$, and s is the specific entropy. Recall that the subscript o refers to the value to of the quantity in the undisturbed medium and that the internal energy e and the enthalpy h are $c_v T$ and $c_p T$, respectively. This is a substantially simplified version of Myers' result since we have no mean flow, viscosity, or heat conduction effects.

We can better understand this corollary if we consider each of the terms separately. Our starting point will be the conservative form of the total energy equation, which is given as

$$\frac{\partial \rho E}{\partial t} + \nabla \cdot \left((\rho E + p)\vec{q}\right) = 0 \tag{5}$$

when ρE is the total energy per unit volume, $\rho(e + u^2/2)$. This is the last equation in (1) if we use fixed coordinates. We need to recognize that the statement of the conservation of energy (5) is not unique since we can add any multiple of the continuity equation to it. This fact can be used to our advantage if we subtract h_o times the continuity equation to account for energy changes in the open system which are due only to mass flux across the control volume boundary. Doing this, the energy equation may be written

$$\frac{\partial}{\partial t}\left(\rho(e + \frac{u^2}{2} - h_o)\right) + \nabla \cdot \left(\rho(h - h_o)\vec{q}\right) = 0. \tag{6}$$

If we recall that an alternative form of the energy equation is

$$\frac{\partial}{\partial t}(\rho s) + \nabla \cdot (\rho s \vec{q}) = 0 \tag{7}$$

when written in terms of the specific entropy s, we can likewise account for energy changes due to changes in entropy by writing the energy equation as

$$\frac{\partial}{\partial t}\left(\rho\left[e + \frac{u^2}{2} - h_o - T_o(s - s_o)\right]\right) + \nabla \cdot \left(\rho\left[h + \frac{u^2}{2} - h_o - T_o(s - s_o)\right]\vec{q}\right) = 0. \tag{8}$$

This is exactly Myers' energy corollary if we add $\partial p_o/\partial t$, which is identically zero. This energy equation will be the basis for defining the energy densities

$$\varepsilon_k = \frac{\rho u^2}{2} \tag{9}$$

$$\varepsilon_p = \rho(\Delta h - T_o \Delta s) - \Delta p \tag{10}$$

$$\varepsilon_s = \rho T_o \Delta s \tag{11}$$

which are the kinetic, potential, and entropy energy densities, respectively. The kinetic energy has its normal physical meaning and is the only component of energy in the incompressible limit. The potential energy is related to the compression of the fluid, and the entropy energy is energy corresponding to the increase of entropy in the fluid. We can use these definitions to rewrite the energy balance as

$$\frac{\partial}{\partial t}(\varepsilon_k + \varepsilon_p + \varepsilon_s) + \nabla \cdot \left((\varepsilon_k + \varepsilon_p + \varepsilon_s)(\vec{q} - \vec{v}) + p\vec{q}\right) = 0 \tag{12}$$

for a moving control volume. If we integrate over a volume V and use the divergence theorem, we find that

$$\frac{\partial}{\partial t}(E_k + E_p + E_s) + \dot{F}_a + \dot{F}_s = \dot{W} \tag{13}$$

when we define

$$E_k = \int_V \varepsilon_k \, dV \tag{14a}$$

$$E_p = \int_V \varepsilon_p \, dV \tag{14b}$$

$$E_s = \int_V \varepsilon_s \, dV \tag{14c}$$

$$F_a = \int_{t_o}^{t} \int_{g=0} \left[(\varepsilon_k + \varepsilon_p)(q_n - v_n) + p q_n \right] \, dS d\tau \tag{14d}$$

$$F_s = \int_{t_o}^{t} \int_{g=0} \varepsilon_s (q_n - v_n) \, dS d\tau \tag{14e}$$

$$W = \int_{t_o}^{t} \int_{f=0} p v_n \, dS d\tau. \tag{14e}$$

Here E_k, E_p, and E_s refer to the total amount of kinetic, potential, and entropy energy in the volume at a particular time. F_a and F_s are the total flux of acoustic energy and entropy energy out of the volume since time $t = t_o$, and W is the total work done by the body on the fluid since $t = t_o$. The dot over F_a, F_s and W in equation (13) represents time differentiation. The integration on $f = 0$ is over the body surface and on $g = 0$ is over the outer surface of the control volume V, see figure 5. Notice that we have used the outward normal to the body rather than to the volume in the definition of W along with $q_n = v_n$ on $f = 0$. The value of F_a is only truly acoustic energy flux if the control volume boundary is sufficiently far from the body to be relatively unaffected by the local aerodynamic field. We have not separated the acoustic flux into its kinetic and potential energy components because of the additional work term in the defining integral. This is normally not any problem since we are only interested in the total acoustic energy flux.

Time History of the Energy Transport.

We have defined these energy quantities in order to gain an understanding of the transport of energy from the body surface to the near and far fields. In figures 6, 7, and 8, we can observe the transport of kinetic, potential, and entropy energy for the impulsively started Mach 0.4 translation by examining the time sequence of the appropriate energy

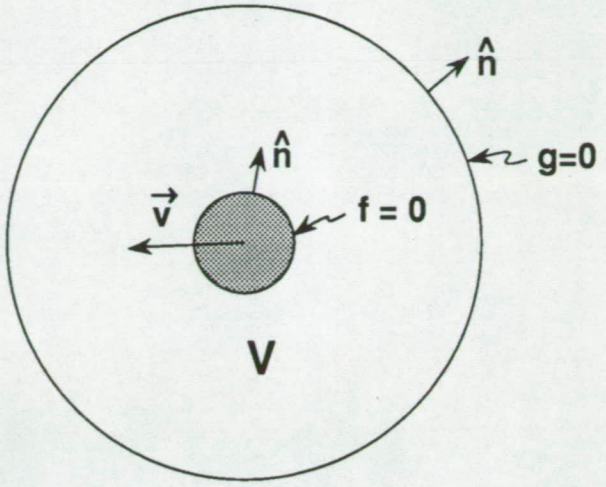

Figure 5. The geometry of the cylinder and control volume used in the calculation of the total energy in the control volume. Notice that the normal vector on $f = 0$ is an outward normal to the body and not to the volume V.

density contours. Note that in each of these figures the energy is scaled by r to account for the cylindrical spreading.

In figure 6 we clearly see that the kinetic energy is concentrated both near the cylinder surface and in the acoustic wavefronts. The shock is evident in the local kinetic energy contours as a discontinuity in the contours near the cylinder, from $t = 4.0$ to $t = 8.0$, in figures 6c-e. The shock becomes even more apparent when we compare figures 6c-e with the smooth distribution at $t = 22.0$ in figure 6l. Notice that the local kinetic energy in the aerodynamic field distributes itself uniformly around the cylinder. This is not true for the potential energy in figure 7. Again the shock wave is evident, but now we see that the potential energy, which is due to compressibility, is primarily found in the wave fronts and near the top of the cylinder in the region of maximum fluid velocity.

We can also see from figures 6 and 7 that more kinetic and potential energy is radiated in front of the cylinder than behind. This effect is at least partially numerical, due to the increased wave speed of the rightward moving expansion wave. We see evidence in figure

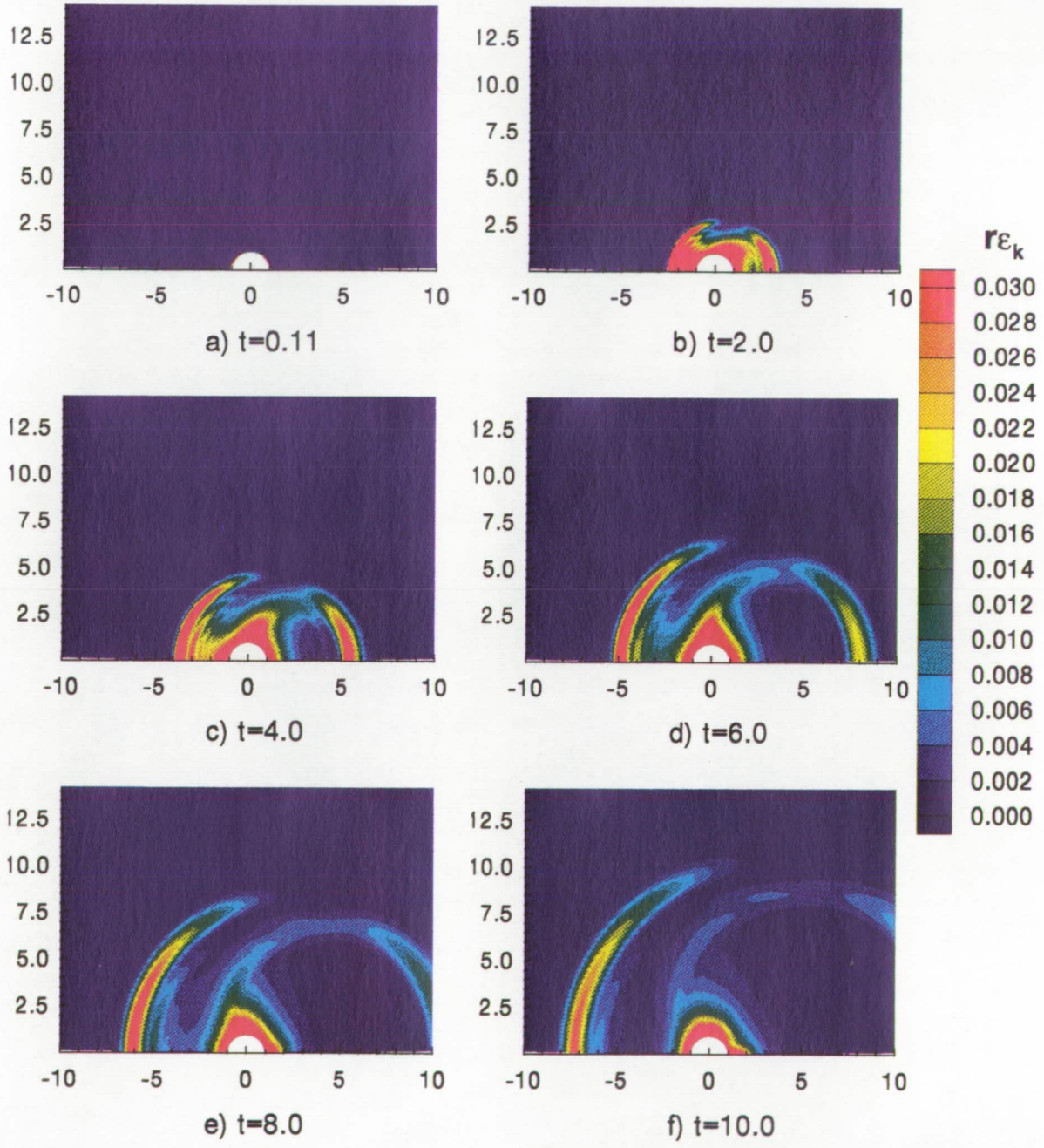

Figure 6. The time history of the kinetic energy field ε_k is shown in these figures for a cylinder which has been impulsively started to Mach 0.4 translation. Notice that the energy has been scaled here by r.

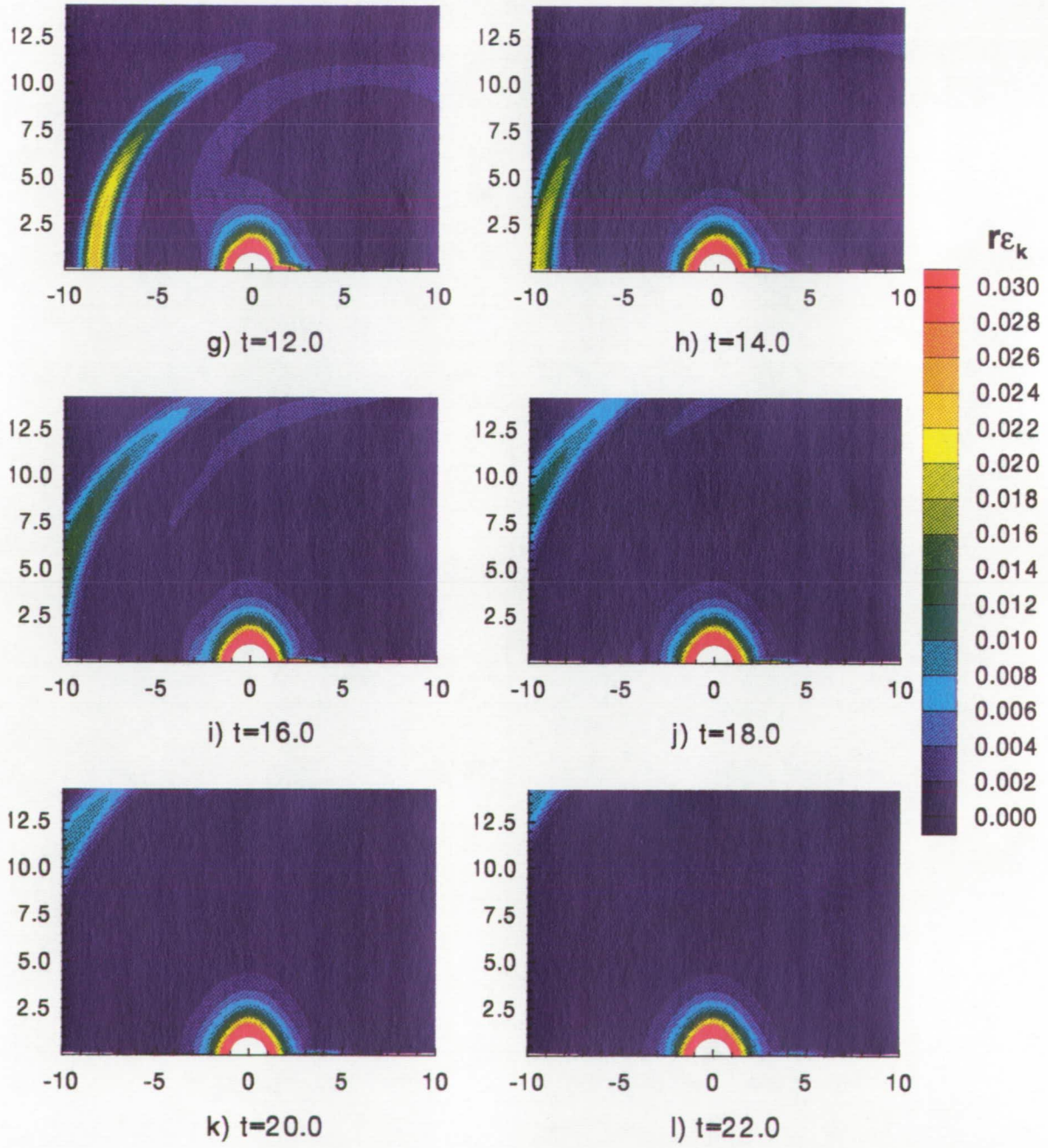

Figure 6.(continued) The time history of the kinetic energy field ε_k is shown in these figures for a cylinder which has been impulsively started to Mach 0.4 translation. Notice that the energy has been scaled here by r.

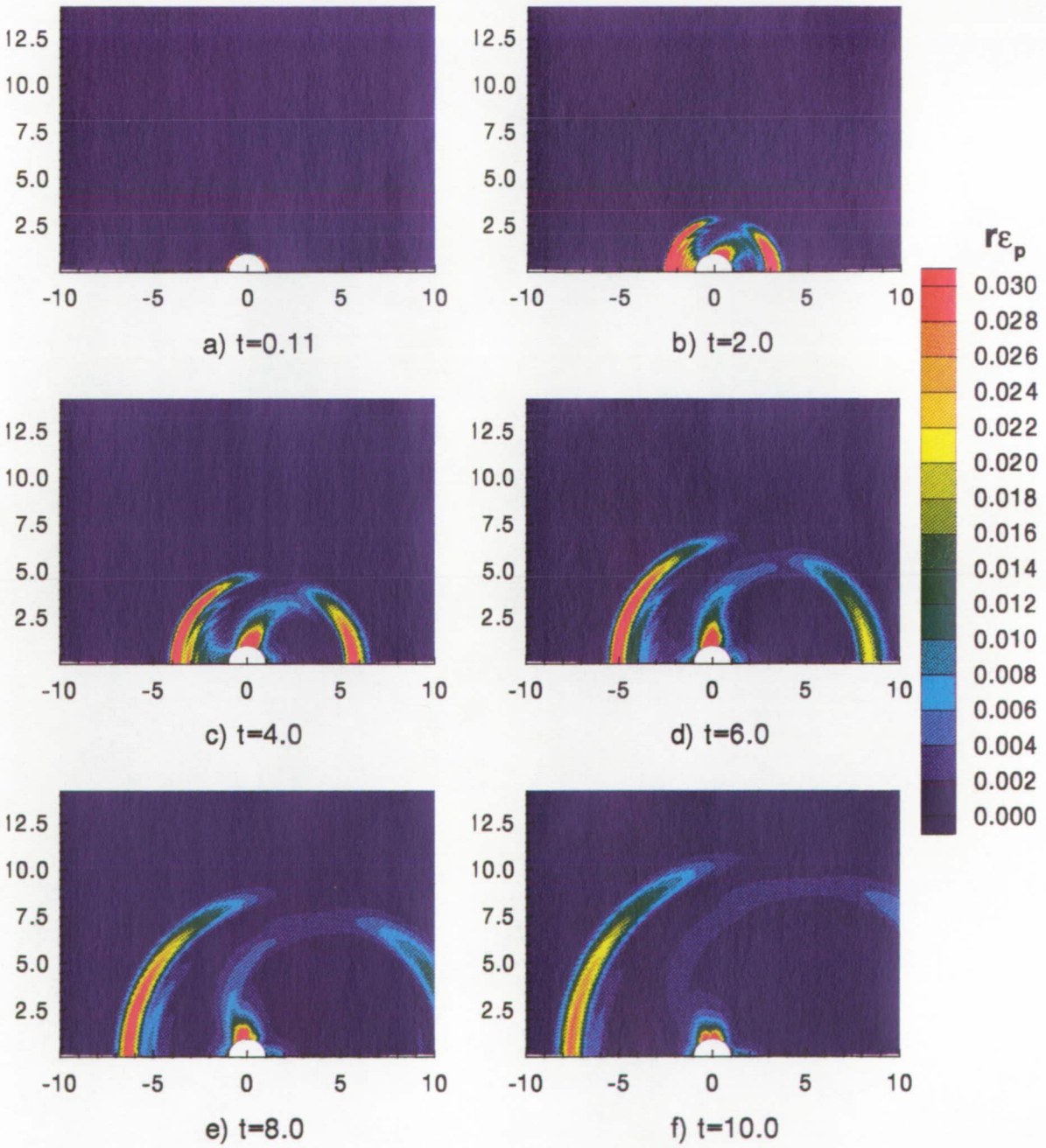

Figure 7. The time history of the potential energy field ε_p is shown in these figures for a cylinder which has been impulsively started to Mach 0.4 translation. Notice that the energy has been scaled here by r.

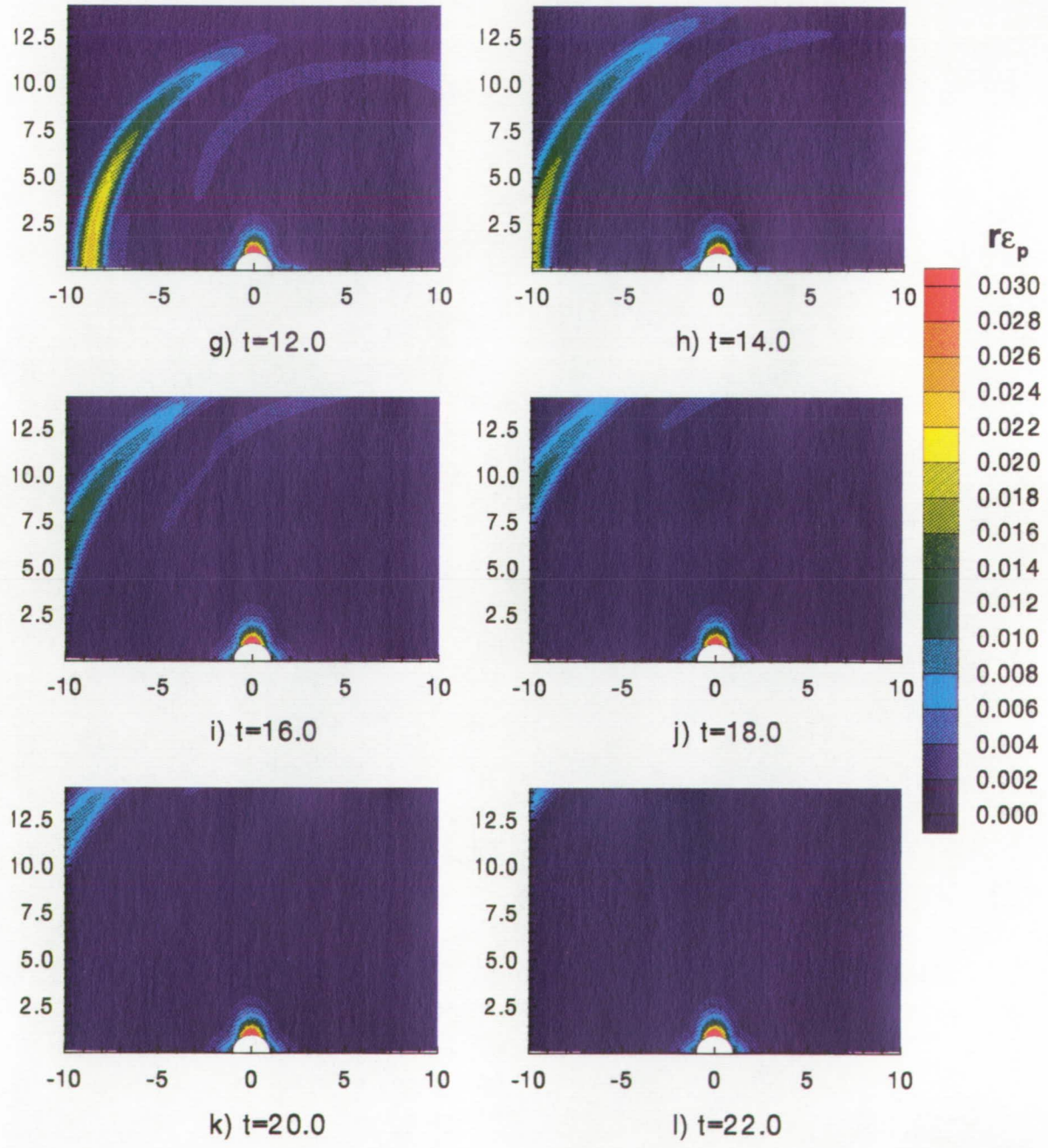

Figure 7.(continued) The time history of the potential energy field ε_p is shown in these figures for a cylinder which has been impulsively started to Mach 0.4 translation. Notice that the energy has been scaled here by r.

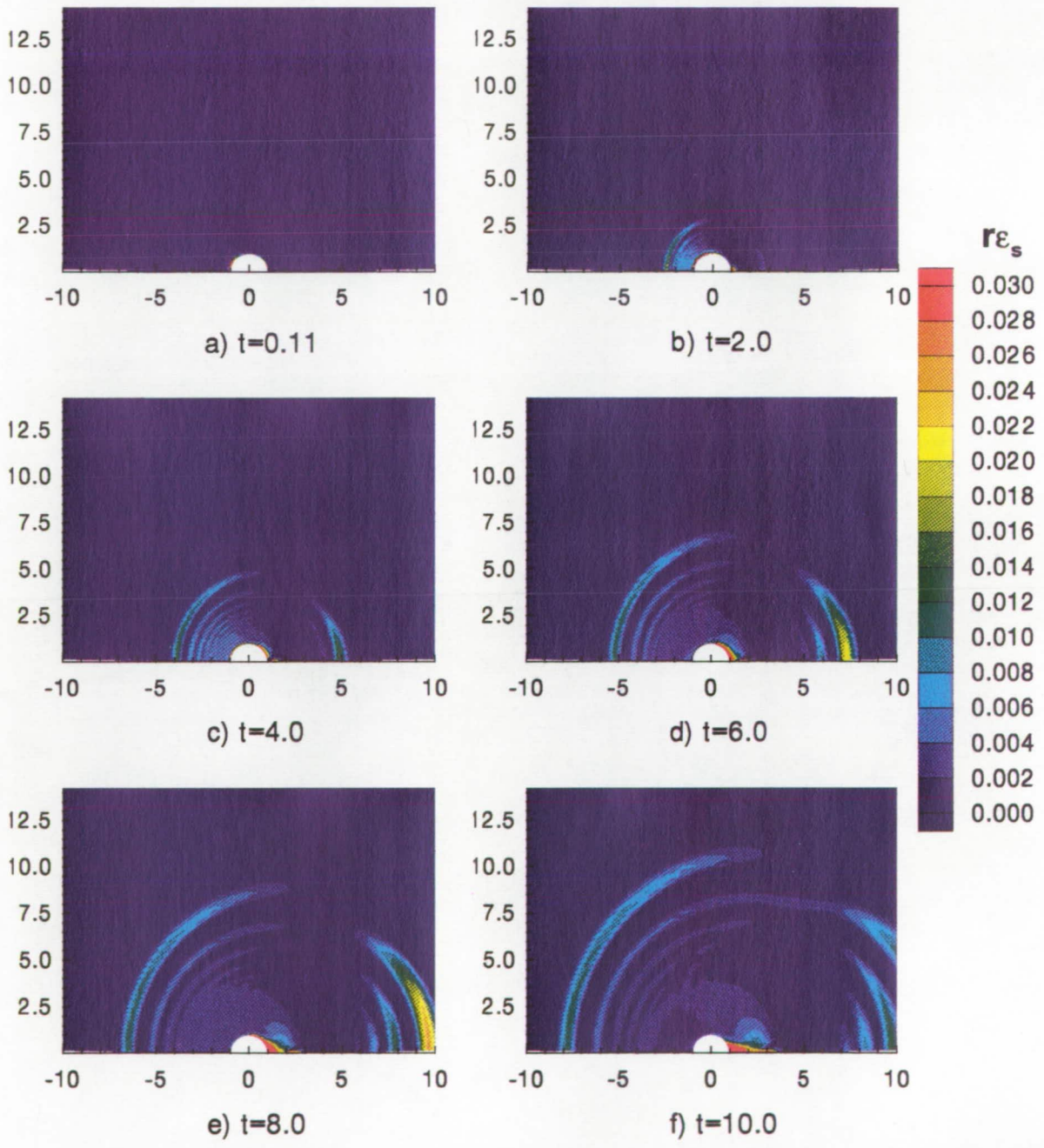

Figure 8. The time history of the entropy energy field ε_s is shown in these figures for a cylinder which has been impulsively started to Mach 0.4 translation. Notice that the energy has been scaled here by r.

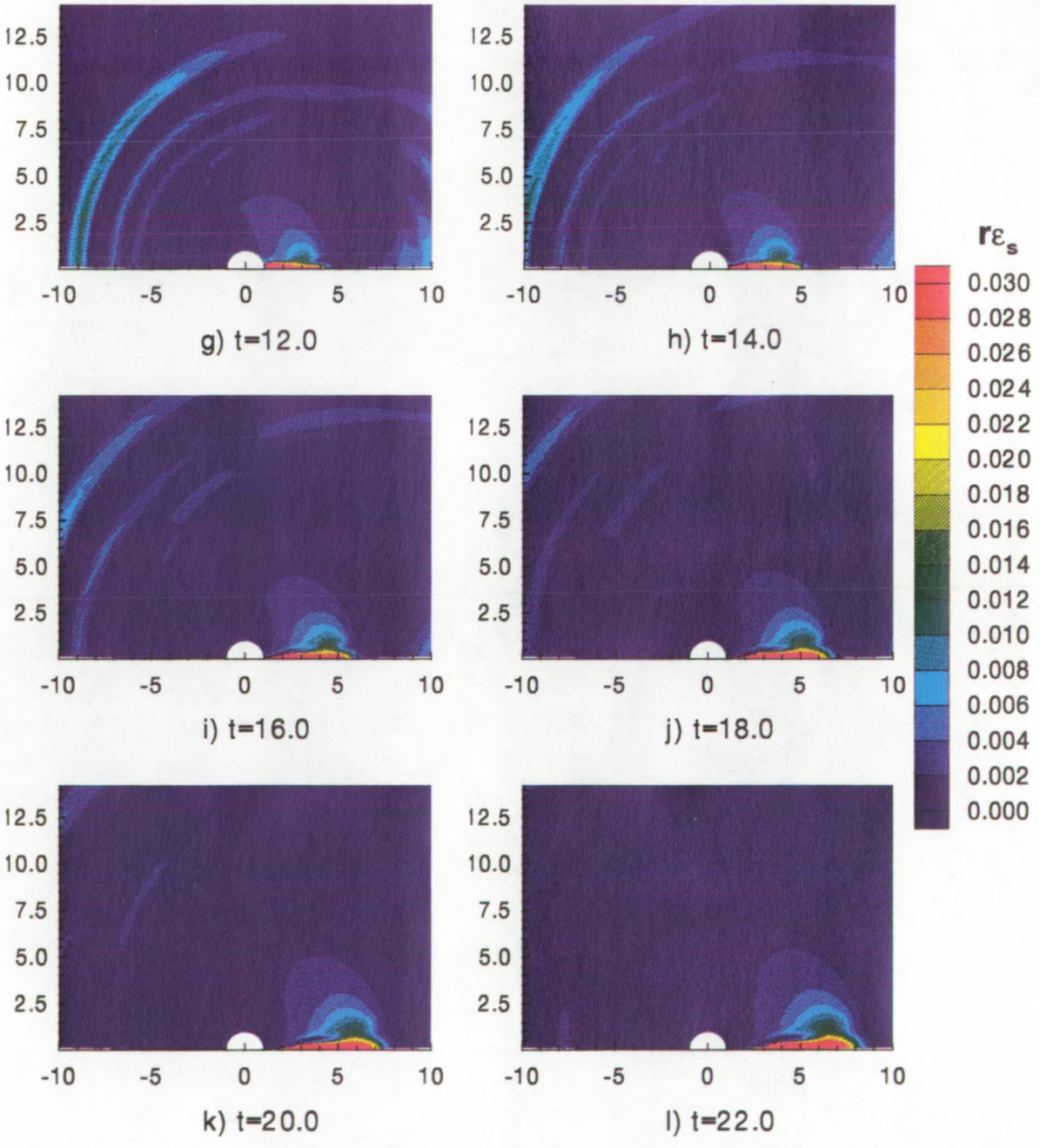

Figure 8.(continued) The time history of the entropy energy field ε_s is shown in these figures for a cylinder which has been impulsively started to Mach 0.4 translation. Notice that the energy has been scaled here by r.

8, especially 8d, that some of the energy in the rightward moving expansion has been transferred to the entropy form. This should not happen for a inviscid fluid; hence it must in some way be related to the numerical viscosity of the discrete algorithm. Upon closer examination of figure 8 we find that the most intense feature roughly corresponds to the vortex shown in figure 3. This should have been anticipated from Crocco's theorem. What is not expected in figure 8 is the elevated level of entropy energy which is clearly due to the passage of the acoustic waves. The entropy field has features which correspond to the oscillations in the density perturbation in figure 2. These figures seem to suggest that the numerically induced errors or damping are identified by the entropy energy term. This is significant since it gives a quantitative local measure of the numerical error which we can use to judge the acceptability of the CFD solution for acoustics. We shall consider this in some detail as we proceed.

Now that we have some idea of how the components of energy are spatially and temporarily distributed, it is useful to consider the balance of energy for the control volume as a function of time. We shall consider the total kinetic, potential, and entropy energy in a cylindrical control volume of radius 10 around the cylinder along with the acoustic and entropy energy flux out of the control volume for different starting scenarios. The definitions for these quantities are given in equation (14), and each of the values are nondimensionalized by the total kinetic energy of the incompressible limit, $\rho\pi a^2 v^2/2$, which is the added mass times $v^2/2$. In figure 9 and following, the energy components are added up such that the envelope of the curve represents the total work input into the fluid by the cylinder. Notice that the kinetic energy, potential energy and acoustic energy flux are the first three components. They are plotted in this order because any acoustic energy will be counted as kinetic and potential energy while inside the control volume and acoustic

energy flux as it leaves the control volume. Likewise entropy energy and entropy energy flux are plotted together for the same reason. Hence when the cylinder is impulsively started to Mach 0.4 in figure 9a for example, we see that most of the work goes initially into kinetic and potential energy modes and eventually a significant entropy energy component before $t = 10.0$, at which time acoustic energy begins to leave the control volume. By time $t = 40.0$ all of the acoustic energy has left and the entropy energy begins to leave. The entropy energy convects with the fluid velocity rather than the sound speed, thus accounting for the delay in leaving the control volume. We can predict the time in which acoustic energy and entropy energy will leave the control volume based on a local sound speed which is approximately unity and a convection velocity of 0.4.

Notice that some of the energy input into the fluid by the cylinder is subsequently recovered as the steady state is approached. This overshoot in energy input can also be found in Longhorn's calculations for the sphere*[25]*. We can also see that the total work required to reach steady state after an impulsive start, i.e. the sum of all the energy components at large t, is equally divided between the sum of kinetic and potential energy in the control volume and the other energy components. This result is an extension of the equipartition of energy found by Taylor*[39]*, Longhorn*[25]*, Ffowcs Williams and Lovely*[38]*, and Hill*[40]* since we have no low Mach number restriction and the local flow field has a significant potential energy component. In figure 9a, we find that the equipartition of energy exists even though a shock and vortices form during the transient startup process. These phenomenon have not been found in the previous work even though there is some evidence following (nonnegligible entropy energy) that a shock may be forming for Mach numbers as low as 0.2.

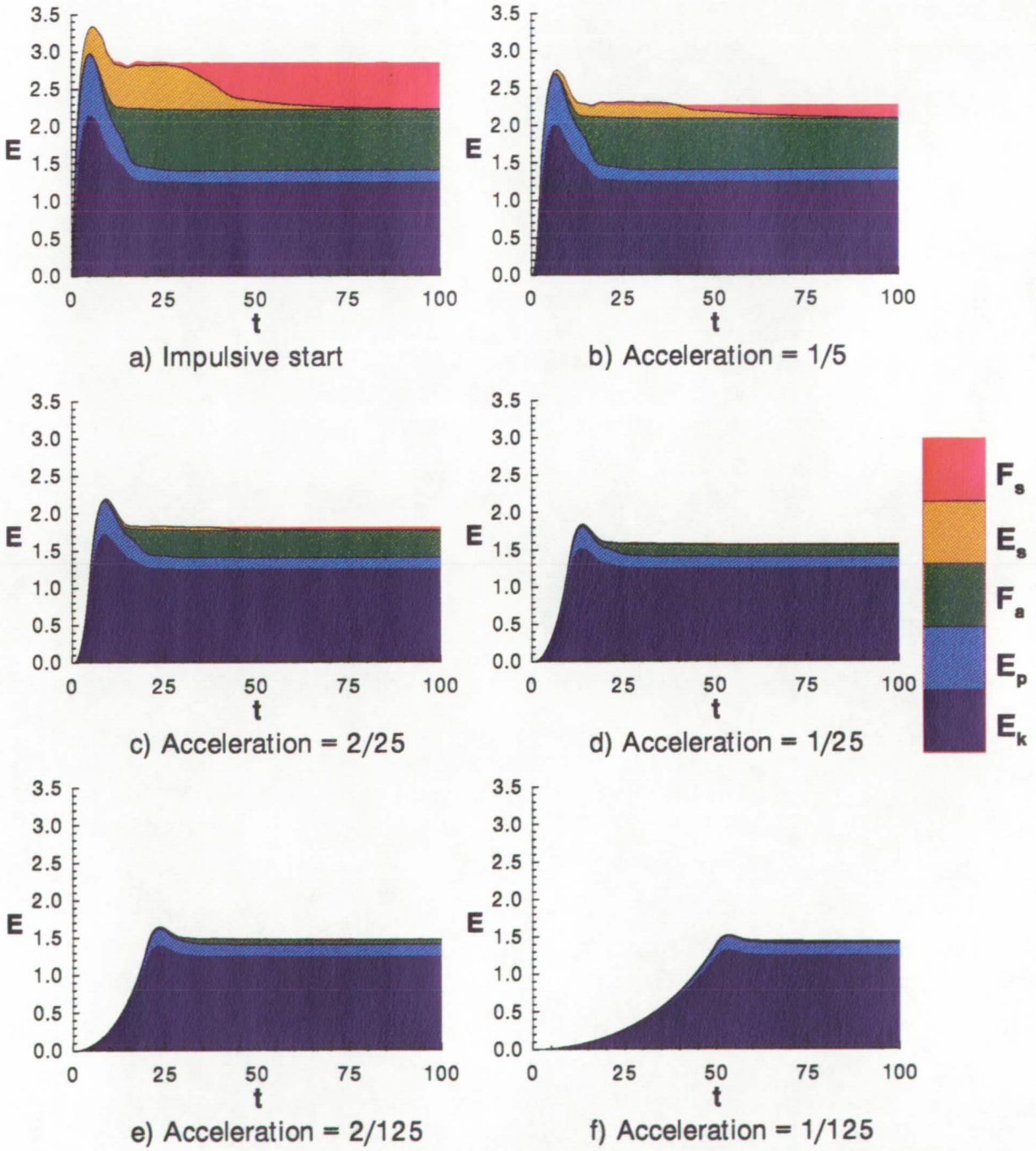

Figure 9. Time history of total kinetic energy E_k, potential energy E_p, acoustic energy flux F_a, entropy energy E_s, and entropy energy flux F_s for a control volume with a radius of 10. Energy is nondimensionalized by the total incompressible kinetic energy, $\rho\pi a^2 v^2/2$, where v is the steady state velocity Mach 0.4.

Figure 9 b-f shows the energy transfer for a cylinder accelerated at various constant acceleration rates. The final velocity is Mach 0.4 in each case. As we compare the accelerations in figure 9, we find that the amount of work required to reach steady state declines significantly with reduced acceleration. As the rate of acceleration is decreased, the production of entropy and acoustic energies decline until in figure 9f only the work needed to energize the local aerodynamic field is input into the system. Thus a negligible amount of acoustic energy leaves the control volume.

We find similar results for lower Mach numbers in figures 10-12. When the cylinder is translated at Mach 0.1 in figure 10, we see that the kinetic energy in the aerodynamic field is essentially that for an incompressible fluid. The compressible energy radiates as sound, although part of the energy we expect to radiate is contained in the entropy term. This is thought to be due to the numerical damping, which we will describe in more detail later. Also notice the oscillations in the entropy energy near time $t = 10.0$, in figure 10a-d. These oscillations are not apparent when the work is calculated directly from the surface pressure. The error here is attributed to the inaccuracy of the numerical method at this Mach number. Recall that the accuracy of the numerical scheme depends upon the grid resolution and time step size, neither of which vary with Mach number even though the low Mach number perturbations are much smaller. Since the values in figure 10 are nondimensionalized by $\rho\pi a^2 v^2/2 = .005\pi$, the error is more apparent.

As we consider intermediate velocities in figures 11 and 12, we see there are no particular surprises. The work required to bring the cylinder into steady state translation for each Mach number and velocity is summarized in figure 13. This figure shows that more energy is imparted to the system for all acceleration rates when the steady state Mach number is raised. This additional energy goes into both the kinetic energy and the the

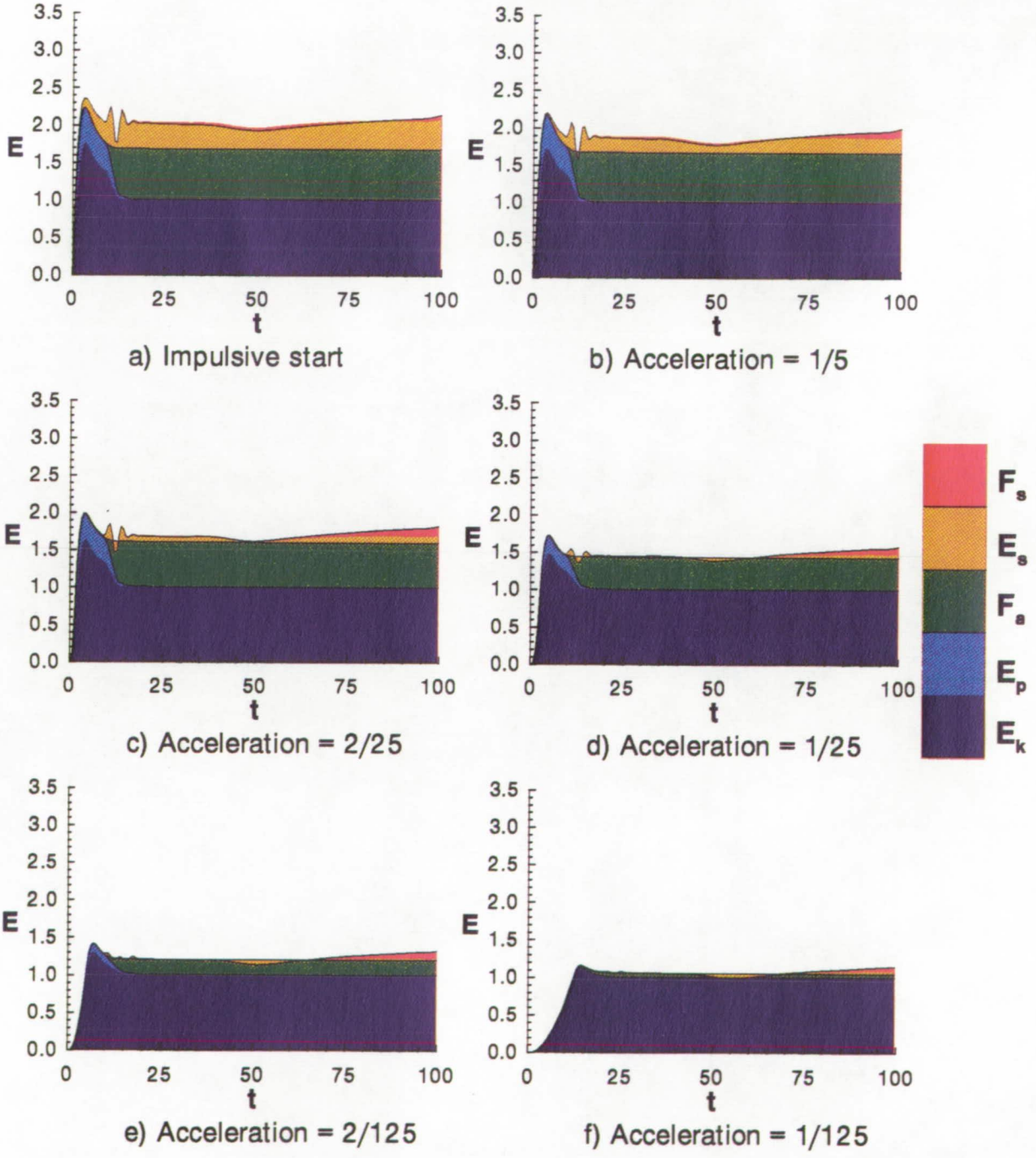

Figure 10. Time history of total kinetic energy E_k, potential energy E_p, acoustic energy flux F_a, entropy energy E_s, and entropy energy flux F_s for a control volume with a radius of 10. Energy is nondimensionalized by the total incompressible kinetic energy, $\rho\pi a^2 v^2/2$, where v is the steady state velocity Mach 0.1.

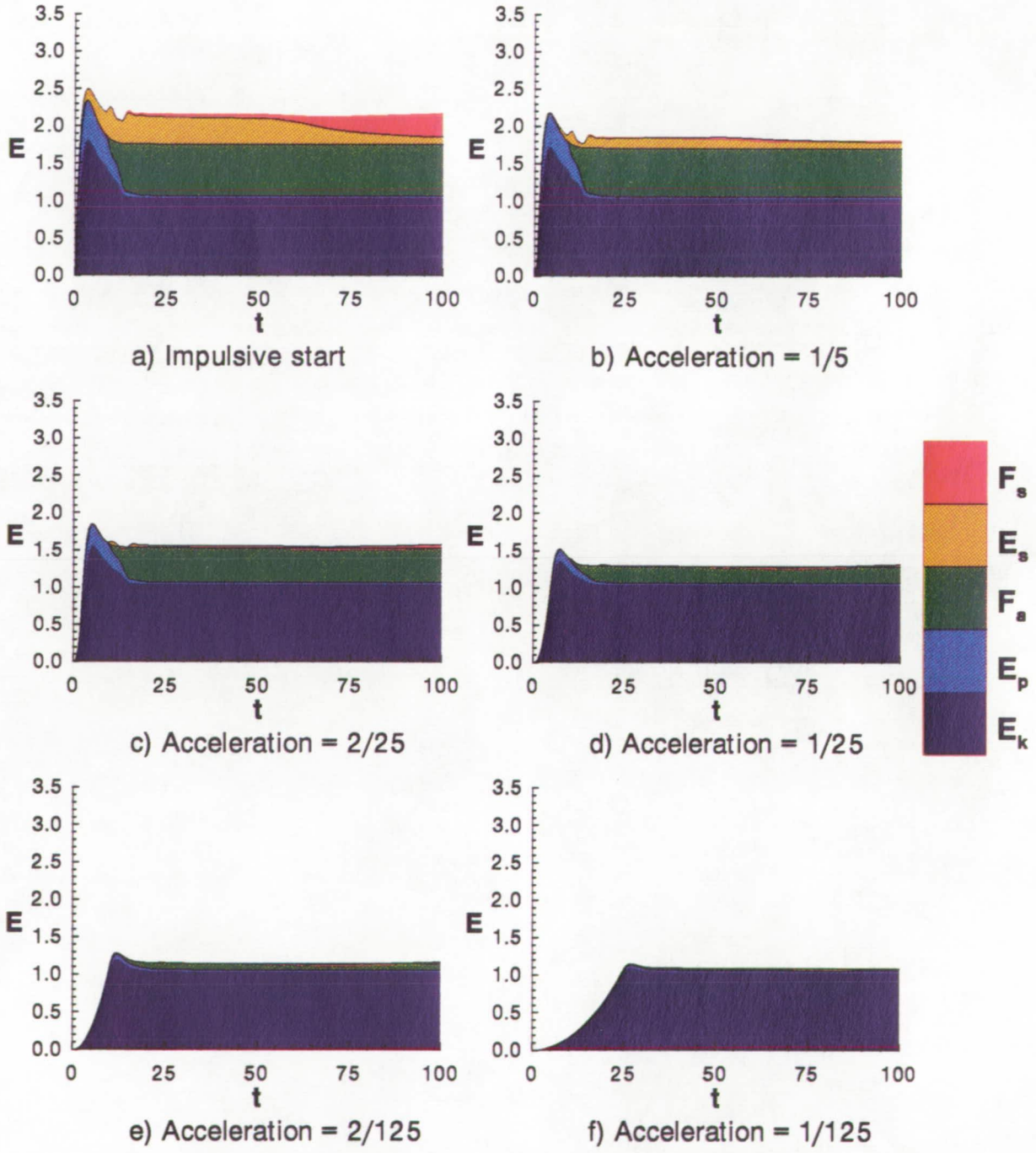

Figure 11. Time history of total kinetic energy E_k, potential energy E_p, acoustic energy flux F_a, entropy energy E_s, and entropy energy flux F_s for a control volume with a radius of 10. Energy is nondimensionalized by the total incompressible kinetic energy, $\rho\pi a^2 v^2/2$, where v is the steady state velocity Mach 0.2.

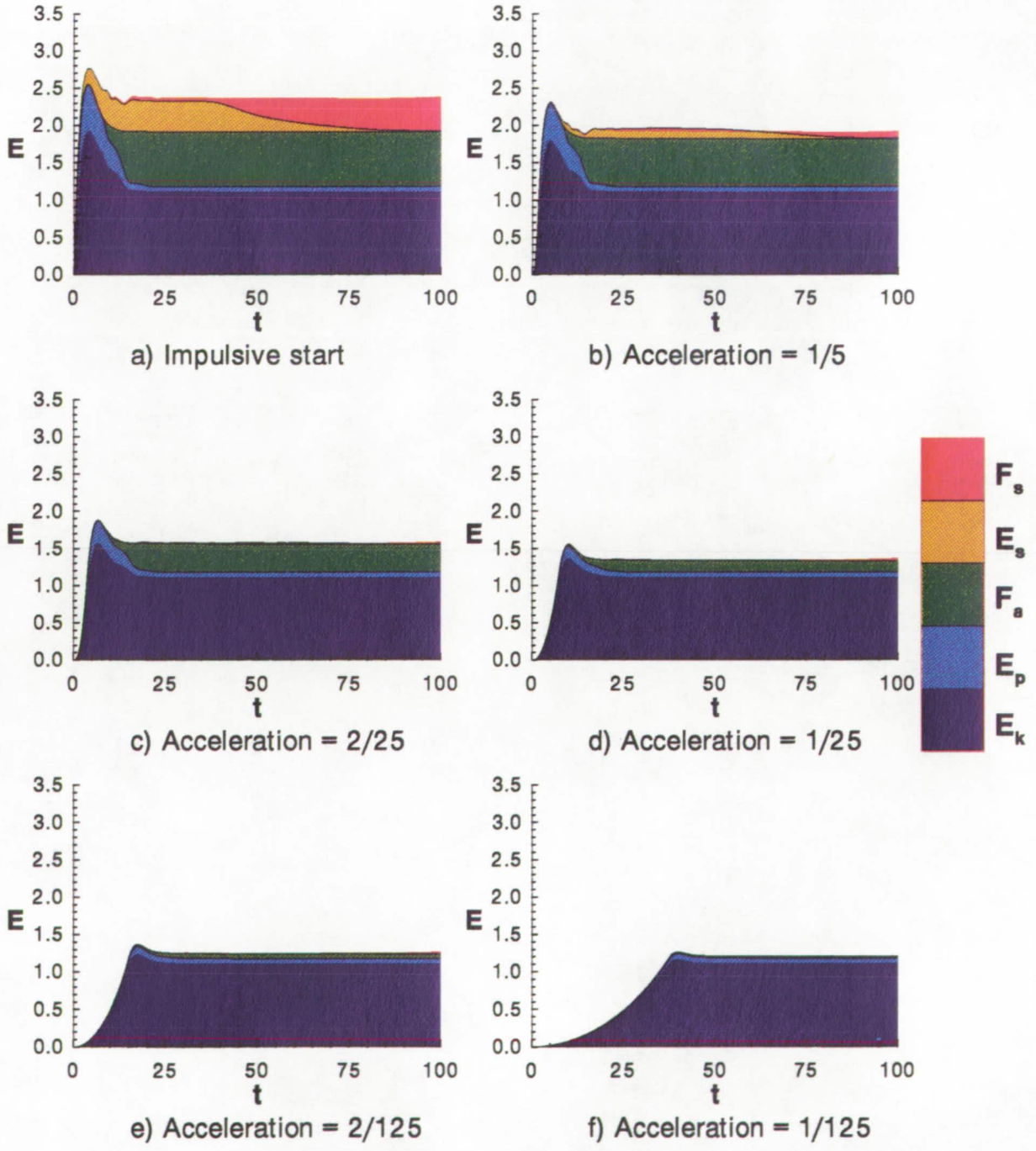

Figure 12. Time history of total kinetic energy E_k, potential energy E_p, acoustic energy flux F_a, entropy energy E_s, and entropy energy flux F_s for a control volume with a radius of 10. Energy is nondimensionalized by the total incompressible kinetic energy, $\rho\pi a^2 v^2/2$, where v is the steady state velocity Mach 0.3.

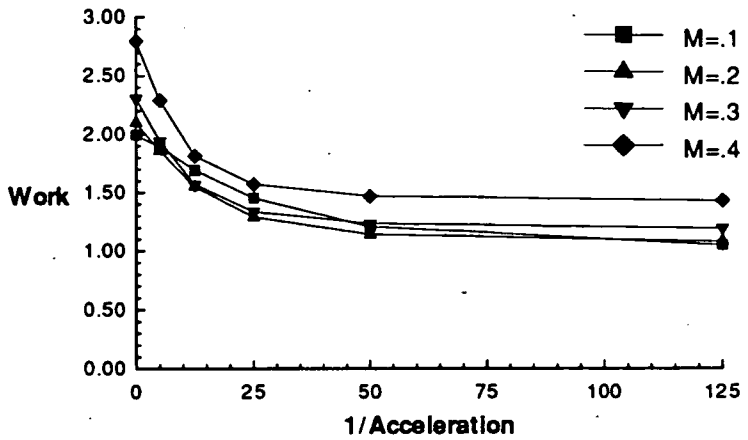

Figure 13. A comparison, as a function of Mach number, of work required to reach steady state using various accelerations. No additional work is required to maintain the translation after steady state has been reached for these Mach numbers. Work is nondimensionalized by the total kinetic energy of the incompressible case, $\rho\pi a^2 v^2/2$.

potential energy components as is clearly seen in figure 14. From this figure it is evident that the potential energy component does not become significant until around Mach 0.2, hence the low Mach number solutions should be valid up to this Mach number. Again in figure 13, we find for all Mach numbers 0.1 to 0.4, twice as much energy is required to impulsively accelerate the cylinder as is required when we accelerate it very slowly, thus for the impulsive start an equipartition of the energy in evident.

When the final cylinder velocity is above the critical Mach number 0.4, the character of the energy time history changes and no equipartition exists. Figure 15 shows the energy time history for Mach 0.5 translation. This case is fundamentally different from the others since a shock exists in the steady flow. This alters the surface pressure distribution in such a way that energy is continually input into the system to maintain the cylinder velocity. This additional energy goes into the entropy energy mode and then is convected out of the control volume, thus the flux of entropy continues to increase with time. The oscillations

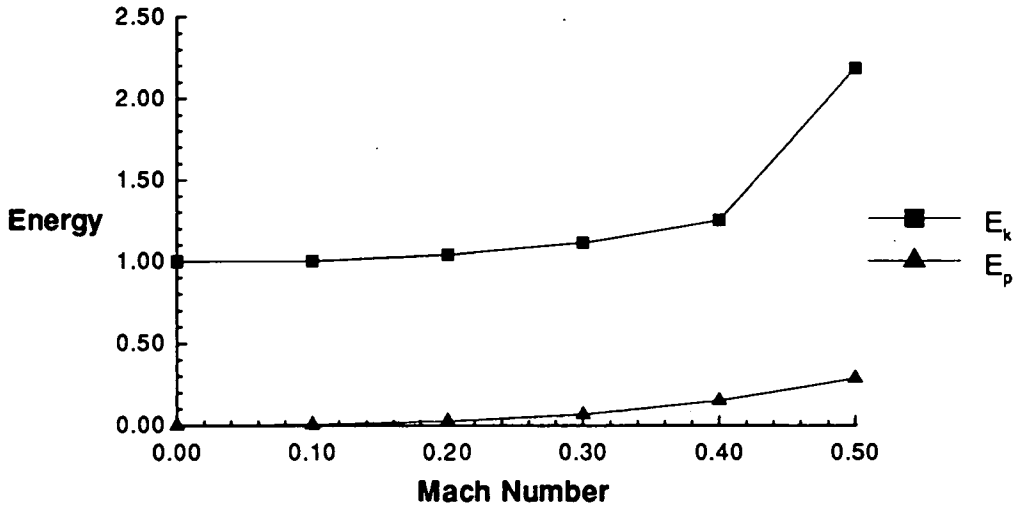

Figure 14. A comparison of kinetic and potential energy in the steady state, local aerodynamic field as a function of Mach number. A control volume of radius 10 is used for these calculations and energy is nondimensionalized by the total kinetic energy of the incompressible case, $\rho\pi a^2 v^2/2$.

between the entropy energy and entropy energy flux are an indication of concentrated vorticity convecting out of the control volume.

Deceleration of the Cylinder.

Now that we have examined the energy transport from an accelerating cylinder into the surrounding fluid, it is informative to examine the related problem of a decelerating cylinder. For a cylinder impulsively brought to rest from a low Mach number translation, we would expect all of the energy contained in the local aerodynamic field to radiate as sound. For our compressible calculations, we must also entertain the possibility of energy going to the entropy mode. We will only consider two Mach numbers and a few decelerations because the results are all somewhat similar. We will plot the time histories of the total kinetic energy, potential energy, etc., as before, but instead of using the final velocity for the incompressible kinetic energy used in nondimensionalization, we shall use

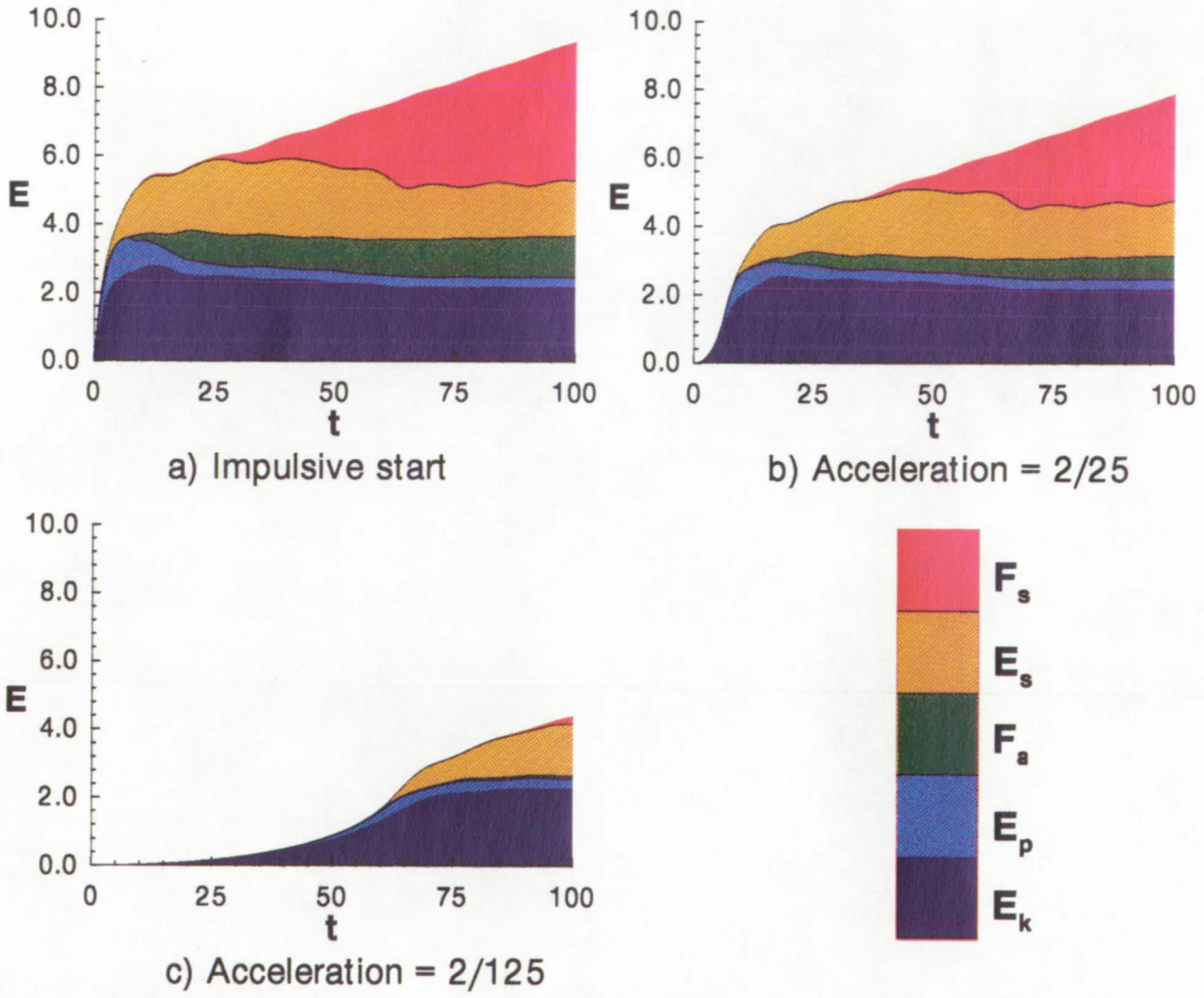

Figure 15. Time history of total kinetic energy E_k, potential energy E_p, acoustic energy flux F_a, entropy energy E_s, and entropy energy flux F_s for a control volume with a radius of 10. Energy is nondimensionalized by the total incompressible kinetic energy, $\rho\pi a^2 v^2/2$, where v is the steady state velocity Mach 0.5.

the initial velocity. In figures 16 and 17 we show various decelerations in which the cylinder is brought to rest from initial velocities of Mach 0.2 and Mach 0.4, respectively. Upon first glance we notice that while we have entropy energy generated in the rapid decelerations,

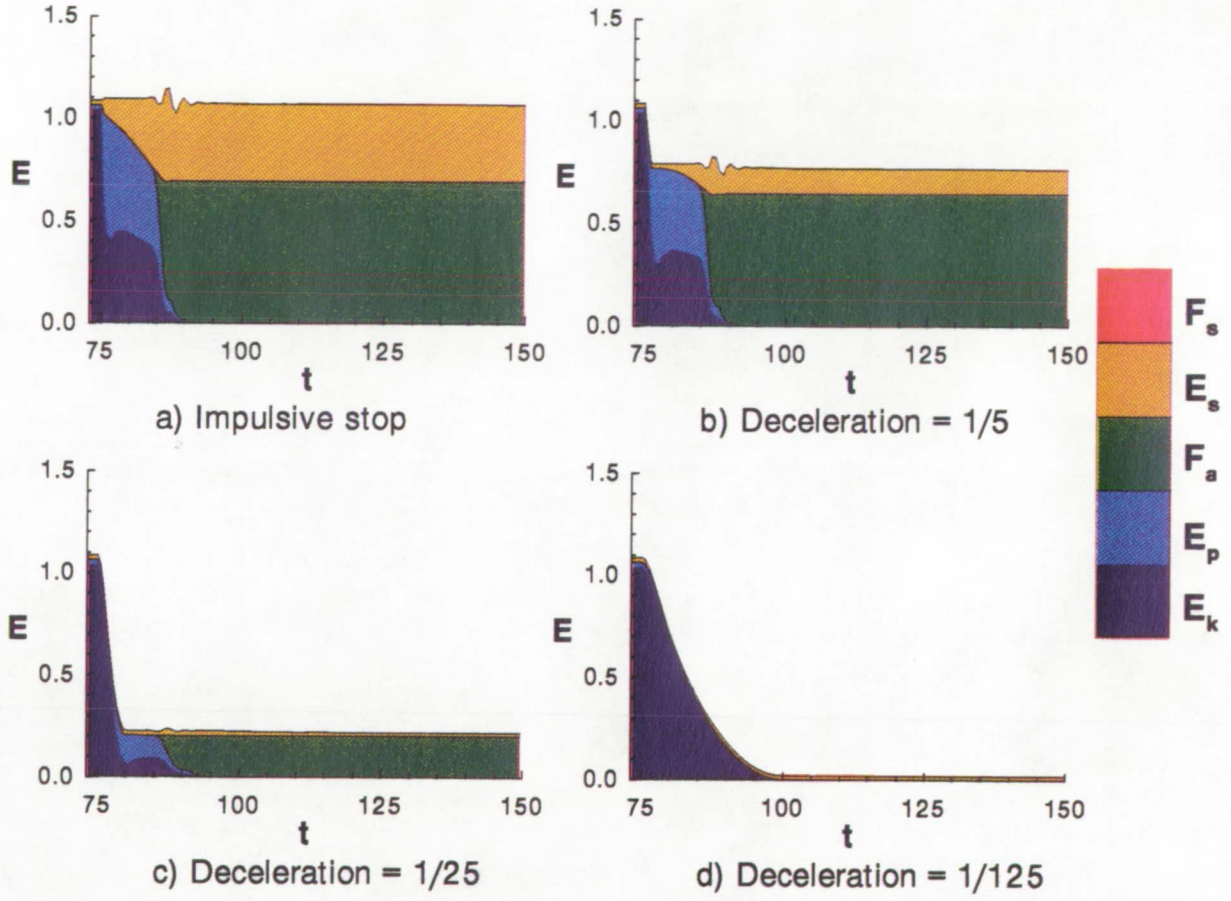

Figure 16. Time history of total kinetic energy E_k, potential energy E_p, acoustic energy flux F_a, entropy energy E_s, and entropy energy flux F_s for a control volume with a radius of 10. Energy is nondimensionalized by the total incompressible kinetic energy, $\rho\pi a^2 v^2/2$, where $v = 0.2$ is the velocity before the deceleration is initiated.

there is no apparent flux of entropy energy out of the control volume. This is because the transport of entropy energy depends upon fluid convection, a mechanism which no longer exists when the cylinder is brought to rest.

Another feature of this problem, seen for high deceleration, is the nearly linear increase in entropy energy before the acoustic waves leave the control volume. Since the entropy

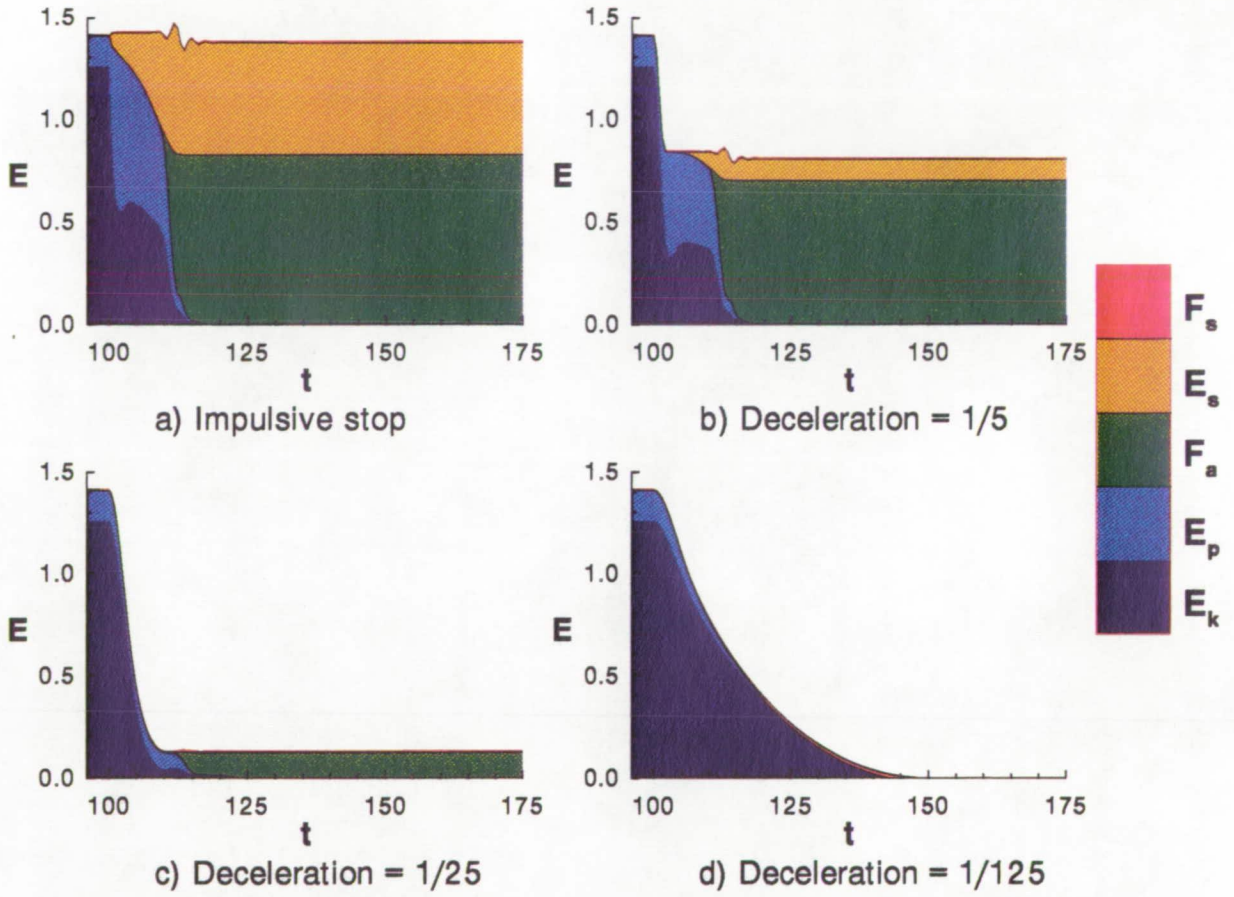

Figure 17. Time history of total kinetic energy E_k, potential energy E_p, acoustic energy flux F_a, entropy energy E_s, and entropy energy flux F_s for a control volume with a radius of 10. Energy is nondimensionalized by the total incompressible kinetic energy, $\rho\pi a^2 v^2/2$, where $v = 0.4$ is the velocity before the deceleration is initiated.

energy component does not continue to grow after the acoustic waves have left the control volume, we may surmise that the acoustic energy is being transferred to the entropy term in our numerical calculations. This is true of both the kinetic and potential energy components and the effect is much less pronounced in the low deceleration cases. If we look back to the accelerating cylinder, we find evidence of the transfer of acoustic energy

to entropy energy in the rapid acceleration cases as well. We speculate that this is due in part to the inability of the discrete computational grid to resolve the high frequency content of the acoustic waves and therefore the numerical method damps out that part of the solution. Hence, the nonphysical damping arising from the discrete nature of our grid is seen through an increase in entropy. We will examine this idea by using different grid resolutions in the next section.

A final feature we can understand in figures 16 and 17 is the rapid increase in potential energy shortly after the cylinder has been stopped. In both figure 16 a-c and 17 a-c, we can see that the potential energy increase is the same as the kinetic energy decrease, aside from the loss to entropy energy. We can understand this if we consider that the fluid around the cylinder has inertia, and hence will interact with the cylinder as both are stopped. Thus, any fluid adjacent to the cylinder will tend to stop, transferring its kinetic energy into potential energy.

Sources of Entropy

Before we conclude, one nagging question must still be addressed – How much of the entropy energy results from numerical error and how much is real? For a cylinder which is rapidly stopped, it is clear that the acoustic waves transfer some of their energy into the entropy energy term. This is unfortunate since it implies that as an acoustic wave propagates, its energy will be gradually dissipated when it should continue to propagate. This damping of acoustic waves is evident if we examine the amount of acoustic and entropy energy flux out of various size control volumes. In figure 18, we find that for a control volume radius of 10 the acoustic flux out is greater than the entropy energy flux, while the opposite is true for a control volume of radius 25. This is clearly a serious problem if we

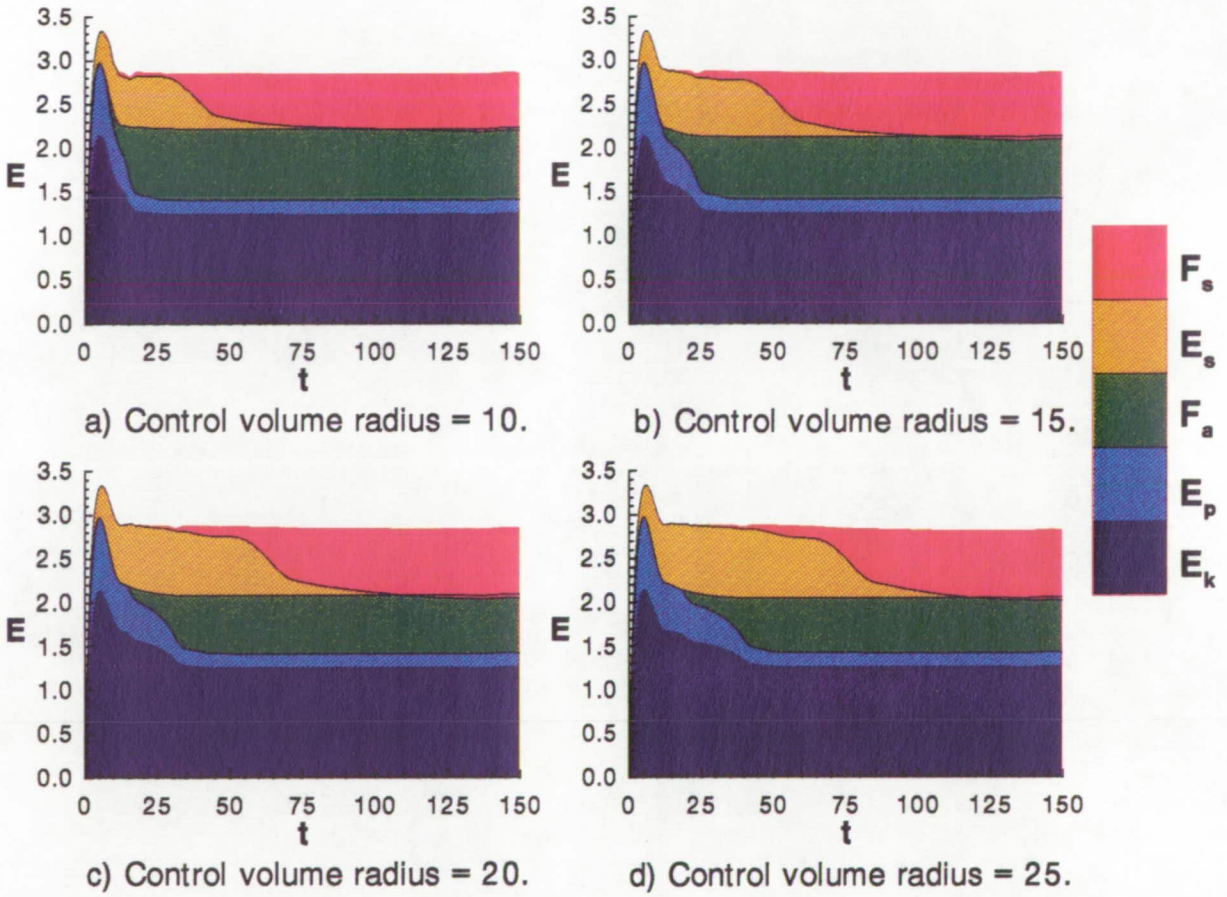

Figure 18. A comparison of total energy in control volumes of different radii for a cylinder impulsively started to Mach 0.4 translation.

intend to use CFD methods to calculate the acoustic field directly as part of an unsteady calculation.

We do have some hope that this will not be an insurmountable problem since, for lower acceleration rates there is very little energy in the entropy component, and hence even if acoustic energy is dissipated, it may be at negligible levels. To address the question of entropy energy generation, we will consider the original problem of a cylinder impulsively started to Mach 0.4 for the rest of our discussion. In this case some entropy energy is

unavoidable because of the shock wave formation, but we can also envision increases in entropy due to the explicit artificial dissipation added for numerical stability as well as the implicit damping due to the discrete nature of the numerical scheme. We shall examine both of these entropy generation mechanisms separately.

Effect of Artificial Viscosity.

The artificial viscosity we add for numerical stability, which is described in appendix B, seems to be an obvious possible generator of unwanted entropy energy. If we look back over the previous calculations, we see that the total entropy energy E_s in the control volume is negligible when the rate of acceleration is small and it does not grow after the acoustic waves have left the domain. From this we should probably conclude that the second order dissipation is most likely to be the more important part of the artificial viscosity since the fourth order term does not seem to be producing any significant amount entropy after the gradients have left the control volume. We can test this hypothesis by using different values of the coefficients k_2 and k_4 which control the second and fourth order dissipation terms, independently. In figure 19 the effect of changing the damping coefficients on the total potential and entropy energy is shown. We find that even if we triple k_2 or increase k_4 by an order of magnitude, the effect on both energy components is minimal.

Effect of Grid Resolution.

We also expect that the grid resolution may be a strong factor since the impulsive accelerations and decelerations show the most significant levels of entropy energy. To study this effect, three additional computational grids have been generated. The grid used in the previous calculations and shown in figure 1 is designated here as grid 1. Figure 20 shows a comparison of Δr vs r for each of four grids. Grid 2 is a coarser grid in both r and θ directions while grids 3 and 4 both have significantly finer resolution in the r direction.

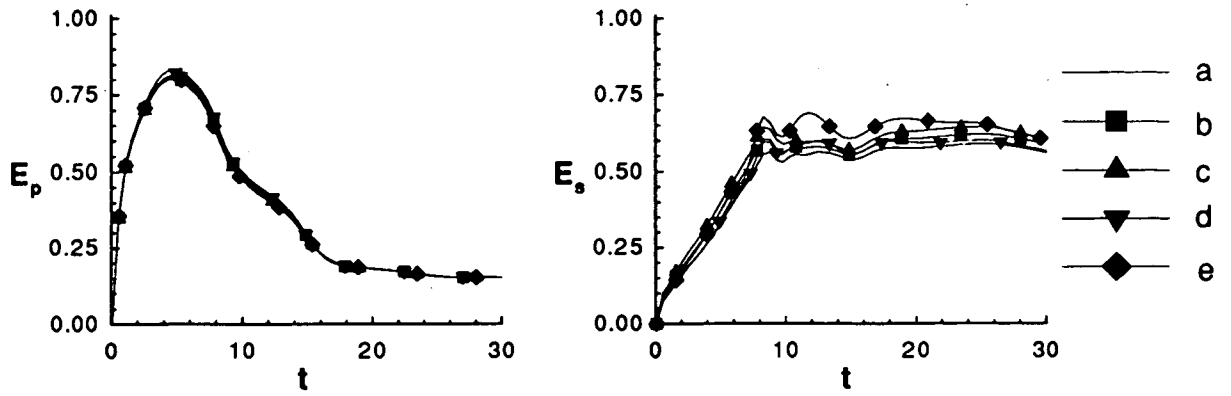

Figure 19. This figure shows the total potential and entropy energy in the control volume after a cylinder has been impulsively started into Mach 0.4 translation. The coefficients of the explicit artificial damping were set at: a) $k_2 = .25$, $k_4 = .003$ – the nominal values; b) $k_2 = .50$, $k_4 = .003$; c) $k_2 = .75$, $k_4 = .003$; d) $k_2 = .25$, $k_4 = .006$; e) $k_2 = .25$, $k_4 = .020$. The energy is nondimensionalized by the total steady state incompressible kinetic energy.

directions while grids 3 and 4 both have significantly finer resolution in the r direction. Grid 3 has the finest azimuthal resolution. The constant radial spacing of the grid 4 starts at a much smaller r than the other grids, giving it the finest radial resolution.

In figure 21, we compare the total potential energy and entropy energy for each of the four grids. Notice that there is some variation in the potential energy for both the impulsive case and the acceleration of 1/5 but there is a substantial variation in entropy energy. We can conclude that the increased entropy energy for the coarser grids corresponds directly to a decrease in acoustic energy flux away from the cylinder. In figures 22-24, we can observe the spatial distribution of kinetic, potential and entropy energies at time $t = 8.0$ for each of these grids. Notice that for grid 3 the increased azimuthal resolution gives a smooth azimuthal variation in energy and both grids 3 and 4 have little entropy energy associated with the acoustic waves. These calculations support the idea that increased

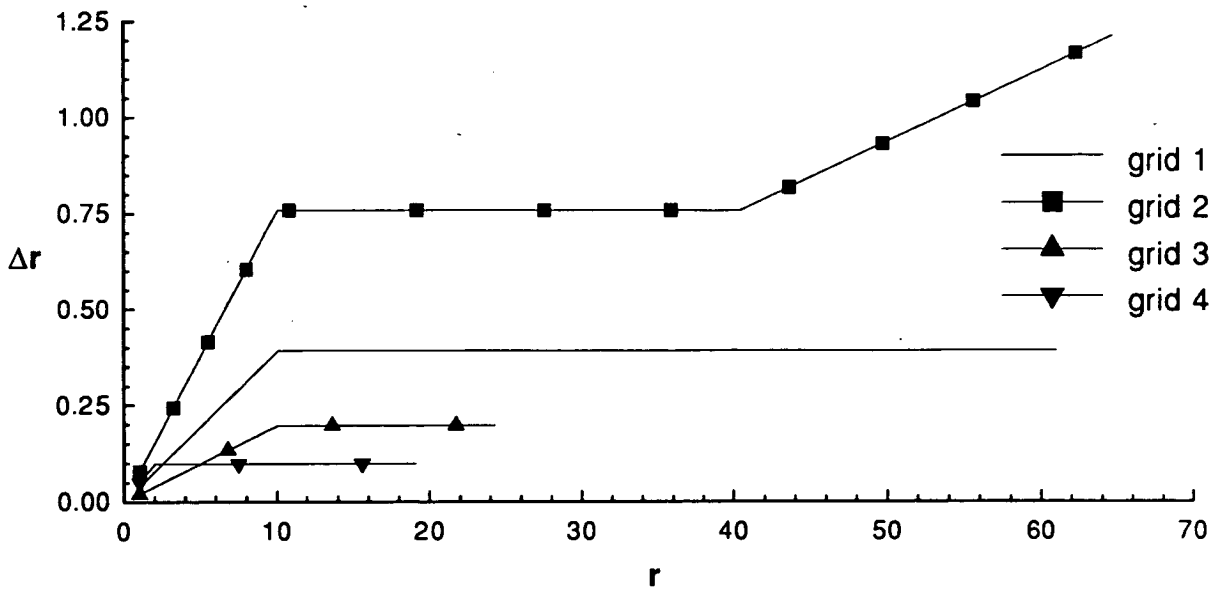

Figure 20. This figures shows the distribution of Δr for the four grids considered. The azimuthal resolution $\Delta\theta$ is constant for each grid and is given as: $\Delta\theta = .0331$ radians for grid 1; $\Delta\theta = .0662$ radians for grid 2; $\Delta\theta = .0165$ radians for grid 3; $\Delta\theta = .0331$ radians for grid 4.

resolution of the computational domain enables the numerical method to better capture the high frequency content associated with rapid accelerations and decelerations. Hence, grid resolution is of primary importance in the calculation of acoustics with CFD methodology.

Although we have refined the grid and achieved improved results, a polar grid may not be the best choice since the azimuthal arc length of the cells grows linearly with r. Other types of grids which maintain the grid cell size uniformly throughout the computational domain, and perhaps even unstructured grids, may be more suitable for acoustics applications. The local aerodynamic field seems to be much less sensitive to the grid resolution away from the body – an observation which explains why stretched grids don't seem to cause problems in aerodynamic calculations.

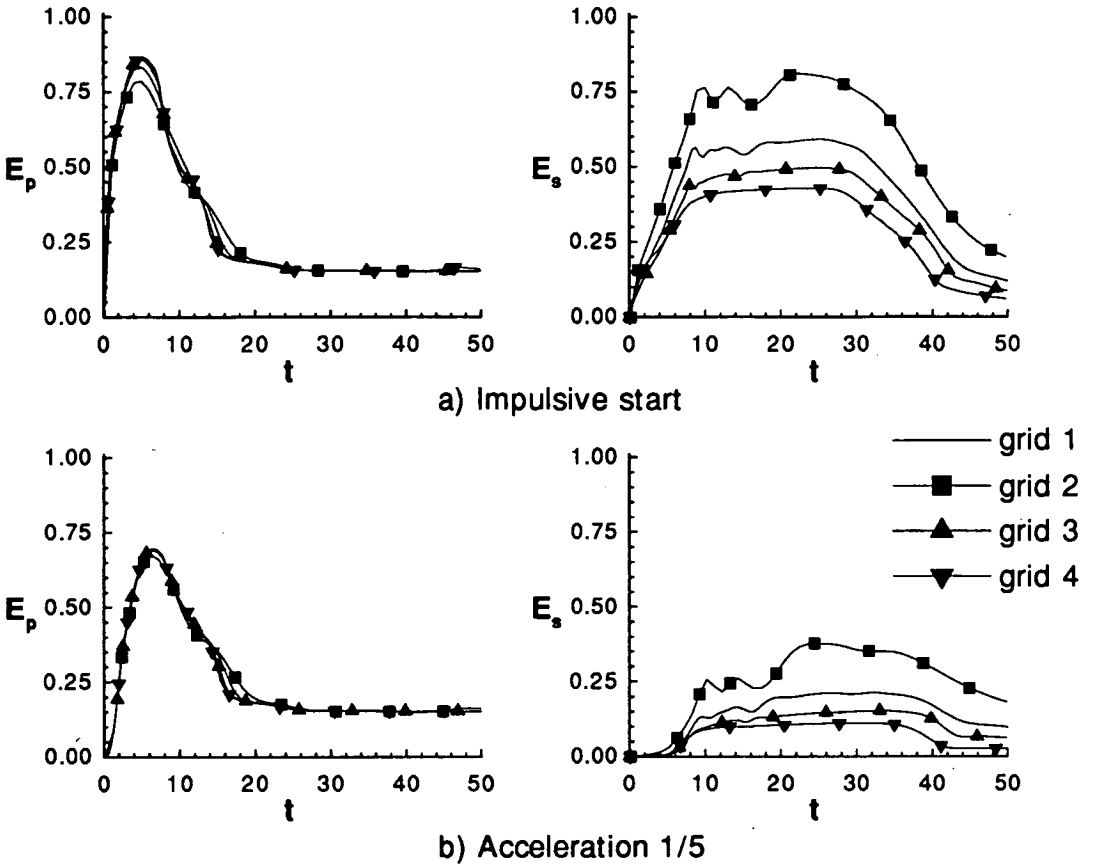

Figure 21. A comparison of potential energy and entropy energy for various grids and accelerations. The final translation velocity is Mach 0.4.

Conclusions

The aim in part B has been twofold: 1) to understand the nonlinear, transient energy transfer from the surface of an accelerating cylinder to the far field; and 2) to better understand the capabilities and limitations of present day CFD methodology as applied to acoustic problems. Both of these aims have be successfully achieved through the numerical study of the circular cylinder.

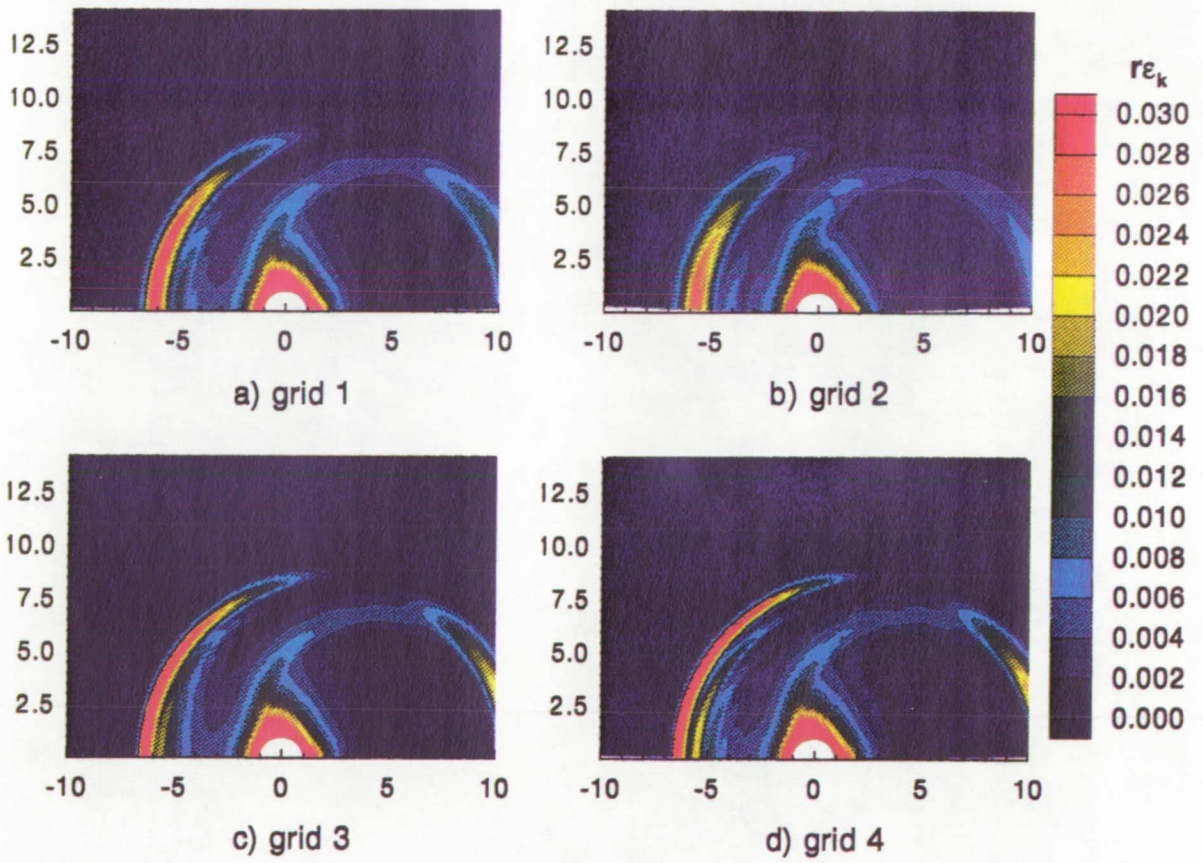

Figure 22. A comparison of the kinetic energy ε_k distribution for various grids at $t = 8.0$. This is for the case of a cylinder impulsively started in Mach 0.4 translational motion.

We have found that the transition from rest to a nonnegligible Mach number is somewhat more complicated than in the low Mach number problems studied previously. When the cylinder is accelerated rapidly, a shock may form in the compressible fluid generating entropy and vorticity in the early stages of the motion. As the shock disappears, the vorticity convects away from the cylinder and the steady flow around the cylinder becomes essentially potential, at least for steady state velocities less than the critical Mach number of the cylinder. We have also shown that as the steady state Mach number increases toward

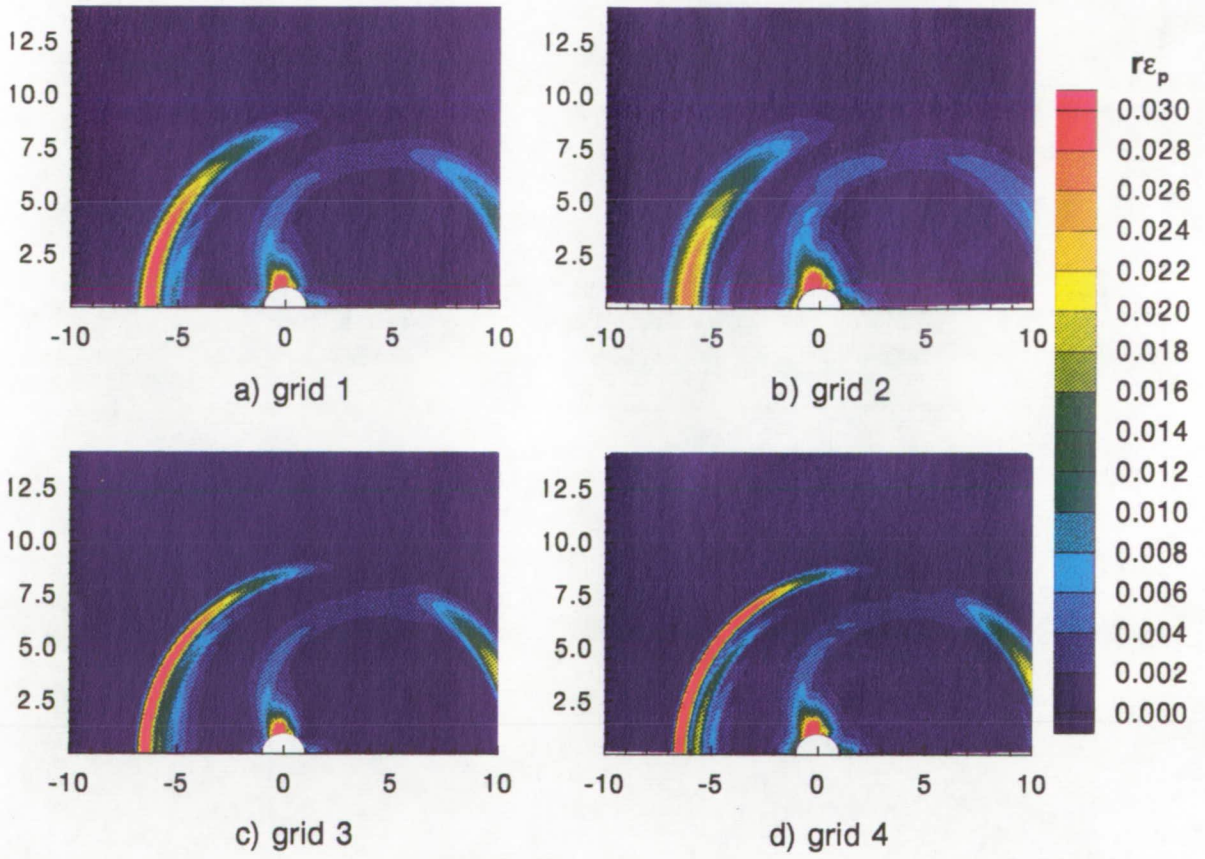

Figure 23. A comparison of the potential energy ε_p distribution for various grids at $t = 8.0$. This is for the case of a cylinder impulsively started in Mach 0.4 translational motion.

the critical Mach number, $\sim M = 0.4$, the aerodynamic field experiences an increase in kinetic energy as well as the addition of potential (compressible) energy. These details are lacking in the low Mach number situation, as demonstrated by the Mach 0.1 calculations.

It is somewhat surprising then that we are able to extend, up to the critical Mach number, the notion of an equipartition of energy between the local kinetic energy and the acoustic energy for an impulsively started body. Nontheless, our calculations show that if we consider the balance of energy in the local aerodynamic field, i.e. the combined kinetic

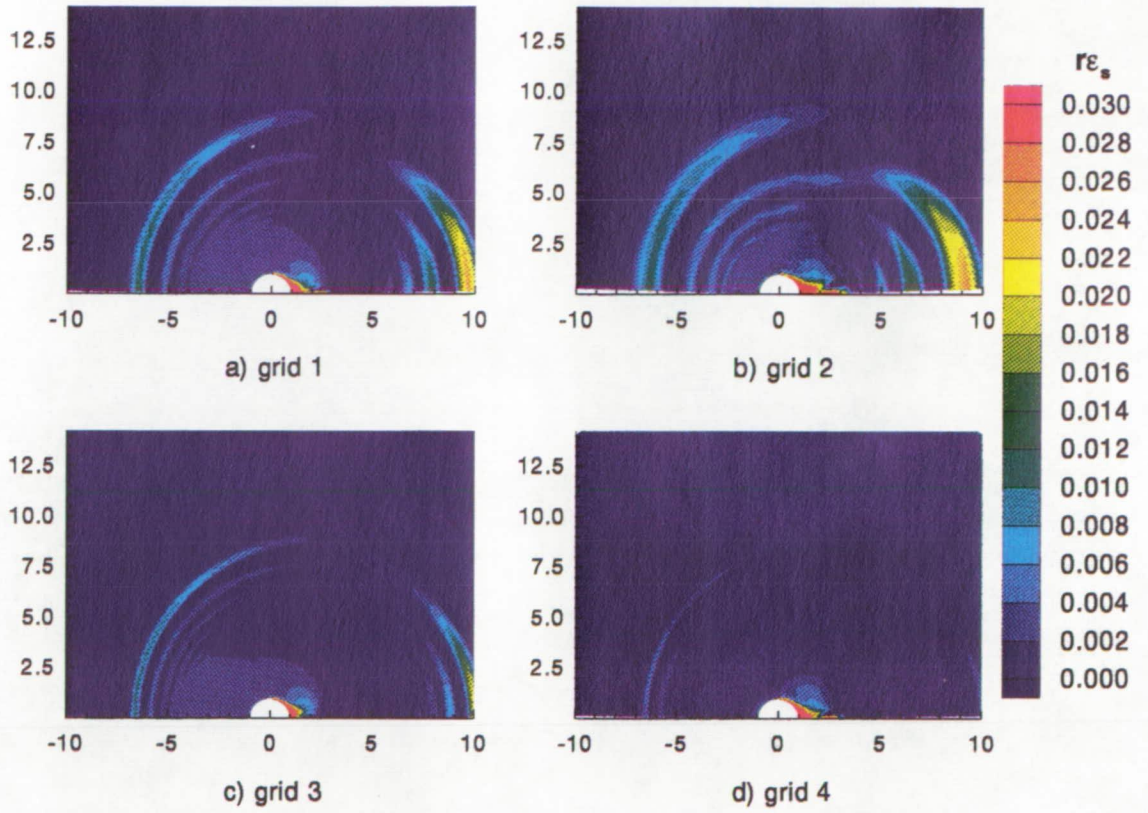

Figure 24. A comparison of the entropy energy ε_s distribution for various grids at $t = 8.0$. This is for the case of a cylinder impulsively started in Mach 0.4 translational motion.

and potential energies, with the energy lost to the far field, i.e. the acoustic and entropy energy, we indeed have an equal division of the energy input into the system. Above the critical Mach number no such equipartition is possible because energy is continually transported from the body to the far field. This is accomplished through the entropy energy component and is due to the presence of the shock in the steady state aerodynamic field.

We have also found that separating the energy into its kinetic, potential, and entropy energy components is useful in understanding both the physics of the problem and the effect of the numerical damping. The entropy term is especially useful because it gives a quantitative measure that we can use to compare the effect of algorithms and grids on the transient solution. This use of energy is apparently new.

In part B we have shown that for the cylinder the implicit damping in the numerical scheme, which is related to the resolution of the grid, is of primary importance for the calculation of the time dependent acoustic field. If the grid is too coarse, acoustic energy is transferred to entropy energy as it propagates. We have also found that the role of the explicitly added artificial viscosity has a small effect on the time dependent energy solution.

Summary

The first goal of this work was to address the importance of the quadrupole source term in the FW–H equation. This was necessary since the acoustic analogy based theory has been somewhat abused in application. We concede that the quadrupole source term is both difficult to interpret and to evaluate. Nevertheless, we have shown in Part A that the quadrupole source contains fundamental components of the complete fluid mechanics problem, which are ignored only at the risk of error. One of the contributions of this research was to demonstrate that the aerodynamics problem may be solved completely only if the vorticity components contained in the quadrupole are retained in the formulation. An integral equation has been put forward which, if extended for compressible flow, could be useful for aeroacoustic and aeroelastic computations. With the results of Part A and previous investigations pointing out the importance of the quadrupole, it should be clear that any application of the acoustic analogy should begin with all of the source terms in the Ffowcs Williams and Hawkings theory.

The second emphasis of this work was to consider the direct calculation of the acoustic field as part of the complete unsteady fluid mechanics problem using CFD. The recovery of the equipartition of energy principle for low Mach numbers gives us confidence that the numerical calculations are consistent with known analytical results. The finding that this principle can be extended to nonnegligible Mach numbers is a bonus. Now with some confidence, we have shown that aeroacoustic calculations can indeed be made with CFD codes. Having said this, the results indicate that the acoustic field is the most susceptible component of the computation to numerical error. Therefore, the ability to measure the damping of acoustic waves is absolutely essential both to develop new algorithms and to

evaluate acoustic computations. Entropy energy seems to be a good quantitative measure for this purpose.

This dissertation has laid essential groundwork for a new approach to the problem of sound generated by moving bodies. Clearly the circular cylinder solution has limited application in and of itself. Nonetheless, one of the main attractions of CFD technology is the ability to treat a wide variety of nonlinear problems with complicated geometries. Now with a tool to identify the numerical damping effect separately from the acoustics, it will be possible to develop improved numerical methods for acoustic applications. In the future other numerical algorithms, especially those with high order of accuracy, should be evaluated using model problems like the circular cylinder. New algorithms may actually take advantage of the entropy generation of the discrete equations by adaptively modifying the calculation in various spatial regions. Also the explicit damping term might be tailored to offset the implicit damping of the algorithm. Finally, it would be useful to separate the numerically generated entropy energy from that of physical origin. This might be done by considering the vorticity in the fluid. This new computational acoustic approach holds the promise of solving many problems hither to pushed aside.

Appendices

Appendix A1 - Calculation of FW–H Source Terms for the Cylinder

The incompressible form of the FW–H equation has three source terms and may be written

$$\nabla^2\left(p'H(f)\right) = -\frac{\partial}{\partial t}\left(\rho v_n \delta(f)\right) + \frac{\partial}{\partial x_i}\left(p' n_i \delta(f)\right) - \frac{\partial^2}{\partial x_i \partial x_j}\left(\rho u_i u_j H(f)\right). \qquad (A1.1)$$

This is equation (3) of Part A. The solution may be obtained by using the two dimensional Green's function for the Laplace equation in unbounded space, $G(\mathbf{x},\mathbf{y}) = \ln|\mathbf{x}-\mathbf{y}|/2\pi$. In what follows, each source term will be evaluated analytically and by linear superposition, all of the contributions can be added at the end to form the final solution. The subscripts t, l, and q will refer to thickness, loading, and quadrupole source terms, respectively. Note that since ρ is a constant, it will not be carried along in the intermediate calculations for convenience.

Thickness Term.

Each term of the FW–H equation may be treated independently since the wave operator is linear, therefore the thickness source will be treated first. The contribution from the thickness source is actually the solution to the equation

$$\nabla^2 p'_t = -\frac{\partial}{\partial t}\left(v_n \delta(f)\right). \qquad (A1.2)$$

The solution to this may be written formally using the Green's function as

$$2\pi p'_t = -\int_{-\infty}^{\infty} \frac{\partial}{\partial t}\left(v_n \delta(f)\right) \ln|\mathbf{x}-\mathbf{y}| d\mathbf{y}. \qquad (A1.3)$$

Now since the operator ∇^2 commutes with $\partial/\partial t$ it is actually beneficial to write (A1.3) as

$$2\pi p_t' = -\frac{\partial}{\partial t}\int_{-\infty}^{\infty} v_n \delta(f) \ln \rho dy \qquad (A1.4)$$

where we define $\rho = |\mathbf{x} - \mathbf{y}|$. To evaluate this integral, it is appropriate for the circular geometry to use polar coordinates, i.e. $dy = RdRd\theta$. Now $\delta(f) = \delta(R-a)$ and $\mathbf{y} = \mathbf{x}_o + R\hat{\mathbf{n}}$ if the cylinder center is labeled $\mathbf{x}_o(t)$. With polar coordinates, (R, θ) are the coordinates of the source position $\mathbf{y}$, relative to the cylinder center. Similarly, we will define the coordinates of the observer position $\mathbf{x}$ relative to the cylinder center as $(r, \tilde{\theta})$. See figure A1-1. We can determine from the geometry that

$$\rho^2 = r^2(1 - 2\alpha\cos(\theta - \tilde{\theta}) + \alpha^2) \qquad (A1.5)$$

where $r = |\mathbf{x} - \mathbf{y}|$ and $\alpha = R/r$. It is useful to recall that $v_n = v_1 \cos\theta + v_2 \sin\theta$ and $\mathbf{v} = d\mathbf{x}_o/dt$. These definitions are used throughout the integration of each of the source terms.

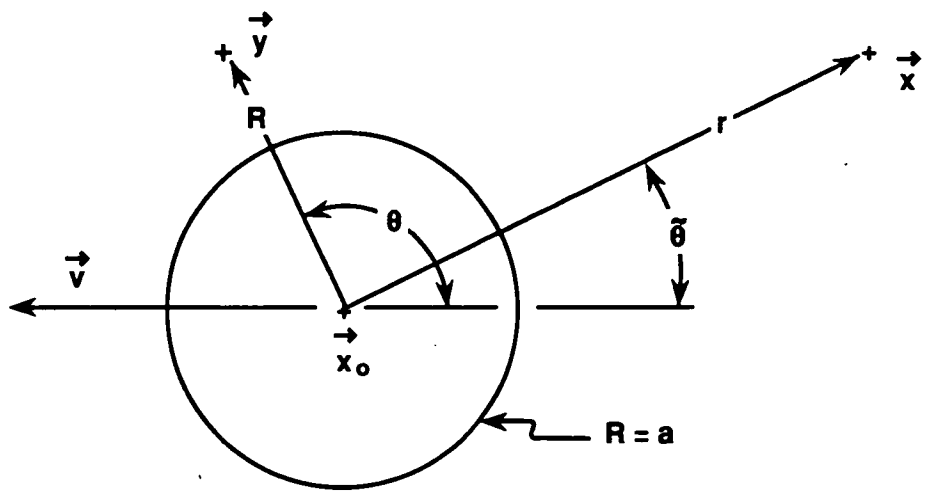

Figure A1-1. This figure shows the definitions of the variables used in the equations.

It is trivial to evaluate the R integration in equation (A1.4) due to the presence of the delta function. The resultant integral is

$$2\pi p_t' = -\frac{\partial}{\partial t}\int_0^{2\pi} a(v_1\cos\theta + v_2\sin\theta)\ln\rho\ d\theta \qquad (A1.6)$$

which may be written as

$$2\pi p_t' = \frac{\partial}{\partial t}\int_0^{2\pi} \frac{a^2(v_1\sin\theta - v_2\cos\theta)\sin(\theta-\tilde{\theta})}{r(1-2\alpha\cos(\theta-\tilde{\theta})+\alpha^2)}d\theta \qquad (A1.7)$$

after an integration by parts. Notice that now $\alpha = a/r$ since we are only dealing with the cylinder surface. Next we make a change of variables $\psi = \theta - \tilde{\theta}$ and recognize that $\tilde{\theta} \le \theta \le 2\pi + \tilde{\theta}$ is an equally valid range of integration in $(A1.7)$. After some algebra we can write

$$2\pi p_t' = \frac{\partial}{\partial t}\int_0^{2\pi} \frac{a^2\left(v_{\tilde{n}}\sin\psi - v_{\tilde{t}}\cos\psi\right)\sin\psi}{r(1-2\alpha\cos\psi+\alpha^2)}d\psi \qquad (A1.8)$$

where $v_{\tilde{n}} = v_1\cos\tilde{\theta} + v_2\sin\tilde{\theta}$ and $v_{\tilde{t}} = -v_1\sin\tilde{\theta} + v_2\cos\tilde{\theta}$. In Gradshteyn and Ryzhik *[43]*, we find

$$\int_0^{2\pi} \frac{\sin(n\psi)}{1-2\alpha\cos\psi+\alpha^2}d\psi = 0 \qquad (A1.9)$$

$$\int_0^{2\pi} \frac{\cos(n\psi)}{1-2\alpha\cos\psi+\alpha^2}d\psi = \frac{2\pi\alpha^n}{1-\alpha^2} \quad ;\ \alpha^2 < 1. \qquad (A1.10)$$

Clearly $\alpha < 1$ will always be true for this case since $\alpha = a/r$ and a is the minimum radius of interest. Substituting these results into $(A1.8)$ gives

$$2\pi p_t' = a^2\pi\frac{\partial}{\partial t}\left(\frac{\mathbf{v}\cdot\tilde{\mathbf{n}}}{r}\right) \qquad (A1.11)$$

with $\mathbf{v}\cdot\tilde{\mathbf{n}} = v_{\tilde{n}}$ and $\tilde{\mathbf{n}} = (\mathbf{x}-\mathbf{x}_o)/|\mathbf{x}-\mathbf{x}_o|$. Now using the relations

$$\frac{\partial}{\partial t}\left(\frac{1}{r}\right) = \frac{\mathbf{v}\cdot\tilde{\mathbf{n}}}{r^2} \tag{A1.12}$$

and

$$\frac{\partial}{\partial t}(\tilde{\mathbf{n}}) = -\frac{1}{r}\mathbf{v} + \frac{(\mathbf{v}\cdot\tilde{\mathbf{n}})}{r}\tilde{\mathbf{n}} \tag{A1.13}$$

the solution for the thickness contribution to the pressure perturbation is found to be

$$p_t'(\mathbf{x},t) = \frac{\rho}{2}\left\{\frac{a^2}{r^2}(v_n^2 - v_t^2) + \frac{a^2}{r}\frac{d\mathbf{v}}{dt}\cdot\hat{\mathbf{r}}\right\} \tag{A1.14}$$

when written in terms of the usual variables and including the fluid density ρ.

Loading Term.

The loading term may be determined in a manner similar to the thickness term, using the above definitions. After the initial manipulations and completion of the radial integration, the loading term is found to be

$$2\pi p_l' = \frac{\partial}{\partial x_i}\int_0^{2\pi} ap|_{r=a}\, n_i \ln\rho \; d\theta \tag{A1.15}$$

where

$$p|_{r=a} = 2v_n^2 - \frac{3v^2}{2} + a\frac{d\mathbf{v}}{dt}\cdot\hat{\mathbf{n}} - \frac{K}{\pi a}v_t - \frac{K^2}{8\pi^2 a^2}. \tag{A1.16}$$

Now we can take the spatial derivatives inside the integrand where they act only on ρ. Noting that

$$\frac{\partial\rho}{\partial x_i} = \frac{(x_i - x_{o_i} - an_i)}{\rho} \tag{A1.17}$$

and

$$n_i\frac{\partial\rho}{\partial x_i} = \frac{r\big(\cos(\theta-\tilde{\theta})-\alpha\big)}{\rho} \tag{A1.18}$$

we can write equation $(A1.16)$ as

$$2\pi p_l' = \alpha \int_0^{2\pi} \frac{(2v_n^2 + a\frac{d\mathbf{v}}{dt}\cdot\hat{\mathbf{n}} - \frac{3}{2}v^2 - \frac{K}{\pi a}v_t - \frac{K^2}{8\pi^2 a^2})(\cos(\theta-\tilde{\theta})-\alpha)}{1-2\alpha\cos(\theta-\tilde{\theta})+\alpha^2}d\theta. \qquad (A1.19)$$

Using some trigonometry and making a change of variables puts this equation in the form

$$\begin{aligned} 2\pi p_l' = \ & \alpha \int_0^{2\pi} \frac{((v_{\tilde{n}}^2 - v_{\tilde{t}}^2)\cos(2\psi) + 2(a\frac{d\mathbf{v}}{dt}\cdot\tilde{\mathbf{n}} - \frac{K}{\pi a}v_{\tilde{t}})\cos\psi)(\cos\psi-\alpha)}{1-2\alpha\cos\psi+\alpha^2}d\psi \\ + \ & \alpha \int_0^{2\pi} \frac{(v_{\tilde{n}}v_{\tilde{t}}\sin(2\psi) + (a\frac{d\mathbf{v}}{dt}\cdot\tilde{\mathbf{t}} + \frac{K}{\pi a}v_{\tilde{n}})\sin\psi - v^2 - \frac{K^2}{8\pi^2a^2})(\cos\psi-\alpha)}{1-2\alpha\cos\psi+\alpha^2}d\psi. \qquad (A1.20) \end{aligned}$$

This is now in a form in which we can apply $(A1.9)$ and $(A1.10)$ quite easily. We find that the second integral is zero, therefore the solution to loading source term contribution to the pressure perturbation is

$$p_l'(\mathbf{x},t) = \frac{\rho}{2}\left\{\frac{a^2}{r^2}(v_n^2 - v_t^2) + \frac{a^2}{r}\frac{d\mathbf{v}}{dt}\cdot\hat{\mathbf{r}} - \frac{Kv_t}{\pi r}\right\} \qquad (A1.21)$$

when written in terms of the usual variables and including the fluid density ρ.

Quadrupole Term.

The quadrupole source term is slighty more complex since the radial integration is no longer trivial. The formal solution for the pressure due to the quadrupole is written as

$$2\pi p_q' = -\int_0^{2\pi}\int_0^{\infty} \frac{\partial^2}{\partial x_i \partial x_j}(u_i u_j H(R-a)) \ln\sqrt{r^2 - 2rR\cos(\theta-\tilde{\theta}) + R^2}\ RdRd\theta. \qquad (A1.22)$$

One way to evaluate this integral is to recognize that

$$\frac{\partial^2}{\partial x_i \partial x_j}(u_i u_j H(f)) = \frac{\partial^2 u_i u_j}{\partial x_i \partial x_j}H(f) + \frac{\partial}{\partial x_i}(u_i u_n \delta(f)) + \left(\frac{\partial}{\partial x_j}(u_i u_j)\right)n_i\delta(f) \qquad (A1.23)$$

and split the problem into three integrals

$$I_1 = -\int_0^{2\pi}\int_a^{\infty} \frac{\partial^2 u_i u_j}{\partial x_i \partial x_j} \ln\sqrt{r^2 - 2rR\cos(\theta-\tilde{\theta}) + R^2}\; RdRd\theta \qquad (A1.24)$$

$$I_2 = -\frac{\partial}{\partial x_i}\int_0^{2\pi}\int_0^{\infty} u_i u_n \delta(R-a) \ln\sqrt{r^2 - 2rR\cos(\theta-\tilde{\theta}) + R^2}\; RdRd\theta \qquad (A1.25)$$

$$I_3 = -\int_0^{2\pi}\int_0^{\infty} \frac{\partial u_i u_j}{\partial x_j} n_i \delta(R-a) \ln\sqrt{r^2 - 2rR\cos(\theta-\tilde{\theta}) + R^2}\; RdRd\theta. \qquad (A1.26)$$

The first integral, I_1, requires more attention than the other two since we must be careful about the radial integration, so we will leave it until last. The second integral, I_2, is in a form which is very similar to the loading term. Here we need $u_i u_n$ evaluated on the surface $r = a$. From the velocity potential we know that

$$u_i = \frac{a^2}{r^2}(v_n n_i - v_t t_i) - \frac{K}{2\pi r} t_i \qquad (A1.27)$$

and hence

$$u_i u_n = \left((v_n n_i - v_t t_i) - \frac{K}{2\pi r} t_i\right) v_n \qquad (A1.28)$$

on the surface. Here n_i and t_i are the components of the unit normal an tangent vectors on the body surface. Now if we integrate radially and bring the spatial derivative in the integral, I_2 becomes

$$I_2 = -\alpha \int_0^{2\pi} \frac{v_{\tilde{n}}^2\left(\cos(\theta-\tilde{\theta}) - \alpha\right) + \left(v_n v_t - K v_n\right)\sin(\theta-\tilde{\theta})}{1 - 2\alpha\cos(\theta-\tilde{\theta}) + \alpha^2} d\theta. \qquad (A1.29)$$

As before, we need to change variables, $\psi = \theta - \tilde{\theta}$, and use the identities $v_n = v_{\tilde{n}}\cos\psi + v_{\tilde{t}}\sin\psi$ and $v_t = -v_{\tilde{n}}\sin\psi + v_{\tilde{t}}\cos\psi$, along with some trigonometry, to get an integral of

the form of $(A1.9)$ and $(A1.10)$. Skipping the details since we have already done most of them for the loading term, we find that

$$I_2 = -\frac{K}{2r} v_t \tag{A1.30}$$

The integral I_3 is slightly different in that we will need to know that

$$\frac{\partial u_i u_j}{\partial x_j} n_i = \frac{\partial u_i}{\partial x_j} u_j n_i \tag{A1.31}$$

for an incompressible fluid. Using the velocity potential, we can write I_3 as

$$I_3 = \int_0^{2\pi} \left(2v^2 + \frac{K^2}{4\pi^2 a^2} + \frac{3K}{2\pi a} v_t\right) \ln \rho \; d\theta. \tag{A1.32}$$

The third term in this integral is of the same form as the integral in $(A1.7)$ and may be evaluated immediately. The integration of the first and second terms is divergent, but it will be seen that these cancel exactly with part of the integral I_1. For this reason we will write the solution to I_3 as

$$I_3 = \int_0^{2\pi} \left(2v^2 + \frac{K^2}{4\pi^2 a^2}\right) \ln \rho \; d\theta \quad - \frac{3K}{2r} v_t. \tag{A1.33}$$

Now to solve the final integral, I_1, we first make use of the fact that for incompressible flow the relationship

$$\frac{\partial^2 u_i u_j}{\partial x_i \partial x_j} = \frac{\partial u_i}{\partial u_j} \frac{\partial u_j}{\partial x_i} = \frac{8a^4}{r^6} v^2 + \frac{4K}{\pi r^5} v_t + \frac{K^2}{2\pi^2 r^4} \tag{A1.34}$$

is true for the circular cylinder. Thus the integral to be evaluated is

$$I_1 = -\int_0^{2\pi} \int_a^{\infty} \left(\frac{8a^4}{R^5} v^2 + \frac{4K}{\pi R^4} v_t + \frac{K^2}{2\pi^2 R^3}\right) \ln \sqrt{r^2 - 2rR\cos(\theta - \tilde{\theta}) + R^2} \; dR d\theta. \tag{A1.35}$$

If we integrate by parts this integral becomes

$$I_1 = -\int_0^{2\pi} (2v^2 + \frac{K^2}{4\pi^2 a^2} + \frac{4K}{3\pi a} v_t) \ln\rho \; d\theta$$
$$+ \int_0^{2\pi}\int_a^{\infty} \left(\frac{2a^4}{R^4}v^2 + \frac{4Ka^2}{3\pi R^3}v_t + \frac{K^2}{4\pi^2 R^2}\right) \frac{(\cos(\theta-\tilde{\theta})-\alpha)}{r(1-2\alpha\cos(\theta-\tilde{\theta})+\alpha^2)} dR d\theta \quad (A1.36)$$

with α again defined as $\alpha = R/r$. If we call the first integral in $(A1.36)$ I_{1a}, we can immediately write down the solution

$$I_{1a} = -\int_0^{2\pi} (2v^2 + \frac{K^2}{4\pi^2 a^2}) \ln\rho \; d\theta \quad + \frac{4K}{3r} v_t \quad (A1.37)$$

by looking at I_3. The second integral in $(A1.36)$, I_{1b}, can be solved by reversing the order of integration and breaking the integration in two parts to make use of the formulas from Gradshteyn and Ryzhik, $(A1.9)$,$(A1.10)$, and

$$\int_0^{2\pi} \frac{\cos(n\psi)}{1-2\alpha\cos\psi+\alpha^2} d\psi = -\frac{2\pi}{(1-\alpha^2)\alpha^n} \quad ; \; \alpha^2 > 1. \quad (A1.38)$$

When this written out we find that

$$I_{1b} = \int_a^r + \int_r^{\infty} dR \int_0^{2\pi} \left(\frac{2a^4}{R^4}v^2 + \frac{4Ka^2}{3\pi R^3}v_t + \frac{K^2}{4\pi^2 R^2}\right) \frac{(\cos(\theta-\tilde{\theta})-\alpha)}{r(1-2\alpha\cos(\theta-\tilde{\theta})+\alpha^2)} d\theta. \quad (A1.39)$$

Notice that for the first integral, $\int_a^r dR$, the range of integration restricts α to $\alpha < 1$ while in the second integral, $\int_r^{\infty} dR$, $\alpha > 1$ is true. For $\alpha < 1$ the θ integration has been done previously in $(A1.19)$-$(A1.21)$, with different coefficients. For $\alpha > 1$ we can write the θ integration as

$$I = \int_0^{2\pi} \left(\frac{2a^4}{R^4}v^2 + \frac{K^2}{4\pi^2 R^2} + \frac{4Ka^2}{3\pi R^3}(-v_{\tilde{n}}\sin\psi + v_{\tilde{t}}\cos\psi)\right) \frac{(\cos\psi-\alpha)}{r(1-2\alpha\cos\psi+\alpha^2)} d\psi. \quad (A1.40)$$

Upon application of $(A1.9)$, $(A1.10)$, and $(A1.38)$ to this we can write I_{1b} as

$$I_{1b} = \int_a^r \frac{4Ka^2}{3rR^3} v_{\hat{i}} dR - \int_r^\infty 2\pi \left(\frac{2a^4}{R^5} v^2 + \frac{K^2}{4\pi^2 R^3}\right) + \frac{4Ka^2 r}{3R^5} v_{\hat{i}} dR. \qquad (A1.41)$$

It is straightforward to complete the integration in R and we find that

$$I_1 = -\int_0^{2\pi} \left(2v^2 + \frac{K^2}{4\pi^2 a^2}\right) \ln \rho \, d\theta - \frac{\pi a^4}{r^4} v^2 - \frac{K^2}{4\pi r^2} - \left(\frac{Ka^2}{r^3} - \frac{2K}{r}\right) v_t. \qquad (A1.42)$$

Combining I_1, I_2, and I_3 gives the full quadrupole contribution of the pressure perturbation as

$$p'_q(\mathbf{x}, t) = -\frac{\rho}{2}\left(\frac{a^4}{r^4} v^2 + \frac{Ka^2}{\pi r^3} v_t + \frac{K^2}{4\pi^2 r^2}\right) \qquad (A1.43)$$

when written in terms of the usual variables and including the fluid density ρ.

Appendix A2 - Derivation of New Quadrupole Formulation

The quadrupole source in the FW–H equation can be arranged into various forms which can be useful in the interpretation of the role of this source term. We can derive equation (17) by first expanding the quadrupole into the form

$$\frac{\partial^2 (\rho u_i u_j H(f))}{\partial x_i \partial x_j} = \nabla \cdot \left\{ \left(\rho \mathbf{u} \nabla \cdot \mathbf{u} + \mathbf{u} \cdot \nabla(\rho \mathbf{u})\right) H(f) + \rho \mathbf{u} v_n \delta(f) \right\} \qquad (A2.1)$$

where we have used $\nabla H(f) = \hat{\mathbf{n}} \delta(f)$ and $u_n = v_n$ on $f = 0$. Now if we use the relation

$$\mathbf{u} \cdot \nabla \mathbf{u} = \nabla \frac{1}{2} u^2 + \boldsymbol{\zeta} \times \mathbf{u}, \qquad (A2.2)$$

where $\boldsymbol{\zeta} = \nabla \times \mathbf{u}$, and the fact that for an incompressible flow, $\nabla \cdot \mathbf{u} = 0$ and ρ constant, we can write the quadrupole

$$\frac{\partial^2 (\rho u_i u_j H(f))}{\partial x_i \partial x_j} = \nabla \cdot \left\{ \left(\nabla \frac{1}{2} \rho u^2 + \rho \boldsymbol{\zeta} \times \mathbf{u}\right) H(f) + \rho v_n \mathbf{u} \delta(f) \right\}. \qquad (A2.3)$$

Now if we take the Heaviside function inside the $\nabla\frac{1}{2}\rho u^2$ term we get

$$\frac{\partial^2(\rho u_i u_j H(f))}{\partial x_i \partial x_j} = \nabla^2(\frac{1}{2}\rho u^2 H(f)) + \rho\nabla\cdot(\boldsymbol{\zeta}\times\mathbf{u}H(f)) + \nabla\cdot\big((\rho v_n\mathbf{u} - \frac{1}{2}\rho u^2\hat{\mathbf{n}})\delta(f)\big) \quad (A2.4)$$

which is the desired result. Notice that the vector quantities in the surface term may also be written as

$$v_n\mathbf{u} - \frac{u^2}{2}\hat{\mathbf{n}} = \frac{v_n^2 - u_t^2}{2}\hat{\mathbf{n}} + v_n u_t\hat{\mathbf{t}} = \frac{u^2}{2}\hat{\mathbf{m}} \quad (A2.5)$$

where $\hat{\mathbf{m}}$ is a unit vector.

Now we can also rearrange the thickness source term by some simple manipulations. The thickness source term can be expanded as

$$\frac{\partial}{\partial t}\big(\rho v_n\delta(f)\big) = \rho\frac{\partial\mathbf{v}}{\partial t}\cdot\hat{\mathbf{n}}\delta(f) + \rho\mathbf{v}\cdot\frac{\partial(\hat{\mathbf{n}}\delta(f))}{\partial t}. \quad (A2.6)$$

If we recognize that

$$\frac{\partial f}{\partial t} = -\nabla f\cdot\mathbf{v} \quad (A2.7)$$

and $\nabla f = \hat{\mathbf{n}}$, then with this and some algebra we can also show that

$$\frac{\partial}{\partial t}\big(\hat{\mathbf{n}}\delta(f)\big) = -\nabla\big(v_n\delta(f)\big) \quad (A2.8)$$

which allows us to write equation $(A2.6)$ as

$$\frac{\partial(\rho v_n\delta(f))}{\partial t} = \rho\frac{\partial\mathbf{v}}{\partial t}\cdot\hat{\mathbf{n}} - \rho\mathbf{v}\cdot\nabla(v_n\delta(f)). \quad (A2.9)$$

Now since $\mathbf{v} = \mathbf{v}_o + \boldsymbol{\omega}\times\boldsymbol{\eta}$ we can show that $\nabla\cdot\mathbf{v} = 0$. Here $\mathbf{v}_o$ is the velocity of the center of rotation, $\boldsymbol{\eta}$ is a position vector from the center of rotation, and $\boldsymbol{\omega}$ is the rotation vector. This result is clear when we write $\nabla\cdot\mathbf{v} = \boldsymbol{\eta}\cdot\nabla\times\boldsymbol{\omega} - \boldsymbol{\omega}\cdot\nabla\times\boldsymbol{\eta}$ because $\nabla\times\boldsymbol{\omega}$ and $\nabla\times\boldsymbol{\eta}$ are both zero. Finally we may write the incompressible version of the thickness source as

$$\frac{\partial}{\partial t}\Big(\rho v_n\delta(f)\Big) = \rho\frac{\partial\mathbf{v}}{\partial t}\cdot\hat{\mathbf{n}} - \nabla\cdot\big(\rho v_n\mathbf{v}\delta(f)\big). \quad (A2.10)$$

This form is useful because it can be combined with the new quadrupole description to write the incompressible FW–H equation as

$$\nabla^2\big((p' + \frac{1}{2}\rho u^2)H(f)\big) = \nabla \cdot \big\{\big((p' + \frac{1}{2}\rho u^2)\hat{\mathbf{n}} - \rho v_n(u_t - v_t)\hat{\mathbf{t}}\big)\delta(f)\big\} - \rho\frac{d\mathbf{v}}{dt} \cdot \hat{\mathbf{n}}\delta(f) - \rho\nabla \cdot \big((\boldsymbol{\zeta} \times \mathbf{u})H(f)\big). \quad (A2.11)$$

Dowling *[44]* has suggested an alternate derivation of equation (A2.11) once it is recognized that the quatitity $p' + \frac{1}{2}\rho u^2$ is the quantity of interest. It starts with the conservation of momentum

$$\rho\big(\frac{\partial \mathbf{u}}{\partial t} + \mathbf{u} \cdot \nabla \mathbf{u}\big) = -\nabla p = -\nabla p' \quad (A2.12)$$

and the relation (A2.2). Now if $B = p' + \rho u^2/2$ we can write

$$H(f)\nabla B = -\rho\big(\frac{\partial \mathbf{u}}{\partial t} + \boldsymbol{\zeta} \times \mathbf{u}\big)H(f) \quad (A2.13)$$

which is valid in the entire space. Next if we replace $H(f)\nabla B$ with $\nabla\{BH(f)\} - B\hat{\mathbf{n}}\delta(f)$ and take the divergence of equation (A2.12) we have

$$\nabla^2\big(BH(f)\big) = \nabla \cdot (B\hat{\mathbf{n}}\delta(f)) - \rho\frac{\partial \mathbf{u}}{\partial t} \cdot \hat{\mathbf{n}}\delta(f) - \rho\nabla \cdot \big((\boldsymbol{\zeta} \times \mathbf{u})H(f)\big) \quad (A2.14)$$

since $\nabla \cdot \mathbf{u} = 0$. Comparing this equation with (A2.11) shows that

$$\frac{\partial \mathbf{u}}{\partial t} \cdot \hat{\mathbf{n}}\delta(f) = \frac{d\mathbf{v}}{dt} \cdot \hat{\mathbf{n}}\delta(f) + \nabla \cdot \big(v_n(u_t - v_t)\hat{\mathbf{t}}\delta(f)\big). \quad (A2.15)$$

Appendix A3 - Comparison of Acoustic Theory to Classical Aerodynamics

In this appendix it is our goal to show that equation (20) can be reduced to classical thin airfoil theory for both the thickness and lifting problems. To do this we need to first start with the differential equation (20)

$$\nabla^2\big(BH(f)\big) = \nabla\cdot\big\{(B\hat{\mathbf{n}} - \rho v_n(u_t - v_t)\hat{\mathbf{t}})\delta(f)\big\} \qquad (A3.1)$$

which has been simplified by the additional assumptions of irrotationality and steady body motion. If we recognize that

$$v_n(u_t - v_t) = v_n u_t - v_t u_n = \mathbf{v}\cdot(\mathbf{u}\times\hat{\mathbf{k}}) \qquad (A3.2)$$

we can write the integral representation of the solution as

$$B = \frac{1}{2\pi}\int_{f=0}\frac{B\cos\theta - \rho\mathbf{v}\cdot(\mathbf{u}\times\hat{\mathbf{k}})\sin\theta}{r}dS \qquad (A3.3)$$

by using the Green's function technique. In this expression we have used $\cos\theta = \hat{\mathbf{r}}\cdot\hat{\mathbf{n}}$, $\sin\theta = \hat{\mathbf{r}}\cdot\hat{\mathbf{t}}$, and $r = |\mathbf{x}-\mathbf{y}|$. This equation is valid for a reference frame in which the body is moving whereas in aerodynamics the body is stationary and the fluid is moving. This difference in point of view is the motivation for comparing the Bernoulli equation for the two reference frames, where we find

$$p' = \frac{1}{2}\rho\big(U_\infty^2 - (u+U_\infty)^2\big) = -\frac{1}{2}\rho u^2 - \rho\frac{\partial\phi}{\partial t}. \qquad (A3.4)$$

Here the first right hand side is the normal, body fixed result from the aerodynamics and the second right hand side is the fluid fixed, acoustics result. In both cases u is the magnitude of the velocity perturbation of the fluid. From this we can infer that

$$B = p' + \frac{1}{2}\rho u^2 = \rho\mathbf{v}\cdot\mathbf{u} \qquad (A3.5)$$

since the constant body velocity $\mathbf{v} = -\mathbf{U}_\infty$. Combining this relation with equation (A3.3) allows us to write the vector equation

$$\mathbf{u} = \frac{1}{2\pi} \int_{f=0} \frac{\mathbf{u}\cos\theta - (\mathbf{u} \times \hat{\mathbf{k}})\sin\theta}{r} dS + \boldsymbol{\omega}. \qquad (A3.6)$$

Here $\boldsymbol{\omega}$ is a vector field everywhere orthogonal to the body velocity $\mathbf{v}$. The vector field $\boldsymbol{\omega}$ must be irrotational, $\nabla \times \boldsymbol{\omega} = 0$, and a solution to the Laplace equation, $\nabla^2 \boldsymbol{\omega} = 0$, for $\mathbf{u}$ to be a solution. This combination of conditions together with the orthogonality to $\mathbf{v}$ requires that $\boldsymbol{\omega}$ is of the form

$$\boldsymbol{\omega} = a + b\eta \qquad (A3.7)$$

where η is a distance in the coordinate direction orthogonal to $\mathbf{v}$ and a and b are constants. Further, a and b must both be zero since the velocity perturbation is required to approach zero at infinity. Therefore we can write equation (A3.6) as

$$\mathbf{u} = \frac{1}{2\pi} \int_{f=0} \frac{\mathbf{u}\cos\theta - (\mathbf{u} \times \hat{\mathbf{k}})\sin\theta}{r} dS \qquad (A3.8)$$

without ambiguity. This equation will be the starting point of our comparison with thin airfoil theory for the separate cases of a symmetric nonlifting airfoil and a thin, cambered airfoil at angle of attack.

Slender Body Theory.

In the first case consider a symmetric slender two dimensional airfoil which is described by the profile

$$y = \pm F(x), \quad 0 < x < 1 \tag{A3.9}$$

and is moving along the x axis with velocity U_∞. If a continuous distribution of sources and sinks is distributed along the axis, it is well known (see Yih*[32]* for example), that the velocity potential may be written

$$\phi = \frac{1}{2\pi} \int_0^1 f(\xi) \ln \sqrt{(x-\xi)^2 + y^2} d\xi \tag{A3.10}$$

where $f(\xi)$ is the source strength at $x = \xi$. The linearized boundary condition on the surface of the body gives

$$v = \pm U_\infty \frac{dF}{dx} \tag{A3.11}$$

where the positive and negative signs are for the upper and lower surfaces respectively. Upon differentiation of (A3.10) with respect to x and y, we find that the fluid velocities are given as

$$u = \frac{1}{2\pi} \int_0^1 \frac{f(\xi)(x-\xi)}{(x-\xi)^2 + y^2} d\xi \tag{A3.12}$$

$$v = \frac{y}{2\pi} \int_0^1 \frac{f(\xi)}{(x-\xi)^2 + y^2} d\xi. \tag{A3.13}$$

For small positive y we can evaluate an approximation to the second integral and after using (A3.11) it follows that

$$f(x) = 2U_\infty \frac{dF(x)}{dx}. \tag{A3.14}$$

While this is all we need for our comparison, usually the first velocity component is given as the finite part of

$$u = \frac{1}{2\pi}\int_0^1 \frac{f(\xi)}{x-\xi}d\xi \qquad (A3.15)$$

for small y.

For the acoustic equation (A3.8), we need the surface normal $\hat{\mathbf{n}} \approx (-dF/dx, \pm 1)$ for the upper and lower surface. We also need

$$\hat{\mathbf{r}}\cdot\hat{\mathbf{n}} = \frac{(x-\xi)n_1 + yn_2}{r} \qquad (A3.16)$$

$$\hat{\mathbf{r}}\cdot\hat{\mathbf{t}} = \frac{-(x-\xi)n_2 + yn_1}{r} \qquad (A3.17)$$

to be able to rewrite equation (A3.8) as

$$\mathbf{u} = \frac{1}{2\pi}\int_0^1 \frac{\mathbf{u}(-(x-\xi)\frac{dF}{dx}+y) - (\mathbf{u}\times\hat{\mathbf{k}})(-(x-\xi) - y\frac{dF}{dx})}{(x-\xi)^2+y^2}d\xi$$

$$+\frac{1}{2\pi}\int_0^1 \frac{\mathbf{u}(-(x-\xi)\frac{dF}{dx}-y) - (\mathbf{u}\times\hat{\mathbf{k}})((x-\xi) - y\frac{dF}{dx})}{(x-\xi)^2+y^2}d\xi. \qquad (A3.18)$$

Here the first integral refers to the upper surface and the second integral to the lower surface. Since the airfoil is symmetric, we know that $u|_{upper} = u|_{lower}$ and $v|_{upper} = -v|_{lower}$. Also we can write $\mathbf{u}\times\hat{\mathbf{k}} = (v, -u)$. Combining this information and dropping second order terms it follows that

$$u = \frac{1}{2\pi}\int_0^1 \frac{2v(x-\xi)}{(x-\xi)^2+y^2}d\xi \qquad (A3.19)$$

$$v = \frac{y}{2\pi}\int_0^1 \frac{2v}{(x-\xi)^2+y^2}d\xi \qquad (A3.20)$$

which is identical to the slender body theory result (A3.12) and (A3.13) when the linearized boundary condition (A3.11) is applied in terms of the upper surface. This result shows

the equivalence of the acoustic equation to the two dimensional slender body theory after these approximations are made.

Munk's Vortex Sheet Theory.

If we have a thin airfoil which is producing lift, we can model the airfoil by its mean line and consider it to be a vortex sheet on the x axis. If we do this, we can write the velocity potential

$$\phi = \frac{1}{2\pi}\int_0^1 f(\xi)\tan^{-1}\frac{y}{x-\xi}d\xi \qquad (A3.21)$$

where $f(\xi)$ is the vortex sheet strength at $x = \xi$. The tangential velocity on the airfoil is approximately

$$u = \frac{\partial\phi}{\partial x} = \frac{y}{2\pi}\int_0^1 \frac{f(\xi)}{(x-\xi)^2+y^2}d\xi \qquad (A3.22)$$

which is similar to (A3.13) and from this we can deduce

$$u|_{upper} = \frac{f(x)}{2} = -u|_{lower} \qquad (A3.23)$$

and hence the vortex sheet strength is $f(x) = [u]$, the discontinuity in u. To find the value of $f(\xi)$, we note that the linear boundary condition gives

$$v = U_\infty(\frac{dy_m}{dx} - \alpha) \qquad (A3.24)$$

with y_m defined as the distance to the mean line from the chord line and α is the angle of attack. We can also find that

$$v = \frac{\partial\phi}{\partial y} = \frac{1}{2\pi}\int_0^1 \frac{f(\xi)(x-\xi)}{(x-\xi)^2+y^2}d\xi. \qquad (A3.25)$$

Therefore if we consider small y, we can write (A3.25) as

$$v = \frac{1}{2\pi}\int_0^1 \frac{f(\xi)}{x-\xi}d\xi \qquad (A3.26)$$

which is an integral equation in terms of $f(\xi)$ when we consider it together with (A3.24). We must solve this integral equation with the Kutta condition $f(1) = 0$ to ensure there is no infinite velocity at the trailing edge. The solution of (A3.26) is then known to be

$$f(x) = \frac{2}{\pi}\sqrt{\frac{1-x}{x}}\int_0^1 \sqrt{\frac{\xi}{1-\xi}}\frac{v(\xi)}{(\xi - x)}d\xi. \qquad (A3.27)$$

This brief outline follows that of Yih*[32]* closely.

Now for the acoustic equation we first write the normal vector as $\hat{\mathbf{n}} \approx (-dy_m/dx + \alpha, 1)$ along with

$$\hat{\mathbf{r}} \cdot \hat{\mathbf{n}} = \frac{(x-\xi)(-\frac{dy_m}{dx} + \alpha) + y}{r} \qquad (A3.28)$$

$$\hat{\mathbf{r}} \cdot \hat{\mathbf{t}} = \frac{-(x-\xi) + y(-\frac{dy_m}{dx} + \alpha)}{r} \qquad (A3.29)$$

for the upper surface. Also for this thin airfoil approximation, $\hat{\mathbf{n}}|_{upper} = -\hat{\mathbf{n}}|_{lower}$, which enables us to write (A3.8) as

$$\mathbf{u} = \frac{1}{2\pi}\int_0^1 \frac{[\mathbf{u}]\big((x-\xi)(-\frac{dy_m}{dx} + \alpha) + y\big) + [\mathbf{u}] \times \hat{\mathbf{k}}\big(-(x-\xi) + y(-\frac{dy_m}{dx} + \alpha)\big)}{r^2} d\xi \qquad (A3.30)$$

if the discontinuity in $\mathbf{u}$ is written $[\mathbf{u}]$. Keeping only the first order terms, it follows that

$$u = \frac{y}{2\pi}\int_0^1 \frac{[u]}{(x-\xi)^2 + y^2} d\xi \qquad (A3.31)$$

$$v = \frac{1}{2\pi}\int_0^1 \frac{[u](x-\xi)}{(x-\xi)^2 + y^2} d\xi \qquad (A3.32)$$

where we have used the fact that $[v] \approx 0$. Notice (A3.31) corresponds to (A3.22) and (A3.32) corresponds to (A3.25). Thus we have shown that we can reduce the acoustic equation to Munk's vortex sheet theory as well as slender body theory.

Appendix B - Description of the Euler Solver

The purpose of this appendix is to give a detailed description of the numerical procedure used in the computations included in Part B. Some description of the methodology is given, but most of the concepts follow Jameson's work. References *[36-39]* give a somewhat broader description of the ideas used in the code developed for this work, while variations from normal practice are pointed out here.

Euler Equations for a Moving Grid.

The Euler equations may be written in vectorial form as

$$\frac{\partial \mathbf{U}}{\partial t} + \nabla \cdot \vec{\mathbf{F}} = 0 \qquad (B1.1)$$

where the dependent variable vector is

$$\mathbf{U} = \begin{Bmatrix} \rho \\ \rho u \\ \rho v \\ \rho E \end{Bmatrix} \qquad (B1.2)$$

and the flux matrix is

$$\vec{\mathbf{F}} = \mathbf{U}\vec{q} + p \begin{Bmatrix} 0 \\ \hat{i} \\ \hat{j} \\ \vec{q} \end{Bmatrix}. \qquad (B1.3)$$

In these equations, ρ is the fluid density, ρu,ρv are the components of the momentum in the x_1 and x_2 directions, ρE is the total energy ($E = c_v T + u^2/2$), while the fluid velocity $\vec{q} = (u, v)$ and $\hat{i}$, $\hat{j}$ are the unit vectors in the x_1 and x_2 coordinate directions. This form of the equations is known as the conservation form and is the correct form to accurately calculate the location and strength of shock waves numerically, if they exist in the flow field.

If we wish to consider a moving control volume, it is useful to make a change of coordinates

$$\mathbf{X}(t) = \mathbf{x} + \int_{t_o}^{t} \vec{v}(\tau) d\tau \qquad (B1.4)$$

where $\vec{v}(t)$ is the velocity the moving coordinate system. When we substitute the moving coordinates $\mathbf{X}$ in the Euler equations (B1.1) we find that

$$\frac{\partial \mathbf{U}}{\partial t} = \left.\frac{\partial \mathbf{U}}{\partial t}\right|_{\mathbf{X}(t)} + \vec{v}(t) \cdot \nabla \mathbf{U} \qquad (B1.5)$$

and

$$\nabla_{\mathbf{X}} \cdot \vec{\mathbf{F}} = \nabla_{\mathbf{x}} \cdot \vec{\mathbf{F}}. \qquad (B1.6)$$

Thus writing the Euler equations in terms of the moving coordinates gives us

$$\frac{\partial \mathbf{U}}{\partial t} + \nabla_{\mathbf{X}} \cdot \left(\vec{\mathbf{F}} - \mathbf{U}\vec{v}\right) = 0. \qquad (B1.7)$$

We can arrive at the integral form of this result if we use generalized functions and extend the Euler equations B1.1 outside of the control volume to the entire 2-D space. If we consider a control volume V where $g > 0$, bounded by $g = 0$, the extended equations would be

$$\frac{\partial}{\partial t}\left(\mathbf{U}H(g)\right) + \nabla \cdot \left(\vec{\mathbf{F}}H(g)\right) - \left(\mathbf{U}\frac{\partial g}{\partial t} + \vec{\mathbf{F}} \cdot \nabla g\right)\delta(g) = 0. \qquad (B1.8)$$

We will define g such that ∇g is a unit normal vector to the surface $g = 0$, pointing into the control volume. Recall that

$$\frac{\partial g}{\partial t} + \vec{v} \cdot \nabla g = 0 \qquad (B1.9)$$

for a surface with velocity $\vec{v}$. Then if we integrate over the entire space, we find

$$\frac{\partial}{\partial t}\int_{V} \mathbf{U} d\mathbf{y} + \int_{-\infty}^{\infty} \nabla \cdot \left(\vec{\mathbf{F}}H(g)\right) d\mathbf{y} + \int_{g=0} \left(\vec{\mathbf{F}} - \mathbf{U}\vec{v}\right) \cdot \hat{n} dS = 0 \qquad (B1.10)$$

where $\hat{n} = -\nabla g$, the outward unit normal and $\vec{v}$ is the velocity of the control volume surface. The second integral in B1.10 is identically zero, which we can see if we use the divergence thereom and realize that the Heaviside function is zero on the integration surface since $g < 0$ outside the control volume. Hence we may write Euler equations for a moving control volume in integral form as

$$\frac{\partial}{\partial t}\int_V \mathbf{U}dV + \int_{g=0} (\vec{\mathbf{F}} - \mathbf{U}\vec{v}) \cdot \hat{n}dS = 0. \qquad (B1.11)$$

If we change the definition of $\vec{\mathbf{F}}$ to include the $\mathbf{U}\vec{v}$ term in either B1.7 or B1.11, the form of the equations is identical to the one we started with. Notice that in any case the fluid velocities are defined in the reference frame fixed to the undisturbed medium.

The Finite Volume Approach.

Starting with the last equation and changing $\vec{\mathbf{F}}$ as indicated, we have

$$\frac{\partial}{\partial t}\int_V \mathbf{U}dV + \int_S \vec{\mathbf{F}} \cdot d\vec{S} = 0 \qquad (B1.12)$$

where S is the boundary of the control volume. For a finite volume method we assume that we can break up the domain of interest into small volumes ΔV and then if we interpret $\mathbf{U}$ to be the value of the dependent variables for the volume, in the sense of the mean value theorem, we can write a system of ordinary differential equations for each ΔV. This idea leads to the semi-discrete version of the conservation law

$$\frac{d}{dt}(\mathbf{U}\Delta V) + \sum_{faces} \vec{\mathbf{F}} \cdot \Delta\vec{S} = 0. \qquad (B1.13)$$

The surface integral has been written here as the sum of the flux through each face of ΔV, with $\Delta\vec{S}$ an outward normal vector to the face with magnitude ΔS. Here ΔS is the surface

area of the particular face rather than of the complete volume ΔV. For two dimensions the volume ΔV should be interpreted as the area of the cell and the surface area ΔS as the length of an edge of the cell. The value of the dependent variables $[\rho, \rho u, \rho v, \rho E]^T$ at the cell face is approximated as the average value of the two adjacent cells. The pressure at the cell face is directly calculated from the average value of the dependent variables. This scheme reduces to a $O(\Delta x^2)$ accurate central difference scheme on a Cartesian grid and has the property that uniform flow is an exact solution to the difference equations.

One advantage of the finite volume method is that curvilinear coordinates can be used to develop the computational mesh, and therefore ΔV and $\Delta \vec{S}$, while regular Cartesian coordinates of the fluid velocity, (u, v), are used in the specification of the dependent variables. Hence no transformation is needed and the form remains the same for various types of grids. The finite volume method is also readily applicable to triangular grids and unstructured grids. In this work only polar grids with constant azimuthal spacing are used.

Dissipative Terms.

The scheme presented thus far permits high frequency oscillations between odd and even mesh points which may cause the solution to become unstable. Dissipative terms must be added to suppress these spurious oscillations and prevent nonphysical wiggles near shock waves. The semi-discrete form of the equations can be written

$$\frac{d}{dt}(\mathbf{U}_{ij}\Delta V_{ij}) + \mathbf{Q}_{ij} - \mathbf{D}_{ij} = 0. \qquad (B1.14)$$

where $\mathbf{Q}_{ij}$ is the convective flux balance vector for the ijth grid cell and $\mathbf{D}_{ij}$ is the added dissipative term for the same cell. No summation of indices is implied in this equation. Various forms of $\mathbf{D}_{ij}$ are possible, each changing the character of the difference equations as Jameson and Lax*[38]* have shown.

For the present work, Jameson's combination of second and fourth order, adaptive dissipation has been used[37]. This form of dissipative terms is attractive because it is computationally efficient, robust, and in wide use. The dissipation $\mathbf{D}_{ij}$ is written in this form as

$$\mathbf{D}_{ij} = \Delta_i^+ \mathbf{d}_i + \Delta_j^+ \mathbf{d}_j \qquad (B1.15)$$

where Δ^+ is the forward difference operator, $\Delta_i^+ d_i = d_{i+1} - d_i$, and $\mathbf{d}_i$ is

$$\mathbf{d}_i = \left(\frac{\Delta V_i + \Delta V_{i-1}}{2\Delta t}\right)\left(\varepsilon^{(2)}\Delta_i^- \mathbf{U}_{ij} - \varepsilon^{(4)}(\Delta_i^-)^3 \mathbf{U}_{ij}\right). \qquad (B1.16)$$

Here Δ^- is the backward difference operator, $\Delta_i^- \mathbf{U}_{ij} = \mathbf{U}_{ij} - \mathbf{U}_{i-1\ j}$, and $(\Delta_i^-)^3$ means three applications of Δ_i^-. The coefficients $\varepsilon^{(2)}$ and $\varepsilon^{(4)}$ are defined as

$$\varepsilon^{(2)} = k_2 \max(\nu_{i-2}, \nu_{i-1}, \nu_i, \nu_{i+1}) \qquad (B1.17)$$

and

$$\varepsilon^{(4)} = \max(0, k_4 - \varepsilon^{(2)}). \qquad (B1.18)$$

The pressure switch ν_i, which is designed to detect the presence of shocks, is defined as

$$\nu_i = \left|\frac{p_{i+1j} - 2p_{ij} + p_{i-1j}}{p_{i+1j} + 2p_{ij} + p_{i-1j}}\right| \qquad (B1.19)$$

and the constants k_2 and k_4 have been used with nominal values of $k_2 = .25$ and $k_4 = .003$. The value of $\mathbf{d}_j$ is found in an analogous manner. From these definitions we see that the constant k_4 controls the fourth order background dissipation and k_2 controls the second order dissipation around pressure gradients. The effect of the second order term is to make the numerical scheme locally $O(\Delta x)$ accurate and it is clear that the pressure sensor ν_i will interpret any high frequency pressure variation as a shock and try to dampen it. The effect of the coefficients of k_2 and k_4 on the solution is shown in Part B.

Multistage Time Stepping.

If we keep the cell volume ΔV_{ij} time independent, we can write the semi-discrete system of equations for each cell as

$$\frac{d}{dt}(\mathbf{U}_{ij}) + \frac{1}{\Delta V_{ij}}(\mathbf{Q}_{ij} - \mathbf{D}_{ij}) = 0. \qquad (B1.20)$$

Recall that $\mathbf{Q}$ is the convective operator and $\mathbf{D}$ is the dissipative operator. Multistage time stepping schemes are modeled after the Runge-Kutta procedures used for ordinary differential equations. By adding more stages we can either improve the time accuracy or increase the allowable time step size while maintaining stability. A five stage scheme of the form

$$\mathbf{U}_{ij}^{(1)} = \mathbf{U}_{ij}^{n} - \alpha_1 \frac{\Delta t}{\Delta V_{ij}}(\mathbf{Q}_{ij}^{n} - \mathbf{D}_{ij}^{n}) \qquad (B1.21a)$$

$$\mathbf{U}_{ij}^{(2)} = \mathbf{U}_{ij}^{n} - \alpha_2 \frac{\Delta t}{\Delta V_{ij}}(\mathbf{Q}_{ij}^{(1)} - \mathbf{D}_{ij}^{(1)}) \qquad (B1.21b)$$

$$\mathbf{U}_{ij}^{(3)} = \mathbf{U}_{ij}^{n} - \alpha_3 \frac{\Delta t}{\Delta V_{ij}}(\mathbf{Q}_{ij}^{(2)} - \mathbf{D}_{ij}^{(1)}) \qquad (B1.21c)$$

$$\mathbf{U}_{ij}^{(4)} = \mathbf{U}_{ij}^{n} - \alpha_4 \frac{\Delta t}{\Delta V_{ij}}(\mathbf{Q}_{ij}^{(3)} - \mathbf{D}_{ij}^{(1)}) \qquad (B1.21d)$$

$$\mathbf{U}_{ij}^{n+1} = \mathbf{U}_{ij}^{n} - \frac{\Delta t}{\Delta V_{ij}}(\mathbf{Q}_{ij}^{(4)} - \mathbf{D}_{ij}^{(1)}) \qquad (B1.21e)$$

has been used for all the calculations in this work. Notice that only two evaluations of the dissipation are made in order to reduce the number of calculations. The coefficients $\alpha_1 = 1/4$, $\alpha_2 = 1/6$, $\alpha_3 = 3/8$, and $\alpha_4 = 1/2$ have been used. This time discretization is $O(\Delta t^2)$ accurate. Jameson's papers*[36,37,39]* are good references for more detail on the multistage time stepping approach.

Boundary Conditions.

Numerical boundary conditions are needed at all of the computational boundaries to complete the system of equations. For exterior flow problems artificial boundaries are necessary to produce a bounded domain. Improper treatment of these boundary conditions can lead to serious errors and perhaps instabilities, thus for this work the boundary conditions recommended by Schmidt and Jameson have been used*[37]*. Many other formulations of the numerical boundary conditions exist, but it was not within the scope of the present work to consider a wide variety of boundary condition formulations. This section follows Schmidt and Jameson and is given for completeness.

For the outer boundaries in subsonic flow, there is one outgoing characteristic at the inflow boundaries and three outgoing characteristics at the outflow boundaries. According to the theory of Kreiss *[45]*, three conditions need to be specified at the inflow boundary and one at the outflow boundary. The remaining conditions required by the numerical method are determined by extrapolating the outgoing characteristic variables from the interior solution. Thus at the inflow boundaries we have used the linear characteristic relations

$$p - c_o^2 \rho = p_o - c_o^2 \rho_o \qquad (B1.22a)$$

$$q_t = q_{t_o} \qquad (B1.22b)$$

$$p - \rho_o c_o q_n = p_e - \rho_o c_o q_{n_e} \qquad (B1.22c)$$

$$p + \rho_o c_o q_n = p_e + \rho_o c_o q_{n_e} \qquad (B1.22d)$$

where the subscripts o and e refer to the value in the undisturbed medium and the value extrapolated from the interior of the computational domain, respectively. Here q_n and

q_t are the normal and tangential components of velocity. When combined these give the result

$$p = \frac{1}{2}\left(p_e + p_o + \rho_o c_o (q_{n_e} - q_{n_o})\right) \qquad (B1.23a)$$

$$q_n = q_{n_o} + \frac{p - p_o}{\rho_o c_o} \qquad (B1.23b)$$

and the density can be determined from (B1.22a).

For the outflow boundary, a nonreflecting condition which should eliminate incoming waves is

$$\frac{\partial}{\partial t}(p - \rho_o c_o q_n) = 0. \qquad (B1.24)$$

This condition has been used together with the extrapolation of the density and momentum from the interior to minimize non-physical reflections from the outflow boundary. This boundary condition does in fact allow small reflections in actual application, which can lead to instabilities, however for the calculations considered here the time required for acoustic waves to reach the boundary is easily determined. Thus by moving the outflow boundary sufficiently far away from the body and limiting the computational time, any problems with the outflow boundary conditions can be minimized.

For the surface boundary conditions, no flux through the surface is specified, i.e.

$$\vec{\mathbf{F}} \cdot \Delta\vec{S} = p \begin{Bmatrix} 0 \\ \hat{n}_1 \\ \hat{n}_2 \\ v_n \end{Bmatrix} \Delta S \qquad (B1.25)$$

since $q_n = v_n$ on the surface of the body. The pressure at the surface is taken to be the linear extrapolation of the pressure from the interior. Linear extrapolation is used because of its simplicity and because little difference was seen between the results obtained with more sophisticated surface boundary conditions. The success of linear extrapolation is

probably related to the fact that the computational grid used in the present calculations is very fine near the body.

The solution is assumed symmetric about the x axis in the computations presented. Calculations were also made with a full computational grid with no symmetry assumption for the circular cylinder, but the results were identical. The boundary conditions used in this work should be considered representative of those in common use even though more advanced boundary condition formulations are under development.

References

[1] Lighthill, M. J., "On Sound Generated Aerodynamically," *Proceedings of the Royal Society*, Series A, Vol. 211, 1952, pp. 564-587.

[2] Curle, N.,"The influence of solid boundaries upon aerodynamic sound," *Proceedings of the Royal Society*, Series A, Vol. 231, 1955, pp. 505-514.

[3] Ffowcs Williams, J. E. and Hawkings, D. L., "Sound Generated by Turbulence and Surfaces in Arbitrary Motion," *Philosophical Transactions of the Royal Society*, Series A, Vol. 264, No. 1151, 1969, pp. 321-342.

[4] Farassat, F., "Theory of Noise Generation from Moving Bodies with an Application to Helicopter Rotors," NASA TR R-451, 1975.

[5] Hanson, D. B. and Fink, M., "The Importance of Quadrupole Sources in the Prediction of Transonic Tip Speed Propeller Noise," *Journal of Sound and Vibration*, 62(1), 1979, pp. 19-38.

[6] Schmitz, F. H. and Yu, Y. H., "Transonic Rotor Noise - Theoretical and Experimental Comparisons," *Vertica*, Vol 5, 1981, pp. 55-74.

[7] Ffowcs Williams, J. E., "On the Role of Quadrupole Source Terms Generated by Moving Bodies," AIAA 79-0576, 1979.

[8] Schultz, K.J. and Splettstoesser, W. R.,"Prediction of helicopter rotor impulsive noise using measured blade pressures," Proceedings of the 43rd AHS Forum, St. Louis, Missouri, May 1987.

[9] Farassat, F.,"Can Shock Waves on Helicopter Rotors Generate Noise? A Study of the Quadrupole Source," Proceedings of the 46th AHS Forum, Washington, DC, May 1990.

[10] Long, L. N., "The Compressible Aerodynamics of Rotating Blades Based on an Acoustic Formulation," NASA TP 2197, 1983.

[11] Farassat, F. and Myers, M. K., "Aerodynamics via Acoustics: Application of Acoustic Formulas for Aerodynamic Calculations," AIAA paper 86-1877, 1986.

[12] Brandão, M. P., "A New Perspective of Classical Aerodynamics," *Proceedings of the AIAA/ ASME/ ASCE/ AHS 28th Structure, Structural Dynamics, and Materials Conference*, Paper AIAA-87-0853-CP, Monterey, California, April 6-8, 1987.

[13] Brandão, M. P., "A New Method for the Aerodynamic Analysis of Lifting Surfaces," Presented at the Thirteen European Rotorcraft Forum, Sept. 8-11, 1987, Paper 2-3.

[14] Lee, Y. J., and Yang, Y. J.,"A Panel Method for Arbitrary Moving Boundary Problems," *AIAA Journal*, Vol. 28, 1990, pp. 432-438.

[15] Hanson, D. B.,"Compressible Helicoidal Surface Theory for Propeller Aerodynamics and Noise," *AIAA Journal*, Vol. 21, 1983, pp. 881-889.

[16] Das, A.,"Wave Propagation from Moving Singularities and a Unified Exposition of the Linearized Theory for Aerodynamics and Acoustics," DFVLR-FB 84-17, 1984.

[17] Morino, L.,Bharadvaj, B. K.,Freedman, M. I., and Tseng, K.,"Boundary Integral Equation for Wave Equation with Moving Boundary and Applications to Compressible Potential Aerodynamics of Airplanes and Helicopters," submitted for publication in Computational Mechanics, 1987

[18] Piva, R. and Morino, L.,"Vector Green's Function Method for Unsteady Navier-Stokes Equations," *MECCANICA*, Vol. 22, 1987, pp. 76-85.

[19] Ffowcs Williams, J. E.,"Hydrodynamic Noise," *Annual Review of Fluid Mechanics*, Vol. 1, 1969, pp. 197-222.

[20] Korkan, K. D., Von Lavante, E., and Bober, L. J.,"Numerical Evaluation of Propeller Noise Including Nonlinear Effects," *AIAA Journal*, Vol. 24, 1986, pp. 1043-1045.

[21] Purcell, T. W., Strawn, R. C., and Yu, Y. H.,"Prediction of High-Speed Rotor Noise with a Kirchhoff Formula," Proceedings of the AHS National Specialist's Meeting on Aerodynamics and Aeroacoustics, Arlington, Texas, Feb. 1987.

[22] Lyrintzis, A. S., and George, A. R.,"Transonic blade-vortex interactions: the far field," Proceedings of the AHS National Specialist's Meeting on Aerodynamics and Aeroacoustics, Arlington, Texas, Feb. 1987.

[23] Farassat, F. and Myers, M. K.,"Extension of Kirchhoff's Formula to Radiation from Moving Surfaces," *Journal of Sound and Vibration*," Vol. 123, 1988, pp. 451-460.

[24] Morgans, W. R.,"The Kirchhoff Formula Extended to a Moving Surface," *Philosophical Magazine*, Vol. 9, 1930, pp. 141-161.

[25] Longhorn, A. L.,"The Unsteady, Subsonic Motion of a Sphere in a Compressible Inviscid Fluid," *Quarterly Journal of Mechanics and Applied Mathematics*, Vol. V, Pt. 1, 1952, pp. 64-81.

[26] Farassat, F.,"Discontinuities in Aerodynamics and Aeroacoustics: The Concept and Applications of Generalized Derivatives," *Journal of Sound and Vibration*, Vol. 55(2), 1977, pp. 165-193.

[27] Powell, A., "Theory of Vortex Sound," *Journal of the Acoustical Society of America*, Vol. 36, No. 1., 1964, pp. 177-195.

[28] Howe, M. S., "Contributions to the Theory of Aerodynamic Sound with Applications to Excess Jet Noise and the Theory of the Flute," *Journal of Fluid Mechanics*, Vol. 58, Part 4, 1973, pp. 625-673.

[29] Milne-Thomson, L. M.,*Theoretical Hydrodynamics*, 4th edition, The Macmillan Company, 1960.

[30] Powell, A., "Aerodynamic Noise and the Plane Boundary," *Journal of the Acoustical Society of America*, Vol. 32, No. 8, 1960, pp. 982-990.

[31] Ffowcs Williams, J. E., "Sound Radiation from Turbulent Boundary Layers formed on Compliant Surfaces," *Journal of Fluid Mechanics*, Vol. 22, Part 2, 1965, pp. 347-358.

[32] Yih, Chia-Shun,*Fluid Mechanics*, West River Press, 1977, pp 153-155.

[33] Myers, M. K.,"Transport of Energy by Disturbances in Arbitrary Steady Flows," accepted for publication in the *Journal of Fluid Mechanics* in 1991.

[34] Jameson, A., Schmidt, W., and Turkel, E.,"Numerical Solution of the Euler Equations by Finite Volume Methods Using Runge-Kutta Time-Stepping Schemes," AIAA paper 81-1259, 1981.

[35] Schmidt, W. and Jameson, A.,"Recent Developments in Finite-Volume Time-Dependent Techniques for Two and Three Dimensional Transonic Flows," Von Karman Lecture Series 1982-04, March 29 - April 2,1982.

[36] Jameson, A., and Lax, P. D.," Conditions for the Construction of Multi-point Total Variation Diminishing Difference Schemes," *Applied Numerical Mathematics*, Vol. 2, No 3-5, October 1986, pp. 335-345.

[37] Jameson, A.,"A Nonoscillatory Shock Capturing Scheme Using Flux Limited Dissipation," *Lectures in Applied Mathematics*, Vol 22, 1985, pp. 345-370.

[38] Ffowcs Williams, J. E., and Lovely, D. J.,"An Approximate Method for Evaluating the Sound of Impulsively Accelerated Bodies," *Journal of Sound and Vibration*, Vol. 50(3), 1977, pp. 333-343.

[39] Taylor, G. I.,"The Motion of a Body in Water When Subjected to a Sudden Impulse," in *Scientific Papers of G. I. Taylor*, Vol. III, Aerodynamics and the Mechanics of Projectiles and Explosions, (G. K. Batchelor, editor), Cambridge University Press, 1971, pp. 306-308.

[40] Hill, D. C., "Starting mechanics of an evanescent wave field," *Journal of Fluid Mechanics*, Vol. 165, 1986, pp 319-333.

[41] Liepmann, H. W., and Roshko, A., *Elements of Gas Dynamics*, John Wiley and Sons, Inc., 1957.

[42] Walatka, P. P., and Buning, P. G.,"PLOT3D User's Manual," NASA TM 101067, 1989.

[43] Gradshteyn, I. S., and Ryzhik, I. M., *Table of Integrals, Series, and Products*, Academic Press, 1980.

[44] Dowling, A. P., personal communication, May 1988.

[45] Kreiss, H. O., "Initial Boundary Value Problems for Hyperbolic Systems," *Communications on Pure and Applied Mathematics*, Vol 23, 1970, pp. 277-298.

Suggested Key Words

Acoustics, Aeroacoustics, Computational Acoustics
Energy Analysis, Exact Quadrupole Calculation